CR160168



[redacted]

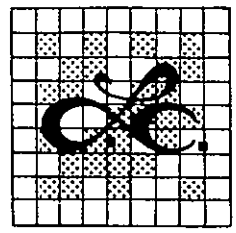

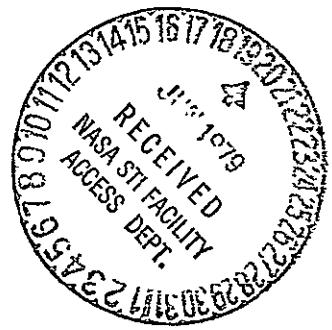


LinCom Corporation

P.O. Box 2793D, Pasadena, Calif. 91105

LinCom

FINAL REPORT

# SHUTTLE/TDRSS MODELLING AND LINK SIMULATION STUDY

PREPARED FOR

NASA LYNDON B. JOHNSON SPACE CENTER
HOUSTON, TX 77058

TECHNICAL MONITORS: W. TEASDALE
S. NOVOSAD

CONTRACT NAS 9-14846

PREPARED BY

W. R. BRAUN
T. M. McKENZIE
L. BIEDERMAN
W. C. LINDSEY

LINCOM CORPORATION
P.O. BOX 2793D
PASADENA, CA 91105

APRIL 20, 1979

TR-7904-0476a

LinCom

TABLE OF CONTENTS


| | | PAGE |
|---|---|---|
| 1.0 | INTRODUCTION | 1 |
| 1.1 | General | 1 |
| 1.1.1 | Final Report Contents | 1 |
| 1.2 | Summary and Recommendations | 3 |
| 1.2.1 | Shuttle S-Band Return Link Performance Summary | 3 |
| 1.2.2 | Attached Spacelab Bit Jitter Performance Summary | 3 |
| 1.2.3 | Shuttle Bent-Pipe Mode Subcarrier Performance Summary | 6 |
| 2.0 | DESCRIPTION OF LinCsim | 11 |
| 2.1 | Introduction | 11 |
| 2.2 | Link Models | 12 |
| 2.2.1 | Introduction | 12 |
| 2.2.2 | Channel Model Description | 13 |
| 2.2.3 | Forward Link Model and Design Values | 17 |
| 2.2.4 | Return Link Models and Design Values | 17 |
| 2.2.5 | Dedicated vs Composite Channel Model for the S-band Return Link | 17 |
| 2.2.6 | Ideal Channel Model | 31 |
| 2.3 | Subsystem Models | 31 |
| 2.3.1 | Introduction | 31 |
| 2.3.2 | Modulator | 31 |
| 2.3.3 | Filters | 32 |
| 2.3.4 | Power Amplifiers | 34 |

TABLE OF CONTENTS (Cont'd)


| | PAGE |
|---|---|
| 2.3.4.1 Introduction | 34 |
| 2.3.4.2 Linear Amplifier | 34 |
| 2.3.4.3 TWT Characteristic | 35 |
| 2.3.4.4 Constant AM-AM, AM-PM Model | 37 |
| 2.3.4.5 Definition of Operating Point | 40 |
| 2.3.5 PN Despreader | 40 |
| 2.3.6 Carrier Recovery | 40 |
| 2.3.7 Data Clock Recovery | 40 |
| 2.3.8 Data Detector | 40 |
| 2.4 Definition and Modelling of User Constraints | 44 |
| 2.4.1 Introduction | 44 |
| 2.4.2 User Constraints | 44 |
| 3.0 LinCsim PERFORMANCE PREDICTION | 77 |
| 3.1 Introduction | 77 |
| 3.2 Performance Prediction for Shuttle S-band Return Link | 77 |
| 4.0 ATTACHED SPACELAB PAYLOAD BIT JITTER PERFORMANCE | 106 |
| 4.1 Introduction | 106 |
| 4.2 System Model, Clock Jitter and Data Asymmetry | 107 |
| 4.3 BER at the Spacelab Ku-Band Transmitter Interface | 113 |
| 4.4 Coded Link Bit Jitter Performance | 117 |
| 4.5 Summary and Conclusions | 125 |
| 5.0 SHUTTLE PAYLOAD BENT-PIPE MODE SUBCARRIER RECOVERY | 128 |
| 5.1 Introduction | 128 |

TABLE OF CONTENTS (Cont'd)


| | | PAGE |
|---|---|---|
| 5.2 | Problem Statement | 128 |
| 5.3 | Costas Loop Model (Following Reference 1) | 131 |
| 5.4 | Costas Loop S-Curve | 133 |
| 5.5 | Spectral Density of the Equivalent Noise | 136 |
| 5.6 | Nonlinear Costas Loop Theory | 139 |
| 5.7 | Hard-Limiting Shuttle Repeater | 141 |
| 5.8 | Linear Shuttle Repeater | 144 |
| 5.9 | S-Curve Amplitude Plots | 147 |
| 5.10 | Variance of Loop Phase Error | 154 |
| 5.11 | Filter Bandwidth Selection | 154 |
| 5.12 | Conclusions | 161 |

# 1.0 INTRODUCTION

## 1.1 General

This document presents the final report on the Shuttle/TDRSS Modelling and Link Simulation Study performed for NASA Johnson Space Center under Contract NAS 9-14846 directed by William Teasdale and Sid Novosad. It represents a portion of the work accomplished during the period June 10, 1976 through April 20, 1979.

The general objectives of the overall contract are the following: (1) to develop Shuttle/TDRSS link simulation models which can predict the performance sensitivity of these links to Shuttle transmitted signal distortions, (2) to exercise the simulation to predict the bit error rate performance as a function of the signal distortion parameters, (3) to present these data in a form suitable to support ESTL hardware tests and (4) to provide ESTL with a quick assessment of the basic differences between the ESTL TDRSS simulator hardware and the actual TDRSS system. This last item was covered in informal briefings to pertinent ESTL personnel and is not further addressed in this final report.

In what follows an overall description of the contractual effort and a brief summary of the results is given. This is followed by backup material which includes simulation data and analyses from which our summary results and recommendations have been drawn.

### 1.1.1 Final Report Contents

This report addresses and documents LinCom's findings on the task statements detailed in the Statement of Work. All tasks

pertain to the performance prediction of Shuttle forward and return links through the Tracking and Data Relay Satellite System (TDRSS).

Chapter 2 describes in detail the Shuttle/TDRSS S-band and Ku-band link simulation package, called LinCsim, developed for evaluation of link performance for specific Shuttle signal designs. The link models are described in detail and the transmitter distortion parameters, the so-called User Constraints are defined carefully. A complete list of the present values of all parameters used in the simulation is also included in the description.

Chapter 3 contains the results of extensive simulation of the Shuttle/TDRSS S-band return link. The overall link degradation (excluding hardware degradations) relative to an ideal BPSK channel are shown for various sets of user constraint values and the performance sensitivity to each individual user constraint is illustrated. The results can be used by NASA/JSC as a technical base for negotiating interface parameters between the Shuttle and TDRSS.

Chapters 4 and 5 take an indepth look at two specific problems. The effect of excessive Spacelab clock-jitter on the return link BER performance is analyzed in Chapter 4. This investigation accounts for the effects of the clock clean-up system (scrubber) in the Shuttle as well as for the coding and for the high level of data asymmetry expected on this link. Chapter 5 considers the problem of subcarrier recovery for the K-band Shuttle return link signal when one of the channels contains unprocessed digital data from a detached payload. Two different implementations for the payload interrogator are investigated and their performance compared.

## 1.2 Summary and Recommendations

### 1.2.1 Shuttle S-band Return Link Performance Summary

The performance degradation of the Shuttle/TDRSS return link due to Shuttle signal imperfections has been evaluated for the expected Shuttle distortion values based on current link budgets and TDRS/ground station hardware data. The results show a loss relative to ideal BPSK of 1.65 dB at the nominal bit error probability of $10^{-4}$. The TDRS and ground station contribute .9 dB to this loss and the Shuttle the remaining .75 dB. This is illustrated in Fig. 1.1.

The single biggest contributor to the Shuttle degradation is the phase noise which is specified as 10° rms in the frequency interval 0 to 270 Hz. We recommend to separate the phase noise into components lying inside and outside the carrier tracking loop bandwidth, respectively, since these components affect the bit error rate performance differently. Such a refinement of the specification could greatly improve the accuracy of the predicted performance results. Since our present prediction is based on worst-case assumptions the overall degradation would be reduced.

### 1.2.2 Attached Spacelab Bit Jitter Performance Summary

The functional model of the Spacelab return link is shown in Fig. 1.2. The data and/or clock transitions from the Spacelab into the Shuttle are subject to severe phase jitter. The clock regenerator (scrubber) removes some of this jitter on the reclocked and convolutionally encoded data. However, the coded data may exhibit up to 10% of data asymmetry.

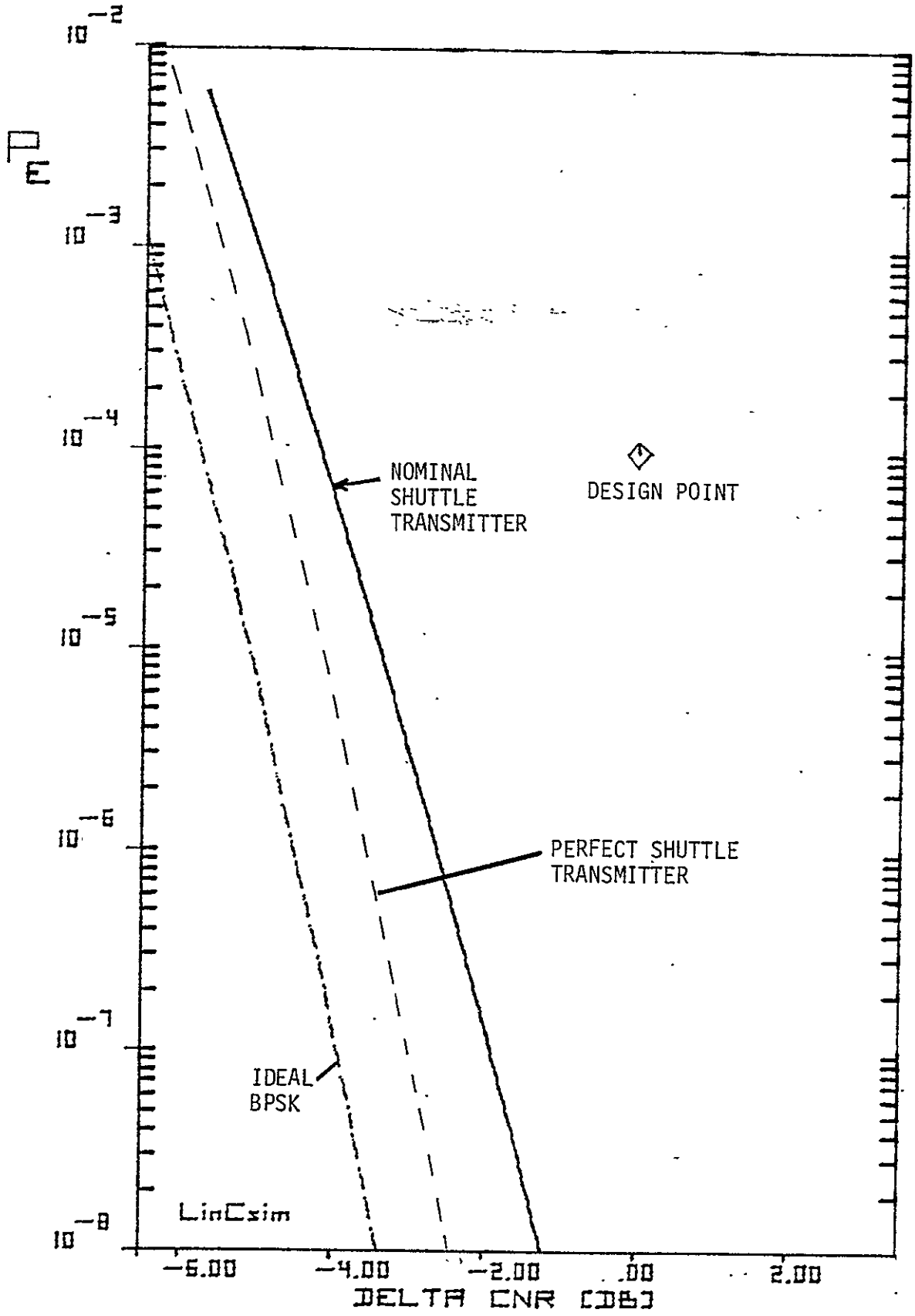


Fig. 1.1. Performance of Shuttle S-Band Return Link.

79 0061

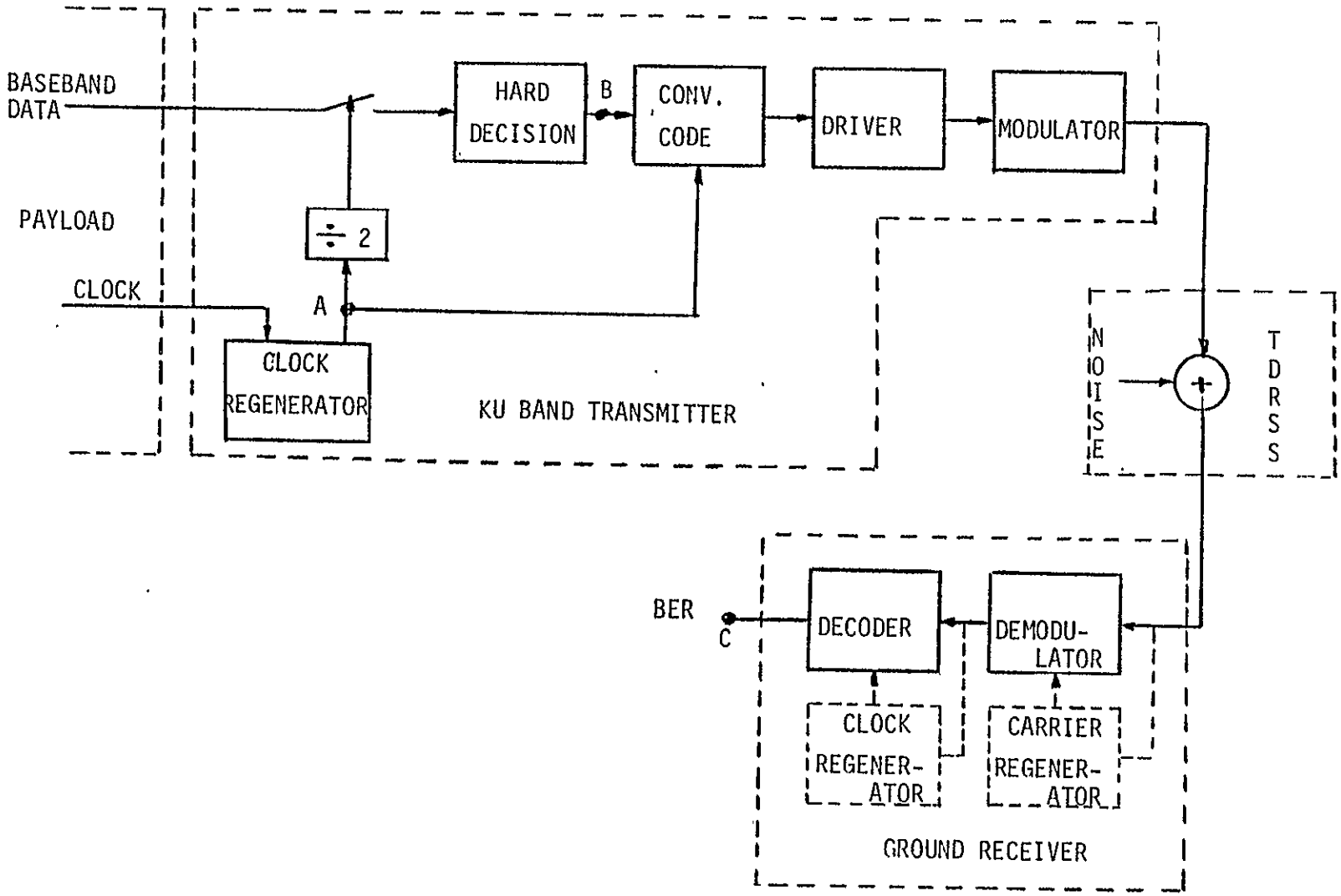


Figure 1.2. Spacelab Return Link Block Diagram.

The effect of bit jitter in the scrubber was analyzed using measured pulse shapes. The results (Fig. 1.3) show that the error rate of the reclocked data is negligible for bit jitter values which can be tolerated on the Shuttle-to-ground link. This holds for the case where the mean sampling instant is in the center of the bit (0% bias in Fig. 1.3) as well as when it is offset by 12.5%, which is the maximum predicted value. It remains then to analyze the effect of the residual bit jitter and of the data asymmetry on the Shuttle-to-ground link performance. The analysis, based on an ideal clock in the ground station receiver, shows that the CNR loss due to 10% data asymmetry amounts to .52 dB for an otherwise perfect signal. The incremental loss due to bit jitter is shown in Table 1.1.

Based on spectral data provided by JSC personnel the clock phase jitter at the scrubber output was estimated to be less than 2%. From Table 1.1 it is then clear that the associated CNR loss is well below .1 dB.

### 1.2.3 Shuttle Bent-Pipe Mode Subcarrier Performance Summary

A typical functional diagram of a detached payload return link is shown in Fig. 1.4. The payload signal is received by the payload processor, converted to baseband, hard-limited and then modulated onto one quadrature component of the K-band return link subcarrier. The recovery of the subcarrier phase from such a signal was investigated and compared with the performance of a similar system, but without the hard-limiter in the interrogator. The results show that both implementations perform adequately over all data rates. Removing the hard-limited improves the tracking performance slightly, however at the expense of reduced power

Figure 1.3. BER PERFORMANCE AT KU BAND ENCODER INPUT (A)

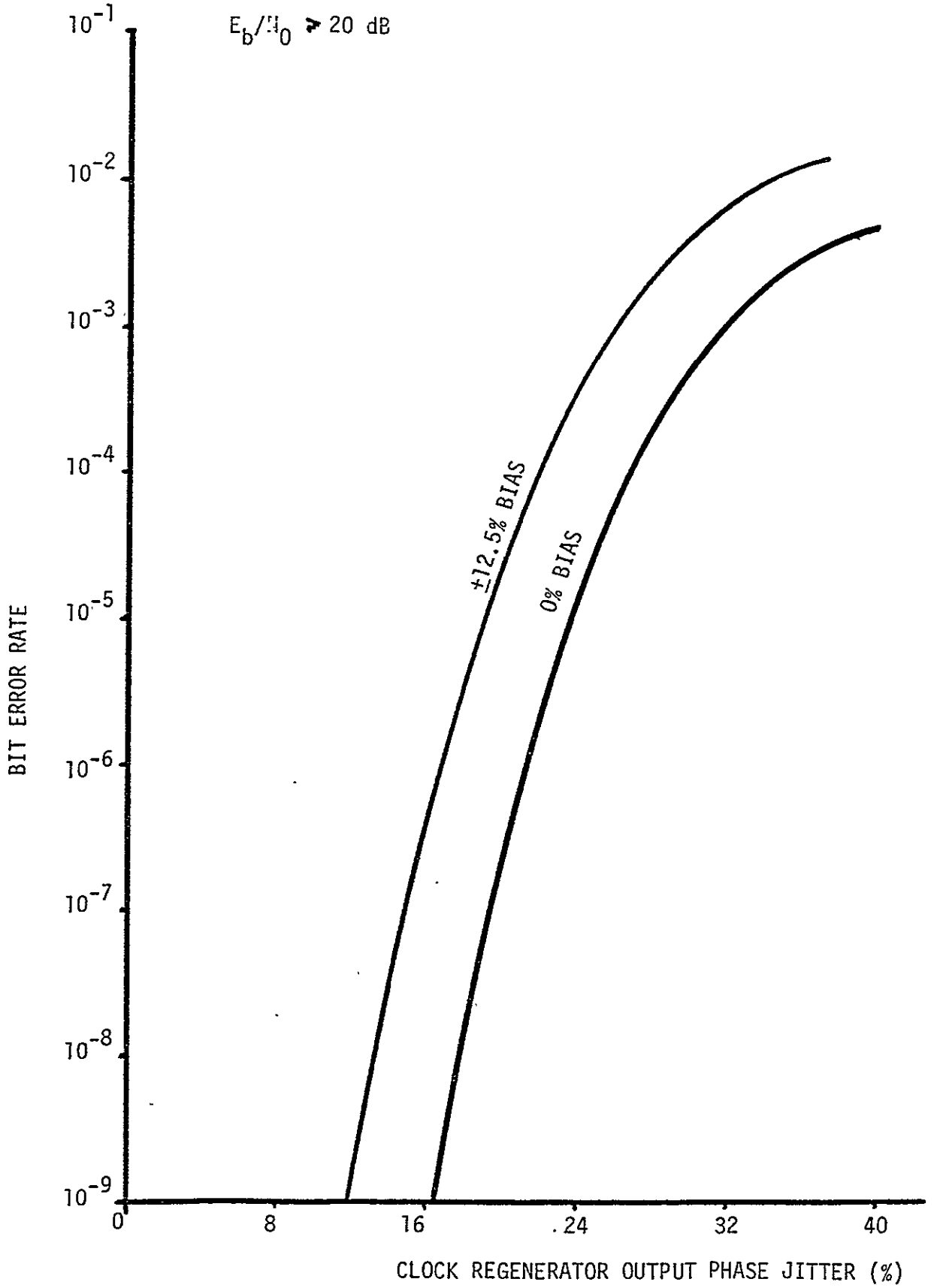


78 3198

Table 1.1. CNR Loss Due to Bit Jitter.

| ΔCNR | Bit Jitter |
|---|---|
| dB | % |
| 0.1 | 5.70 |
| 0.2 | 8.01 |
| 0.3 | 9.75 |
| 0.4 | 11.10 |
| 0.5 | 12.48 |

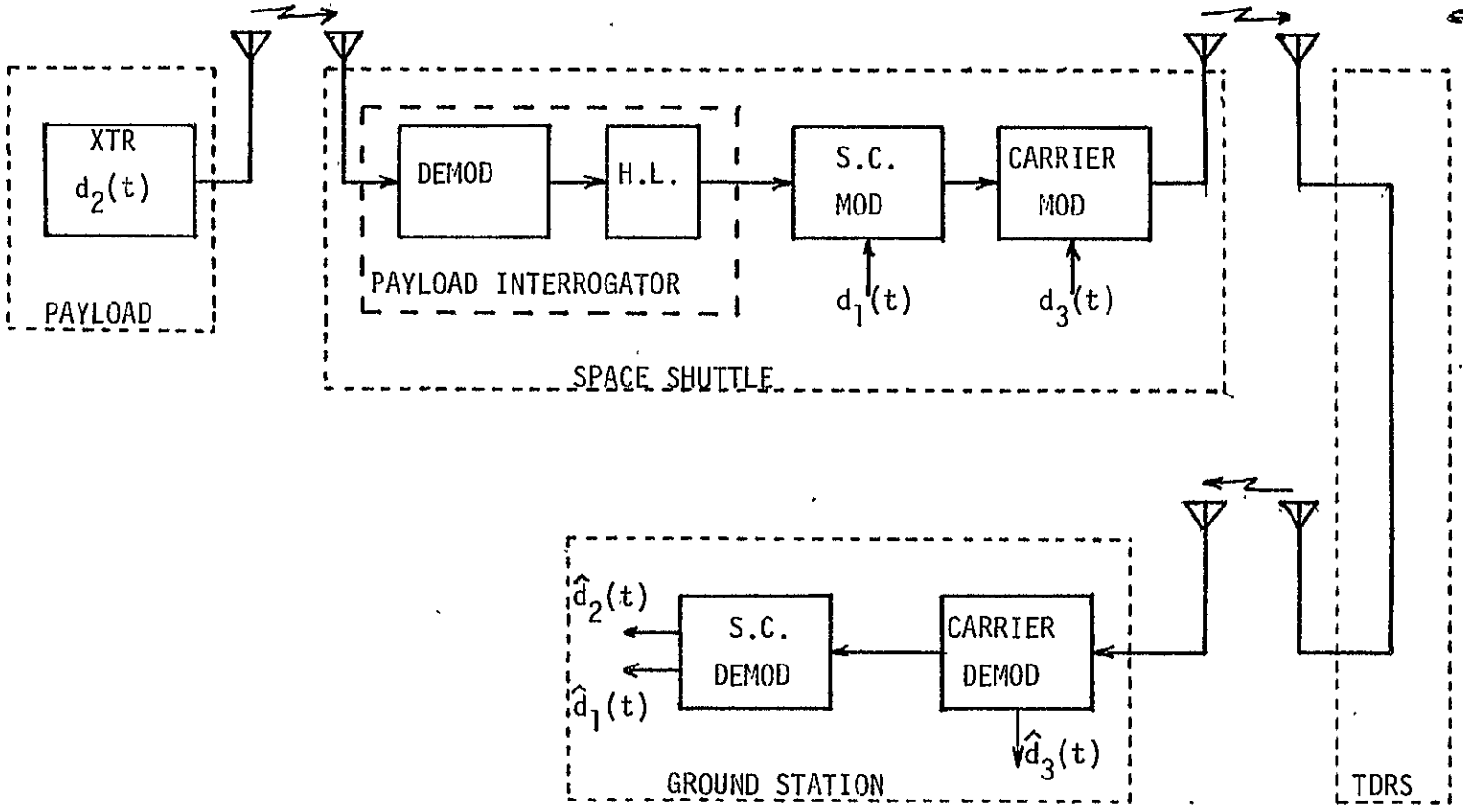


Fig. 1.4. Detached Payload Return Link Block Diagram.

control and hence more crosstalk into the low-rate channel and is therefore not recommended.

The results of our analysis also allow to predict the effect of losing the detached payload signal. With the proper choice for the Costas loop arm filter bandwidths the loop can still track the subcarrier properly. However, if the arm filter bandwidth is less than approximately one fourth of the payload interrogator bandwidth the lock-points of the loop S-curve are shifted by 90 degrees and the channels are interchanged at the detector output.

## 2.0 DESCRIPTION OF LinCsim

### 2.1 Introduction

LinCsim is a software package designed to predict the effect of certain signal distortions in the transmitter (those specified in the TDRSS User's Guide, [1] Table 3-14 as user constraints) on the bit error rate performance of the Shuttle/TDRSS links.

Analytical simulation has been used as the basis for developing a computer simulation model which defines the service performance capability of the TDRSS as a function of the specific subsystem characteristics. The model includes the dynamic effects of the TDRS/ground terminal links and TDRS/Shuttle links. The analytical characterization includes all factors which affect TDRSS services for representative operational conditions. This includes (but is not limited to) the following: channel linear and nonlinear distortions (AM/AM and AM/PM effects, TWT backoff, amplifier limiting), oscillator phase noise sources, additive thermal noise sources, filtering effects in the TDRS and ground station, demodulation and despreading losses for balanced and unbalanced QPSK signals, bit synchronization effects and convolutional coding performance. At present the program has the capability of predicting the bit error rate performance for S-band single access (SSA) and Ku-band single access (KSA) forward and return links. Both coherent and noncoherent turnaround implementations, operating via the hybrid and cross-support tracking modes are available.

The analytical simulation program can be used for several purposes:

(1) To perform a detailed evaluation of several key communication features of the Shuttle services in order to

ensure the consistency of TDRSS and Shuttle user spacecraft transponder performance specifications.

(2) To verify that the TDRSS return link and tracking services are provided without degradation for a Shuttle user with transmitted signal characteristics within the Shuttle user constraints of NASA Specifications [1].

(3) To simulate the full range of permissible Shuttle spacecraft characteristics in order to meet the TDRSS achievable data rate.

(4) As a verification tool of Shuttle spacecraft characteristics with TDRSS operational.

In order to fulfill these purposes the program must accurately model the true signal format, filtering, nonlinear channel effects and any other parameter affecting data transmission or tracking performance. Input and output must be in terms of parameters relevant to the design engineer. In the following we will discuss the models used for the signals and the transmission path and the general set-up of the program. Typical results obtained from LinCsim will be given in Chapter 3.

## 2.2 Link Models

### 2.2.1 Introduction

This chapter presents the models on which the LinCsim computer simulation is based. There is a basic channel model which is general enough to emulate all forward and return services. This generic link model is presented first, followed by channel descriptions for the individual services. To complete the channel definition, a list of the design values of all parameters associated with the link or one

of its subsystems is included. These design values are based on actual system parameter values whenever they are available; otherwise, an estimate was used. The source of each value is indicated.

2.2.2 Channel Model Description

LinCsim is based on a generic channel model which can be modified to fit any particular service (see Sections 2.2.3 and 2.2.4) by specifying the parameters for each subsystem or by bypassing it if necessary. This model is depicted in Figs. 2.1 to 2.3. In Fig. 2.1 $d_1$ and $d_2$ are two binary independent data streams (except for the K-band return link where $d_2$ is a subcarrier with UQPSK modulation). They may be routed through convolutional encoders and NRZ-to-Biphase converters. Then they may be modulated by the independent pseudo-noise sequences $PN_1$, $PN_2$ before they modulate the IF carrier in the modulator. The modulator output is spectrally shaped by the modulator filter. Any linear signal distortions occurring in this part of the transmitter are modeled by a distortion filter. The signal then passes through a high-power amplifier which distorts the signal in a nonlinear fashion. On the uplink, white Gaussian noise is added to the signal.

At the input to the TDRS repeater the signal and noise are filtered. The power level is then adjusted to the specified value. The signal may be combined with other signals in a frequency division multiplex format. A nonlinear TWT amplifier provides the necessary power for the downlink and an output filter limits the transmitted spectrum. At the input to the receiver another white Gaussian noise is added. PN-spread channels are then despread before the carrier phase and bit timing are extracted. The soft-detected bits are

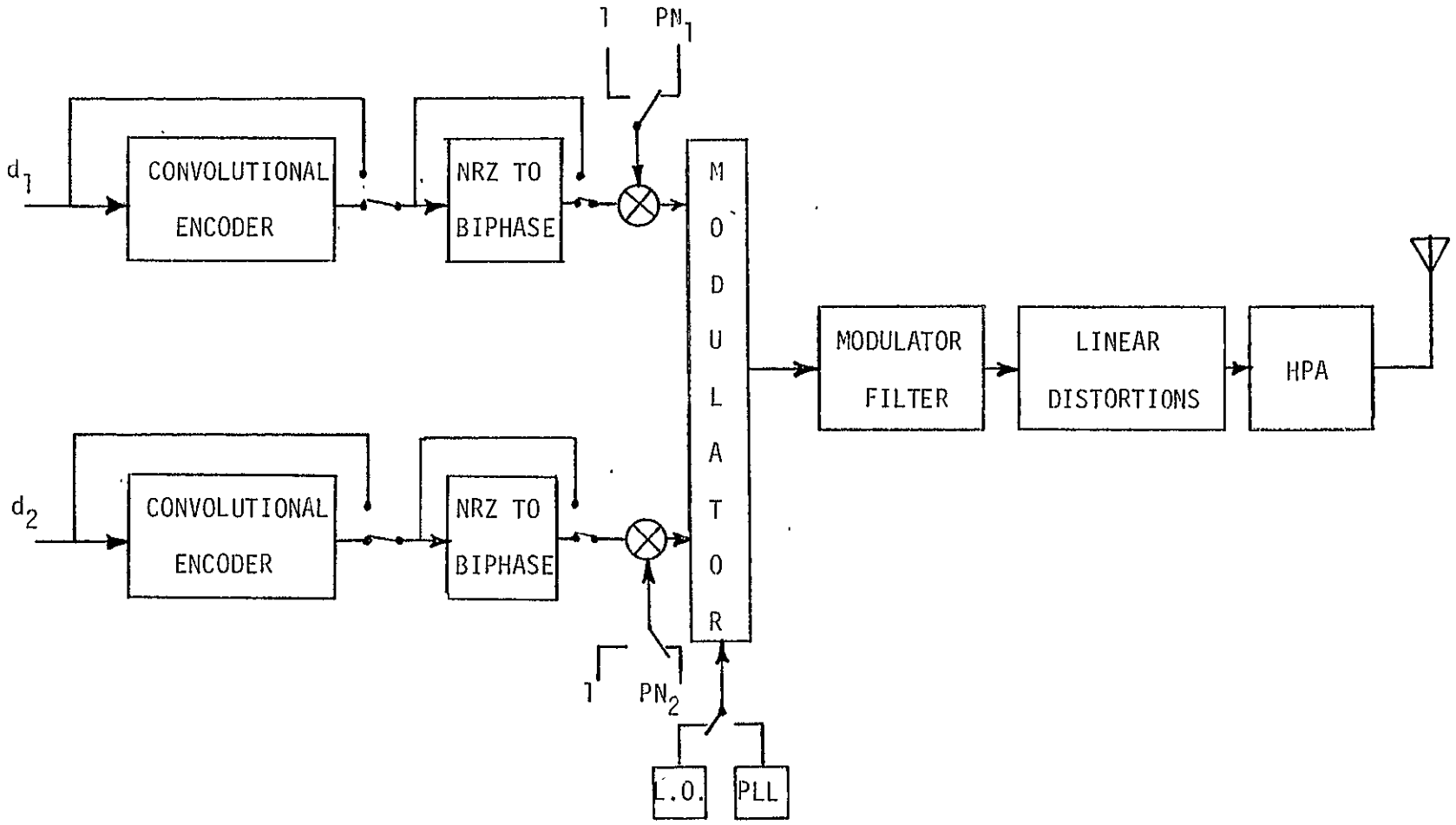


Figure 2.1. Transmitter Model.

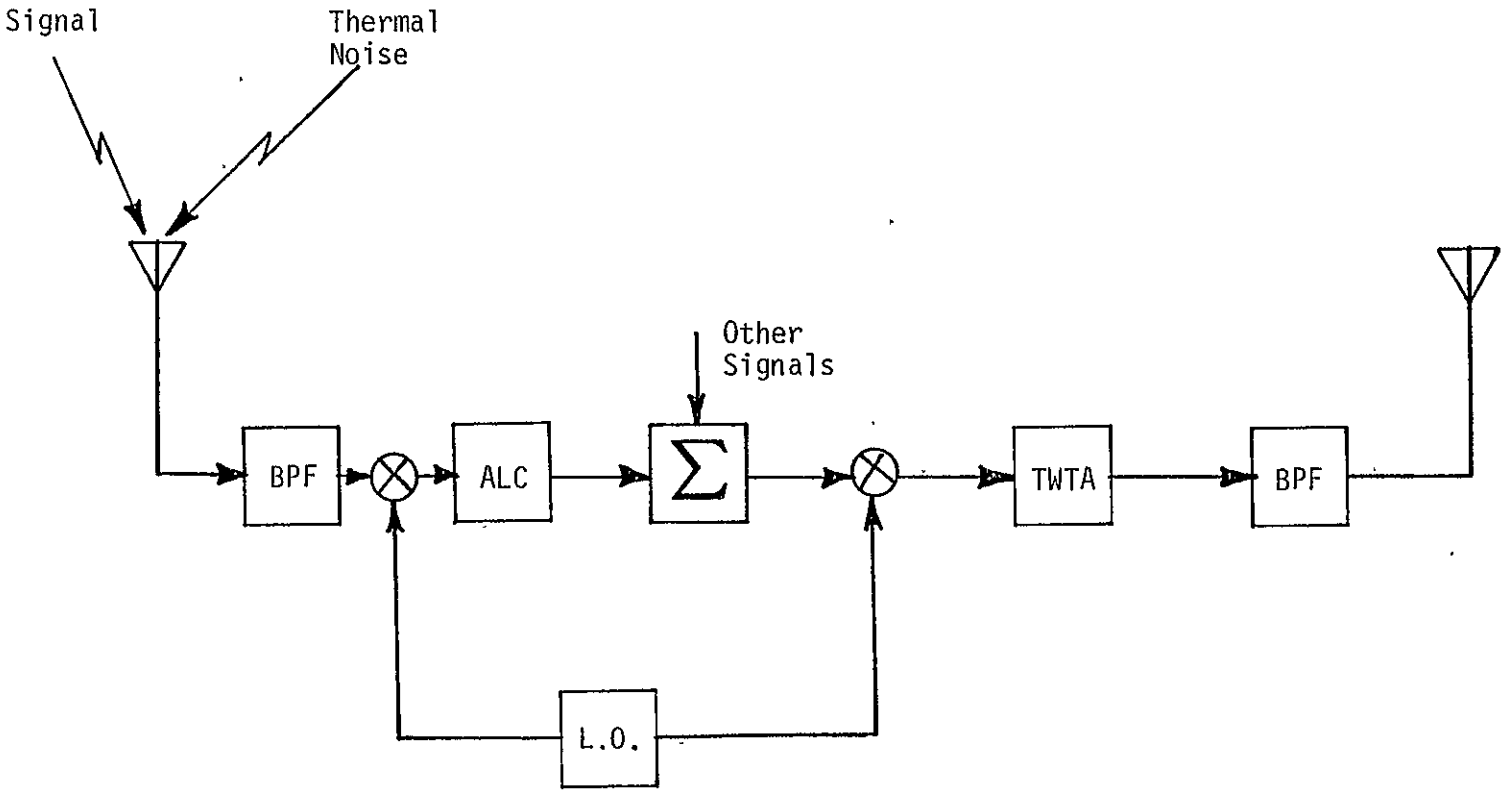


Figure 2.2. TDRS Repeater Model.

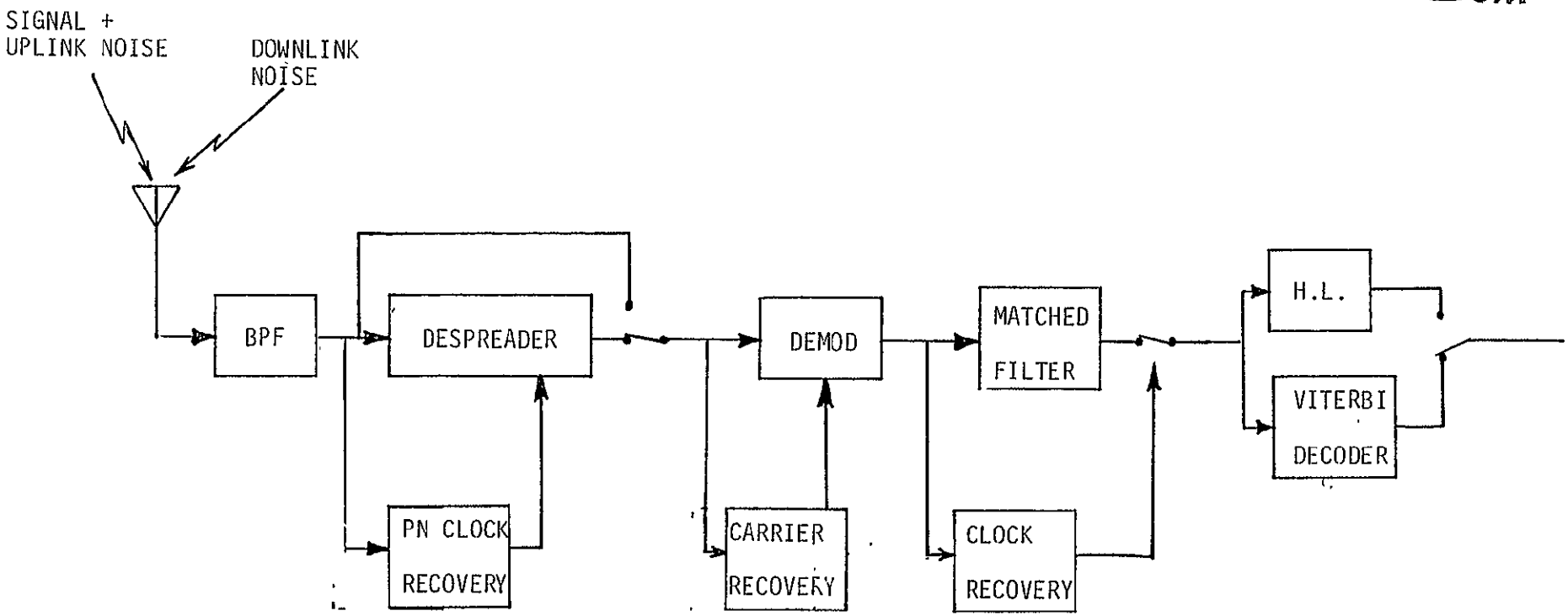


Figure 2.3. Receiver Model.

hardlimited for uncoded data or Viterbi-decoded for coded links.

### 2.2.3 Forward Link Models and Design Values

The models representing the forward service S-band and K-band links are shown in Figs. 2.4 and 2.5, respectively, together with some of the link characteristics. The design values for the parameters defining each one of these models are summarized in Tables 2.1 and 2.2. These values are stored in the program and are used if the operator does not choose to override them.

### 2.2.4 Return Link Models and Design Values

The models for the return link services and their important characteristics are shown in Figs. 2.6 through 2.8. Two different models are defined, one based on a dedicated TWT amplifier (i.e., not shared with other signals), the other assuming a shared TWT amplifier (composite link model). For the K-band link these models correspond to the dedicated and composite links, respectively. For the S-band link the dedicated link model is included to provide a means of assessing the degradation due to the intermodulation effects in the nonlinear amplifier. The two models are discussed in more detail in Section 2.2.5.

The design values for all parameters of the return links are summarized in Tables 2.3 and 2.4. Just as for the forward links, these are the default parameter values stored in the program.

### 2.2.5 Dedicated vs Composite Channel Model for the S-band Return Link

The S-band dedicated link model is provided as a tool to estimate the effects of crosstalk generated in the shared nonlinear TDRS amplifier on the bit error rate. To allow such a comparison the two

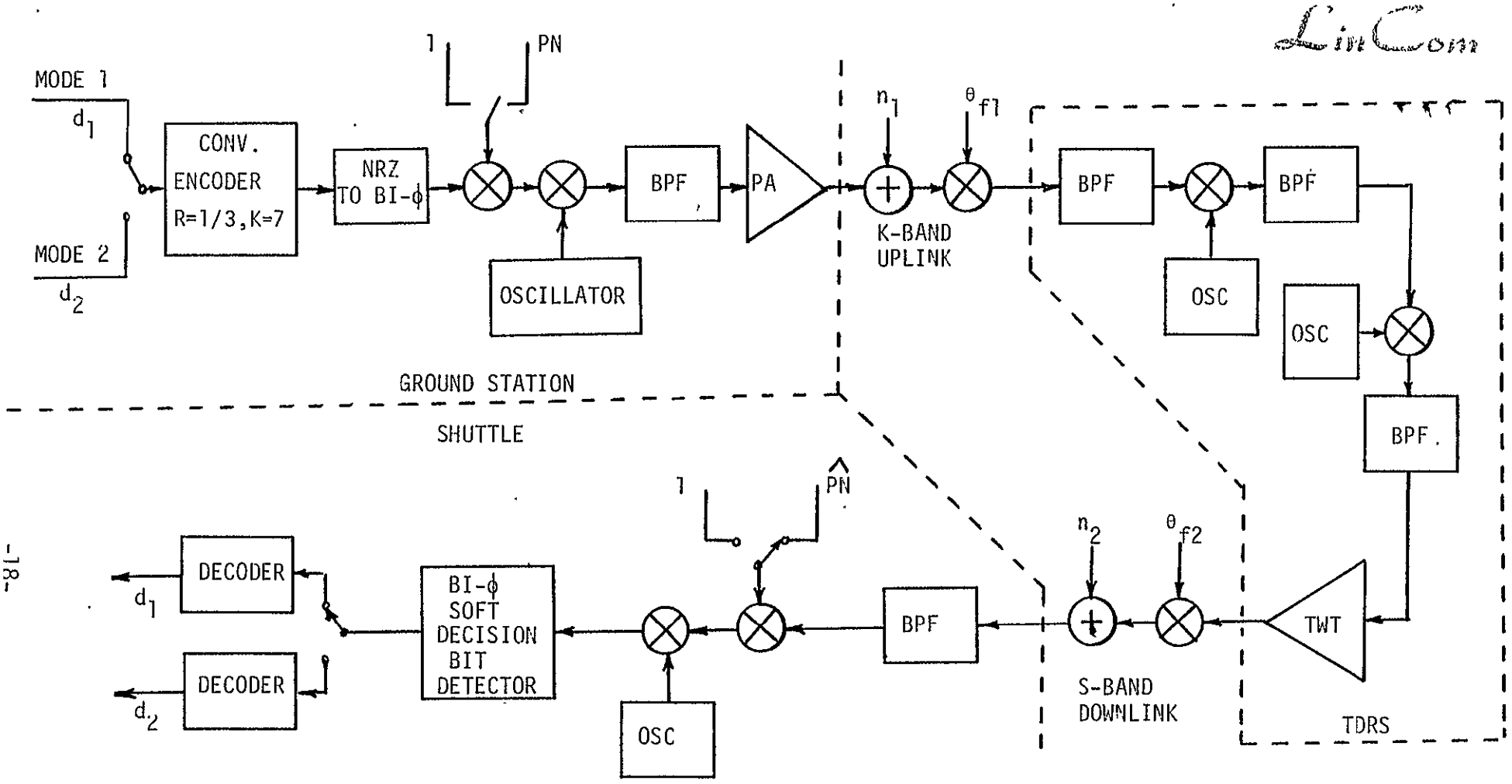


Fig. 2.4. S-Band Shuttle Forward Link

Data Rate: Mode 1: 32 Kbps
Mode 2: 72 Kbps

PN Chip Rate: 11.232 M chips/sec

PN Code Length: 1023 chips

Carrier Modulation: PSK$\pm\pi/2$ radians

Table 2.1 PARAMETER DESIGN VALUES FOR BER PROGRAM - SHUTTLE FORWARD LINK SSA

| PARAMETER | PRESENT VALUE | WHERE OBTAINED | DATE OBTAINED | OLD VALUE | SOURCE OLD VALUE |
|---|---|---|---|---|---|
| | | | | | |
| DATA RATE | 72 Kb/sec | Harris PDR | 3/30/78 | 72 Kb/sec | S-805-1 |
| POWER SPLIT | | | | 1: 0 | S-805-1 |
| MODULATOR PHASE IMBALANCE (BPSK) | ±3° | Harris PDR | 3/30/78 | ± 3° | S-805-1 |
| REL. PHASE BETWEEN I&Q CHANNELS | ±3° peak | Harris PDR | 3/30/78 | ±3° peak | S-805-1 |
| DATA ASYMMETRY | ±3% | Harris PDR | 3/30/78 | +3% peak | S-805-1 |
| PN ASYMMETRY | < 1% | Harris PDR | 3/30/78 | ±1% peak | S-805-1 |
| DATA SKEW | -- | -- | -- | N/A | -- |
| PN SKEW | < 1% | Harris PDR | 3/30/78 | N/A | S-805-1 |
| MODULATOR GAIN IMBALANCE | ±0.25 dB | Harris PDR | 3/30/78 | ±0.25 dB peak | S-805-1 |
| XTR GAIN FLATNESS | | | | ±0.8 dB peak | S-805-1 |
| XTR GAIN SLOPE | .3dB/ MHz | Harris PDR | 3/30/78 | ±.1dB/MHz peak | S-805-1 |
| XTR PHASE NON-LINEARITY | 3° | Harris PDR | 3/30/78 | ±8.6°peak/7MHz | S-805-1 |
| XT FILTER BW | | | | 4.5 MHz | LinCom estimate |
| XT FILTER ORDER | | | | 4 | LinCom estimate |
| XT FILTER RIPPLE | | | | 0.1 dB | LinCom estimate |
| XTR AM/AM | | | | 1 dB / dB | LinCom estimate |
| XTR AM/PM | < 4° dB | Harris PDR | 3/30/78 | 3° | LinCom estimate |
| TDRS TWT MAX AM/PM | 10°/dB | TPM | 3/78 | 10°/dB | LinCom estimate |
| TDRS TWT AM/AM | | | | 0.2 dB/dB | LinCom estimate |
| TDRS TWT AM/PM | 6°/dB | TPM | 3/78 | 6°/dB | LinCom estimate |
| TDRS FRONT END FILTER BW | 20 MHz | Harris PDR | 3/30/78 | 20 MHz | Wu Proposal 7/76 |
| ORDER | | | | 4 | LinCom estimate |
| RIPPLE | | | | 0.1 | LinCom estimate |
| TDRS TRANSMIT FILTER BW | | | | 4.5 MHz | LinCom estimate |
| ORDER | | | | 2 | LinCom estimate |
| RIPPLE | | | | 0.2 | LinCom estimate |
| PN TIMING OFFSET | | | | 1% | LinCom estimate |
| PN TIMING JITTER | | | | 1% peak | S-805-1 |
| DATA TIMING OFFSET | | | | 1% | LinCom estimate |
| DATA TIMING JITTER | | | | 1% peak | S-805-1 |

Table 2.1. PARAMETER DESIGN VALUES FOR BER PROGRAM - SHUTTLE FORWARD LINK SSA

| PARAMETER | PRESENT VALUE | WHERE OBTAINED | DATE OBTAINED | OLD VALUE | SOURCE OLD VALUE |
|---|---|---|---|---|---|
| | LINK BUDGET | | | | |
| XTR EIRP: UNCODED DATA | -- | -- | -- | -- | -- |
| XTR EIRP.: CODED DATA | 71.1 dBW | Harris PDR | 3/30/78 | 71.1 dB | WU Proposal, 7 |
| SPACE LOSS | | | | 208.1 | WU Proposal, 7 |
| POLARIZATION LOSS | | | | 0.1 dB | WU Proposal, 7 |
| ATMOSPHERIC LOSS | | | | 0.8 dB | WU Proposal, 7 |
| TDRS G/T | | | | 10. dB/°K | WU Proposal, 7 |
| TDRS TWT MAX OUTPUT POWER | 14.11 dBW | TPM | 3/78 | 14.1 dBW | WU Proposal, 7 |
| TDRS TWT OUTPUT BACKOFF | | | | 0 | LinCom estimat |
| POWER ALLOCATION | 0 dBW | TPM | 3/78 | 0 dBW | LinCom estimat |
| CHANNEL POWER | 14.11 dBW | TPM | 3/78 | 14.1 dBW | LinCom estimat |
| TDRS HARDWARE LOSS | | | | 3.0 dB | LinCom estimat |
| TDRS ANTENNA GAIN | | | | 35.4 dB | WU Proposal,7/ |
| POINTING LOSS | | | | 0.5 | TDRSS Users Gu |
| SPACE LOSS | 191.4 | SS Circ Marg | 1/77 | 191.6 | TDRSS Users Gu |
| POLARIZATION LOSS | | | | 0.5 | TDRSS Users Gu |
| ATMOSPHERIC LOSS | | | | 0 | SS RF Circuit M |
| RX ANTENNA G/T | | | | -30.1 | SS RF Circuit M |
| | PHASE NOISE BUDGET | | | | |
| T OSCILLATORS 1-10 Hz | | | | 1.5° rms | S-805-1 |
| 10 to 32 Hz | | | | 1.5° rms | S-805-1 |
| 32 Hz to 1 KHz | | | | 4° rms | S-805-1 |
| 1 KHz to 6 MHz | | | | 2° rms | S-805-1 |
| TDRS OSCILLATORS | | | | 3° rms | S-805-1 |
| X Oscillators | | | | 1.4 | S-805-1 |
| X CARRIER TRACK-NG LOOP - STATIC HASE ERROR | | | | 3° | LinCom estimate |
| BANDWIDTH | | | | 32 Hz | LinCom estimate |
| DAMPING | | | | 2 | LinCom estimate |
| SQUARING LOSS | | | | 2 dB | LinCom estimate |

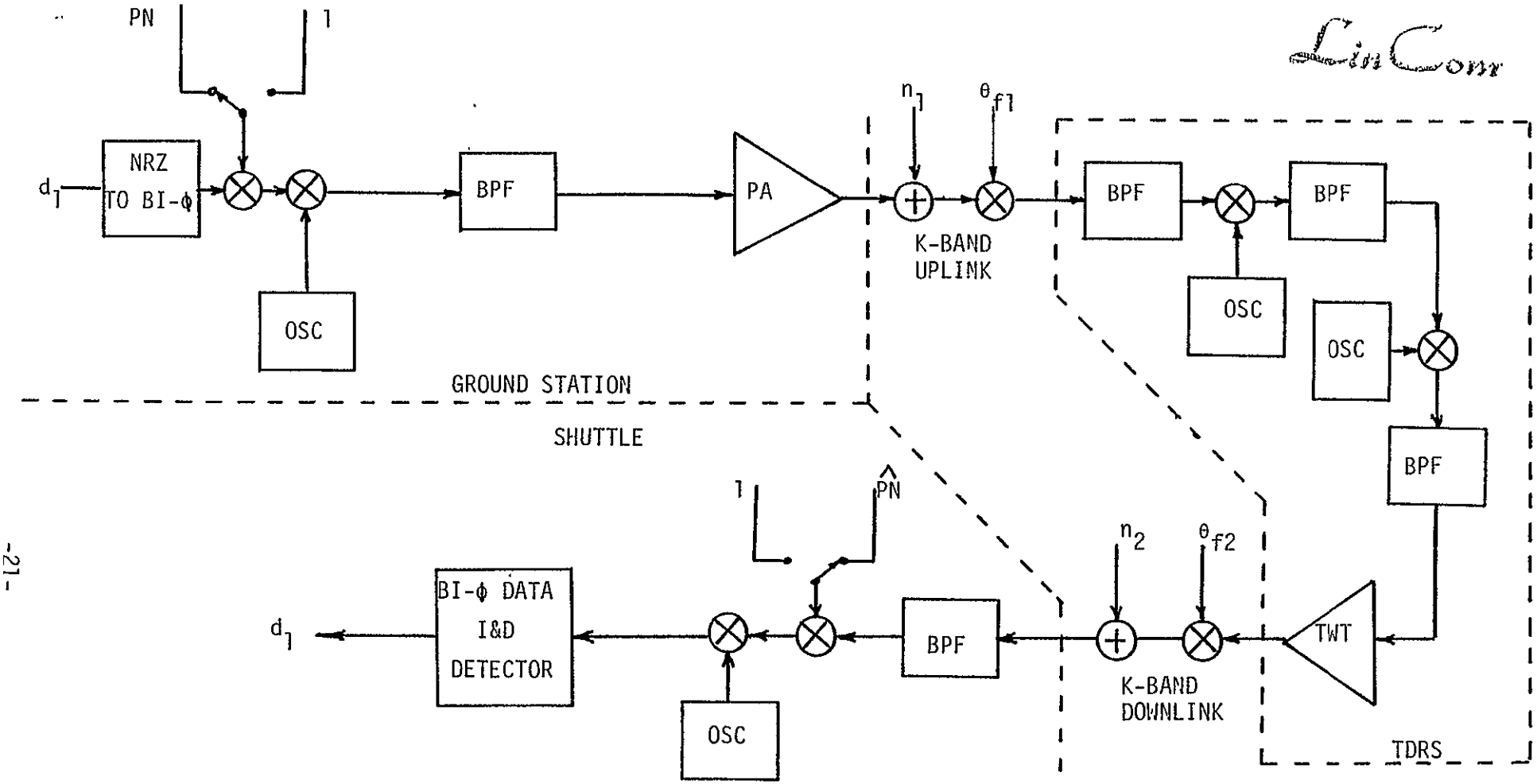


Fig. 2.5. Shuttle Ku-Band Forward Link

Data Rate: 216 Kbps (Mode 1)/72 Kbps (Mode 2)

PN Code: $PN_{f1}$: $(2^{10}-1)$ Chip Gold Code

PN Chip Rate: 3 Mcps

Table 2.2. PARAMETER DESIGN VALUES FOR BER PROGRAM - SHUTTLE FORWARD LINK KSA

| PARAMETER | PRESENT VALUE | WHERE OBTAINED | DATE OBTAINED | OLD VALUE | SOURCE OLD VALUE |
|---|---|---|---|---|---|
| | | | | | |
| TA RATE | | | | 216 Kb/sec | SSO ICD/IRN |
| WER SPLIT | | | | 1: 0 | SSO ICD/IRM |
| DULATOR PHASE BALANCE (BPSK) | ±3° | Harris PDR | 3/30/78 | ±3° peak | S-805-1 |
| L. PHASE BE-EEN I&Q CHANNELS | ±3° | Harris PDR | 3/30/78 | | S-805-1 |
| TA ASYMMETRY | ±3% | Harris PDR | 3/30/78 | ±3° | S-805-1 |
| ASYMMETRY | 1% | Harris PDR | 3/30/78 | 1% | S-805-1 |
| TA SKEW | -- | -- | -- | N/A | -- |
| SKEW | | | | N/A | S-805-1 |
| DULATOR GAIN BALANCE | ±0.75 dB | Harris PDR | 3/30/78 | 0.25 dB peak | S-805-1 |
| R GAIN FLATNESS | | | | 0.8 dB peak | S-805-1 |
| R GAIN SLOPE | ±.3dB/MHz | Harris PDR | 3/30/78 | 0.1dB/MHz | S-805-1 |
| R PHASE NON-NEARITY | 3° | Harris PDR | 3/30/78 | 8.6° | S-805-1 |
| FILTER BW | 40 MHz | Harris PDR | 3/30/78 | 50 MHz | LinCom estimate |
| FILTER ORDER | | | | 4 | LinCom estimate |
| FILTER RIPPLE | | | | 0.1 dB | LinCom estimate |
| R AM/AM | | | | 1 dB/dB | LinCom estimate |
| R AM/PM | 7°/dB | Harris PDR | 3/30/78 | 3°/dB | LinCom estimate |
| RS TWT MAX AM/PM | 7.2°/dB | TPM | 3/78 | 10°/dB | LinCom estimate |
| RS TWT AM/AM | 0.9 dB | TPM | 3/78 | 0.2dB/dB | LinCom estimate |
| RS TWT AM/PM | | | | 6°/dB | LinCom estimate |
| RS FRONT END TER BW | 50 MHz | TPM | 3/78 | 50 MHz | WU Proposal, 7/76 |
| ORDER | | | | 4 | LinCom Estimate |
| RIPPLE | | | | 0.1 dB | LinCom estimate |
| RS TRANSMIT TER BW | | | | 60 MHz | LinCom estimate |
| ORDER | | | | 2 | LinCom estimate |
| RIPPLE | | | | 0.2 dB | LinCom estimate |
| TIMING OFFSET | | | | 1% | LinCom estimate |
| TIMING JITTER | | | | 1% peak | S-805-1 |
| TA TIMING OFFSET | | | | 1% | LinCom estimate |
| TA TIMING JITTER | | | | 1% peak | S-805-1 |

Table 2.2 .PARAMETER DESIGN VALUES FOR BER PROGRAM - SHUTTLE FORWARD LINK KSA

| PARAMETER | PRESENT VALUE | WHERE OBTAINED | DATE OBTAINED | OLD VALUE | SOURCE OLD VALUE |
|---|---|---|---|---|---|
| | LINK BUDGET | | | | |
| XTR EIRP: UNCODED DATA | 75.9 dBW | Harris PDR | 3/30/78 | 75.9 dBW | WU Proposal, 7/ |
| XTR EIRP: CODED DATA | -- | -- | -- | -- | -- |
| SPACE LOSS | | | | 208.4 dB | WU Proposal, 7/7 |
| POLARIZATION LOSS | | | | 0.1 dB | WU Proposal, 7/7 |
| ATMOSPHERIC LOSS | | | | 0.8 dB | WU Proposal, 7/7 |
| TDRS G/T | | | | 10 dB/°K | WU Proposal, 7/7 |
| TDRS TWT MAX OUTPUT POWER | 2.16dBW (spec) | TPM | 3/78 | 1.8 dBW | WU Proposal, 7/7 |
| TDRS TWT OUTPUT BACKOFF | 0 dB | TPM | 3/78 | 0 dBW | LinCom Estimate |
| POWER ALLOCATION | 0 dB | TPM | 3/78 | 0 dB | TDRSS Users Guide |
| CHANNEL POWER | 2.16 dBW | TPM | 3/78 | 0 dB | TDRS Users Guide |
| TDRS HARDWARE LOSS | 1.68 dBW | TPM | 3/78 | 1 dB | TDRS Users Guide |
| TDRS ANTENNA GAIN | 51.85dBW | TPM | 3/78 | 52 dB | TDRS Users Guide |
| POINTING LOSS | | | | 0.7 dB | TDRSS Users Guide |
| SPACE LOSS | | | | 207.7 dB | TDRSS Users Guide |
| POLARIZATION LOSS | | | | 0.3 dB | TDRSS Users Guide |
| ATMOSPHERIC LOSS | | | | 0 dB | TDRSS Users Guide |
| RX ANTENNA G/T | | | | 5.3 dB/°K | TDRSS Users Guide |
| | PHASE NOISE BUDGET | | | | |
| XT OSCILLATORS 1 to 10 Hz | | | | 1.5° rms | S-805-1 |
| 10 to 32 Hz | | | | 1.5° rms | S-805-1 |
| 32 Hz to 1 KHz | | | | 4.0° rms | S-805-1 |
| 1 KHz to 25MHz | | | | 2.0° rms | S-805-1 |
| TDRS OSCILLATORS | | | | 3° | S-805-1 |
| RX OXCILLATORS | | | | 2.8° | S-805-1 |
| RX CARRIER TRACKING LOOP | | | | | |
| STATIC PHASE ERROR | | | | 3° | LinCom estimate |
| BANDWIDTH | | | | 110 Hz | TRW, 8/77 |
| DAMPING | | | | 2 | LinCom estimate |
| SQUARING LOSS | | | | 2 dB | LinCom estimate |

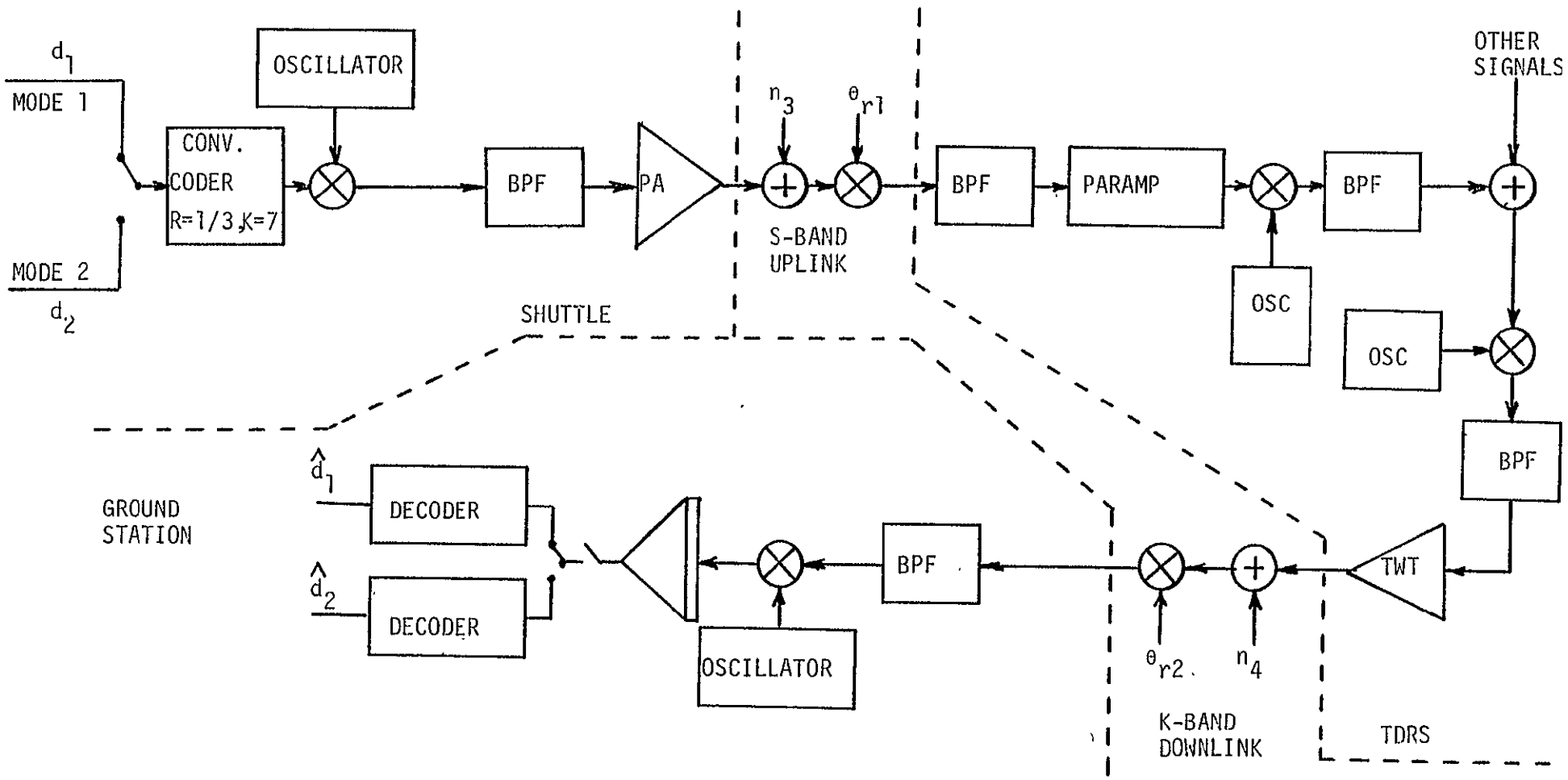


Fig. 2.6. S-Band Shuttle Return Link Model for Data Transmission.

Data Rates: Mode 1: 96 Kbps
Mode 2: 192 Kbps

PN Code: Not Applicable

Convolution Coding: Data Coded in Both Mode 1 & Mode 2

Data Decoding: Rate 1/3, Constraint Length 7

Carrier Modulation: Bi-$\phi$ L Symbols PSK Modulate the Carrier $\pm\pi/2$ Radians

78 0234

Table 2.3. PARAMETER DESIGN VALUES FOR BER PROGRAM - SHUTTLE RETURN LINK SSA.

| PARAMETER | PRESENT VALUE | WHERE OBTAINED | DATE OBTAINED | OLD VALUE | SOURCE OLD VALUE |
|---|---|---|---|---|---|
| DATA RATE - I | | | | 192 Kbps | S-805-1 |
| DATA RATE - Q | | | | 0 | S-805-1 |
| POWER SPLIT | | | | 1:0 | S-805-1 |
| MODULATOR PHASE IMBALANCE (BPSK) | 11° | JSC | 11/78 | ±3° | S-805-1 |
| REL. PHASE BETWEEN I&Q CHANNELS | | | | N/A | S-805-1 |
| DATA ASYMMETRY | 3.8% | JSC | 11/78 | ±3% | S-805-1 |
| PN ASYMMETRY | | | | N/A | S-805-1 |
| DATA SKEW | | | | N/A | S-805-1 |
| PN SKEW | | | | N/A | S-805-1 |
| MODULATOR GAIN IMBALANCE | .1 dB | JSC | 11/78 | ±0.25 dB | S-805-1 |
| XTR GAIN FLATNESS | .4 dB | JSC | 11/78 | ±0.3 dB | S-805-1 |
| XTR GAIN SLOPE | | | | ±0.1dB/MHz | S-805-1 |
| XTR PHASE NON-LINEARITY | | | | ±3° | S-805-1 |
| XT FILTER BW | 100 MHz | JSC | 11/78 | 1.2 MHz | S-805-1 |
| XT FILTER ORDER | | | | 4 | LinCom estimate |
| XT FILTER RIPPLE | | | | 0.1 dB | LinCom estimate |
| XTR AM/AM | | | | 1 dB/dB | LinCom estimate |
| XTR AM/PM | 14°/dB | JSC | 11/78 | 12°/dB | S-805-1 |
| TDRS TWT MAX AM/PM | | | | 10°/dB | LinCom estimate |
| TDRS TWT AM/AM | | | | 0 dB/dB | LinCom estimate |
| TDRS TWT AM/PM | | | | 6°/dB | LinCom estimate |
| TDRS FRONT END FILTER BW | | | | 10 MHz | LinCom estimate |
| ORDER | | | | 4 | LinCom estimate |
| RIPPLE | | | | 0.1 dB | LinCom estimate |
| TDRS TRANSMIT FILTER BW | | | | 621 MHz | LinCom estimate |
| ORDER | | | | 2 | LinCom estimate |
| RIPPLE | | | | 0.2 dB | LinCom estimate |
| PN TIMING OFFSET | | | | 1% | LinCom estimate |
| PN TIMING JITTER | | | | 1% peak | S-805-1 |
| DATA TIMING OFFSET | | | | 1% | LinCom estimate |
| DATA TIMING JITTER | 6% | JSC | 11/78 | 1% peak | S-805-1 |

Table 2.3. PARAMETER DESIGN VALUES FOR BER PROGRAM - SHUTTLE RETURN LINK SSA

| PARAMETER | PRESENT VALUE | WHERE OBTAINED | DATE OBTAINED | OLD VALUE | SOURCE OLD VALUE |
|---|---|---|---|---|---|
| | LINK BUDGET | | | | |
| XTR EIRP: UNCODED DATA | | | | | |
| XTR EIRP: CODED DATA | 16.7 dBW | JSC | 3/78 | 15.2 dBW | SS Circuit Margin, |
| SPACE LOSS | | | | 192.1 dB | SS Circuit Margin, 1/77 |
| POLARIZATION LOSS | | | | 0.5 dB | SS Circuit Margin, 1/77 |
| ATMOSPHERIC LOSS | | | | 0 dB | SS Circuit Margin, 1/77 |
| TDRS G/T | 9.55(nominal) | TPM | 3/78 | 8.3 dB/°K | SS Circuit Margin, 1/77 |
| TDRS TWT MAX OUTPUT POWER | 13.4 dB | TPM | 3/78 | 12.5 dBW | WU Proposal, 7/76 |
| TDRS TWT OUTPUT BACKOFF | 2.0 dB | TPM | 3/78 | 2.0 dB | WU Proposal, 7/76 |
| POWER ALLOCATION | -10.0 dB | TPM | 3/78 | -9.9 dB | WU Proposal, 7/76 |
| CHANNEL POWER | 1.4 dBW | TPM | 3/78 | 0.6 dBW | WU Proposal, 7/76 |
| TDRS HARDWARE LOSS | 2.46dB | TPM | 3/78 | 1.7 dB | WU Proposal, 7/76 |
| TDRS ANTENNA GAIN | 45.90dB | TPM | 3/78 | 41.3 dB | WU Proposal, 7/76 |
| POINTING LOSS | 0.65dB | TPM | 3/78 | 0.7 dB | WU Proposal, 7/76 |
| SPACE LOSS | | | | 207.7 dB | WU Proposal, 7/76 |
| POLARIZATION LOSS | | | | 0.1 dB | WU Proposal, 7/76 |
| ATMOSPHERIC LOSS | | | | 0.8 dB | WU Proposal, 7/76 |
| RX ANTENNA G/T | | | | 40.3 dB/°K | WU Proposal, 7/76 |
| | PHASE NOISE BUDGET | | | | |
| OSC, COHERENT RNAROUND | | | | | |
| to 10 Hz | | | | 1° rms | S-805-1 |
| 0 Hz to 1 kHz | | | | 1° rms | S-805-1 |
| kHz to 6 MHz | | | | 1° rms | S-805-1 |
| OSC NONCOHERENT RNAROUND | | | | | |
| to 10 Hz | | | | 2° rms | S-805-1 |
| 0 to 100 Hz | | | | 1° rms | S-805-1 |
| 00 Hz to 1 kHz | 10° rms | JSC | 11/78 | 1° rms | S-805-1 |
| kHz to 6 MHz | | | | 1° rms | S-805-1 |
| RS OSCILLATORS | 3.2° rms | TPM | 3/78 | 3° | S-805-1 |
| OSCILLATORS | | | | 1° | S-805-1 |
| CARRIER TRACKING OP | | | | | |
| TATIC PHASE ERROR | | | | 3° | LinCom Estimate |
| NDWIDTH | | | | 40 Hz | TRW, 8/77 |
| MPING | | | | 2 | LinCom Estimate |
| QUARING LOSS | | | | DG1: 2 dB<br>DG2: 8 dB | LinCom Estimate |

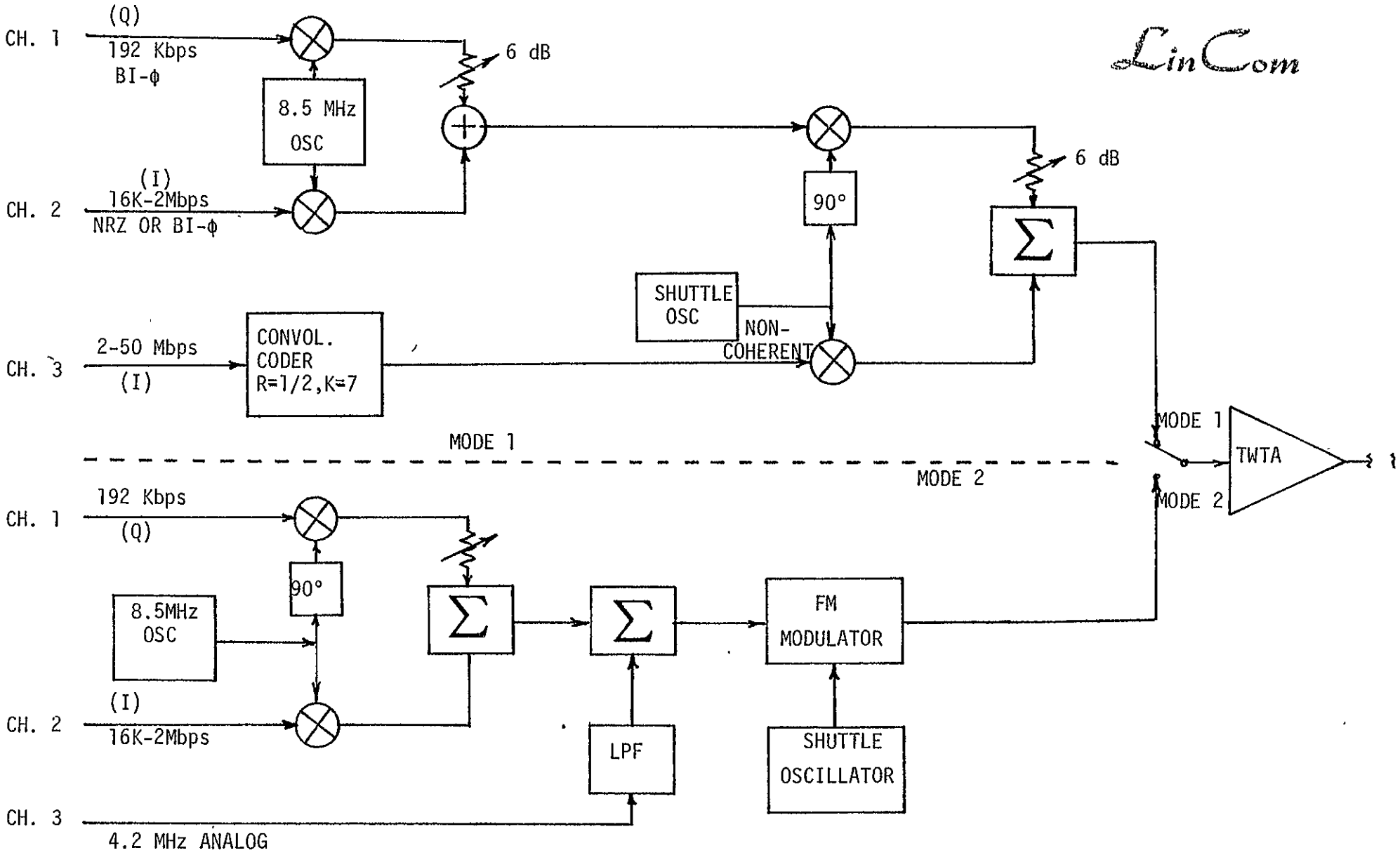


Fig. 2.7. K-Band Shuttle Return Transmitter.

Data Rates: Mode 1

I Channel (Carrier QDSB) 4-50 Mbps

FM: Mode 2

Bandwidth (Predetection) 50 MHz

Table 2.4 PARAMETER DESIGN VALUES FOR BER PROGRAM - SHUTTLE RETURN LINK KSA

LinCom

| PARAMETER | PRESENT VALUE | WHERE OBTAINED | DATE OBTAINED | OLD VALUE | SOURCE OLD VALUE |
|---|---|---|---|---|---|
| ATA RATE - I Ch.1<br>Ch.2<br>Ch.3 | | | | 192 Kb/s<br>2 Mb/s<br>50 Mb/s | S-805-1 |
| OWER SPLIT | | | | 20:-4: 1 | S-805-1 |
| ODULATOR PHASE BALANCE (BPSK) | | | | ±3° | S-805-1 |
| EL. PHASE BE-EEN I&Q CHANNELS | | | | ±3° | S-805-1 |
| TA ASYMMETRY | | | | ±3% | S-805-1 |
| ASYMMETRY | | | | N/A | S-805-1 |
| TA SKEW | | | | N/A | S-805-1 |
| SKEW | | | | N/A | S-805-1 |
| DULATOR GAIN BALANCE | | | | ±0.25 dB | S-805-1 |
| R GAIN FLATNESS | | | | ±0.3 dB | S-805-1 |
| R GAIN SLOPE | | | | ±0.1dB/MHz | S-805-1 |
| R PHASE NON-NEARITY | | | | ±3° | S-805-1 |
| FILTER BW | | | | 225 MHz | LinCom Estimate |
| FILTER ORDER | | | | 4 | LinCom estimate |
| FILTER RIPPLE | | | | 0.1 | LinCom estimate |
| R AM/AM | | | | 1 dB/dB | LinCom estimate |
| R AM/PM | | | | 12°/dB | S-805-1 |
| RS TWT MAX AM/PM | | | | 10°/dB | LinCom estimate |
| RS TWT AM/AM | | | | 0 dB/dB | LinCom estimate |
| RS TWT AM/PM | | | | 6°/dB | LinCom estimate |
| RS FRONT END TER BW | | | | 225 MHz | WU Proposal, 7/76 |
| ORDER | | | | 4 | LinCom estimate |
| RIPPLE | | | | 0.1 | LinCom estimate |
| RS TRANSMIT TER BW | | | | 225 MHz | LinCom estimate |
| ORDER | | | | 4 | LinCom estimate |
| RIPPLE | | | | 0.2 | LinCom estimate |
| TIMING OFFSET | | | | ±1% | LinCom estimate |
| TIMING JITTER | | | | 1%peak | S-805-1 |
| A TIMING OFFSET | | | | 1% | LinCom estimate |
| A TIMING JITTER | | | | 1% peak | S-805-1 |

| PARAMETER | PRESENT VALUE | WHERE OBTAINED | DATE OBTAINED | OLD VALUE | SOURCE OLD VALUE |
|---|---|---|---|---|---|
| | LINK BUDGET | | | | |
| | | | | | |
| XTR EIRP | | | | 48.1 dBW | SSRF Circuit Ma 1/77 |
| SPACE LOSS | | | | 208.5 dB | SSRF Circuit Ma 1/77 |
| POLARIZATION LOSS | | | | -0.3 dB | SSRF Circuit Ma 1/77 |
| ATMOSPHERIC LOSS | | | | 0 dB | SSRF CircuitMarg |
| TDRS G/T | | | | 22.6 dB/°K | SSRF Circuit Mar |
| TDRS TWT MAX OUTPUT POWER | | | | 12.5 dB | WU Proposal, 7/ |
| TDRS TWT OUTPUT BACKOFF | | | | Composite,2.dB Dedicated,.5dB | WU Proposal, 7/ |
| POWER ALLOCATION | -2.5 dB | TPM#8 | 3/78 | -2.4 dB | WU Proposal, 7/ |
| CHANNEL POWER | | | | Composite,8.0dBW Dedicated,12dBW | WU Proposal, |
| TDRS HARDWARE LOSS | | | | 1.2 dB | LinCom estimate |
| TDRS ANTENNA GAIN | | | | 41.3 dB | WU Proposal, 7/ |
| POINTING LOSS | | | | 0.7 dB | WU Proposal, 7/ |
| SPACE LOSS | | | | 207.7 dB | TDRSS Users Gui |
| POLARIZATION LOSS | | | | 0.1 dB | TDRSS Users Gui |
| ATMOSPHERIC LOSS | | | | 0.8 dB | TDRSS Users Gui |
| RX ANTENNA G/T | | | | 40.3 dB | TDRSS Users Gui |
| | PHASE NOISE BUDGET | | | | |
| TX OSC, COHERENT TURNAROUND | | | | | |
| 1 to 10 Hz | | | | 3° rms | S-805-1 |
| 10 Hz to 1 kHz | | | | 3° rms | S-805-1 |
| 1 kHz to 150 MHz | | | | 1° rms | S-805-1 |
| TX OSC, NONCOHERENT TURNAROUND | | | | | |
| 1 to 10 Hz | | | | 15° rms | S-805-1 |
| 10 to 100 Hz | | | | 7.5° rms | S-805-1 |
| 100 Hz to 1 kHz | | | | 2° rms | S-805-1 |
| 1 kHz to 150 MHz | | | | 2° rms | S-805-1 |
| TDRS OSCILLATORS | 3.4° | TPM#8 | 3/78 | 3° | S-805-1 |
| RX OSCILLATORS | | | | 1° | S-805-1 |
| RX CARRIER TRACKING LOOP | | | | | |
| STATIC PHASE ERROR | | | | 3° | LinCom Estimat |
| BANDWIDTH | | | | 1000 Hz | TRW, 8/77 |
| DAMPING | | | | 2 | LinCom Estimat |
| SQUARING LOSS | | | | DG1: 2 dB DG2: 8 dB | LinCom Estimate |

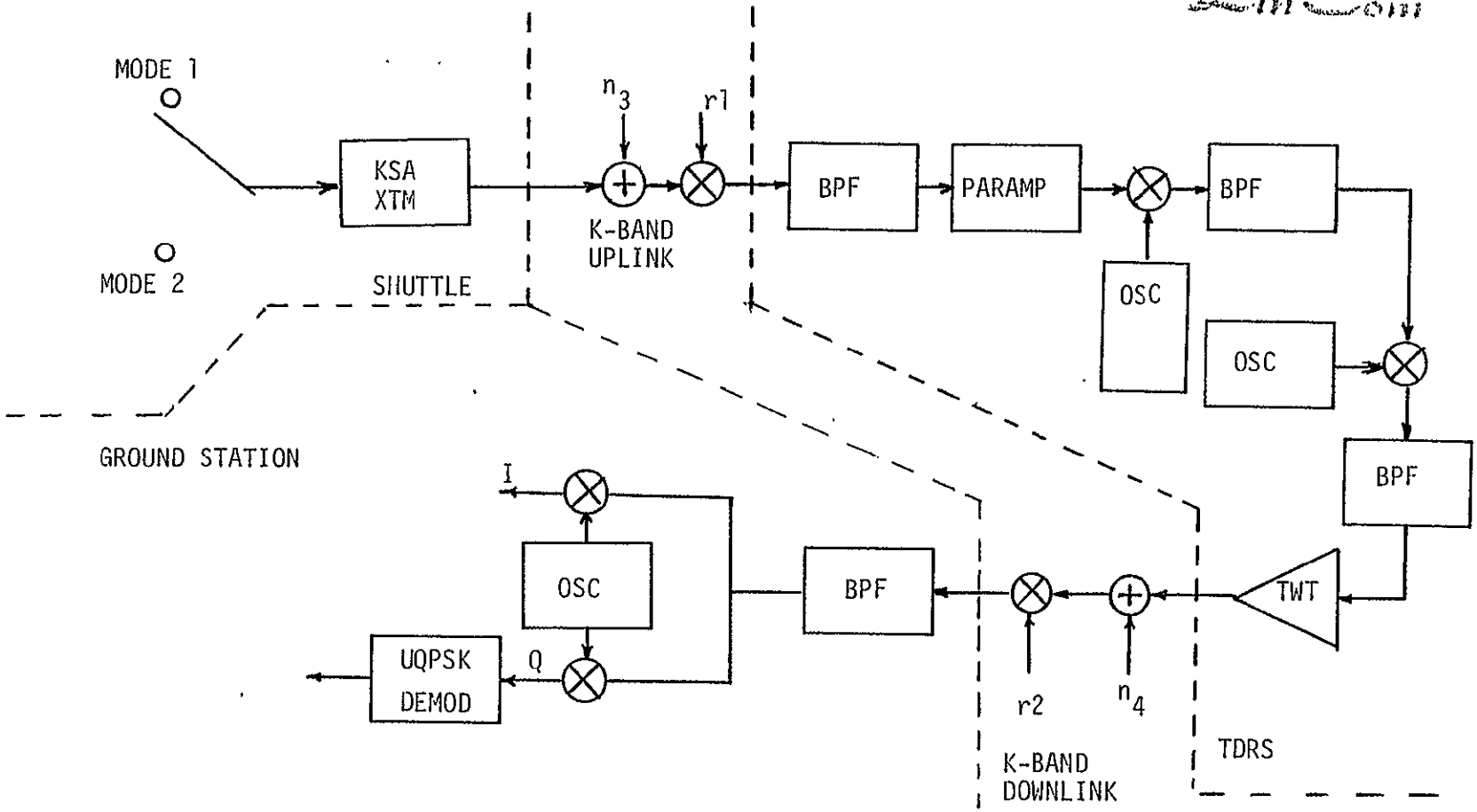


Fig. 2.8. Dedicated KSA Return Link Model.

models are made to agree in every respect except for the sharing of the amplifier. In particular, the S-band channel power into the TWTA and the amplifier characteristic and maximum TWT output power are identical.

### 2.2.6 Ideal Channel Model

Along with the error rate for the specified channel the program prints the error probability for an "ideal channel." This is assumed to be an infinite bandwidth, linear channel with additive white Gaussian uplink and downlink noise as the only distortions. Uplink and downlink carrier-to-noise ratios as well as the repeater input noise bandwidth (affecting the power robbing in the satellite) are matched to the actual channel. The printed error rate is therefore the optimum performance achievable with the given link power budget and a nonprocessing satellite.

## 2.3 Subsystem Models

### 2.3.1 Introduction

This chapter extends the channel model description to the subsystem level. The implementations chosen are based on the actual Shuttle, TDRS or ground station hardware implementation whenever such information was available. Otherwise, a reasonable state-of-the-art guess was used. The Shuttle transmitter implementation has enough flexibility to model the user constraint distortions.

### 2.3.2 Modulator

The modulator accepts two binary switching waveforms and phase-modulates them onto a carrier. The phase transitions are instantaneous. The resulting waveform may exhibit the following types of distortions:

- Gain Imbalance
- Phase Imbalance (for BPSK)
- Nonorthogonal Channels (for QPSK and UQPSK)
- Data Asymmetry
- PN Asymmetry
- I/Q Data Skew (for equal rates and no PN spreading)
- I/Q PN Skew
- Data Bit Jitter
- PN Chip Jitter
- Carrier Phase Jitter

which are defined in Section 2.5.3.

2.3.3 Filters

All filters are modeled as Chebyshev filters. They are defined by the three parameters bandwidth, ripple and number of poles. The number of poles refers to the transfer function of the equivalent baseband filter. The ripple is defined as 20 $\log(v_1/v_2)$ where $v_1, v_2$ are shown in Fig. 2.9. The bandwidth is the two-sided ripple-bandwidth as shown in the figure, i.e. it does usually not agree with either the noise bandwidth or the 3 dB bandwidth. However, if the ripple is specified as 0 dB a Butterworth filter characteristic results and the 3 dB bandwidth is used.

In the transmitter some linear distortion may be specified in terms of the following parameters:

- Gain Flatness
- Gain Slope
- Phase Nonlinearity

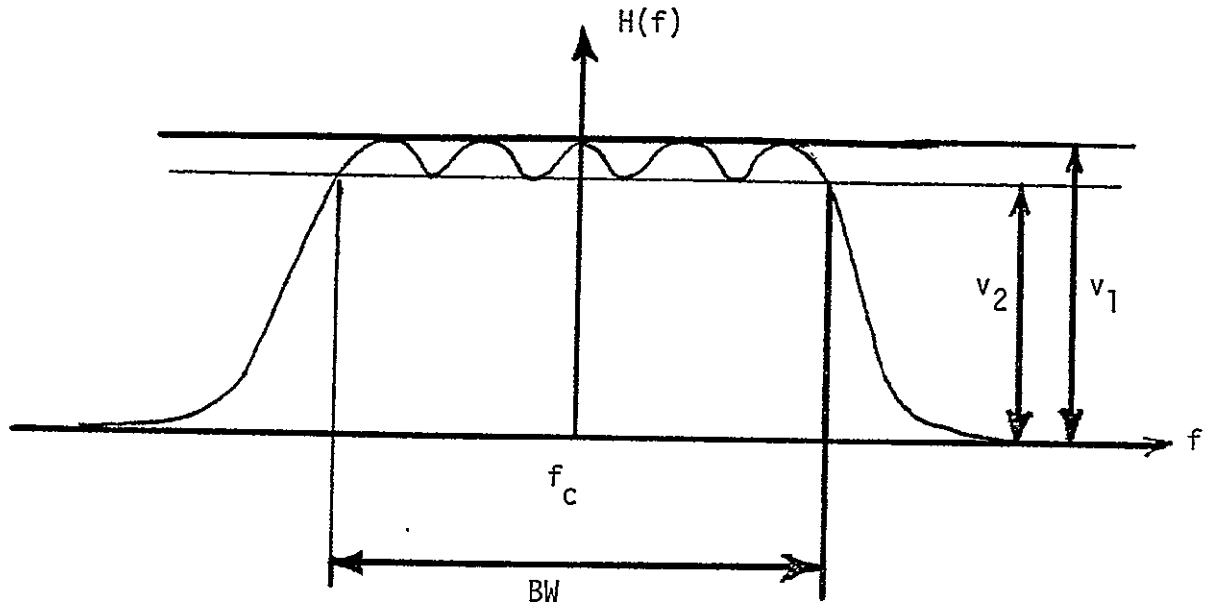


Figure 2.9. Chebyshev Filter Characteristic.

The transfer characteristic used is described in Section 2.5.3. In order to obtain the phase nonlinearity specified and no more, the transmit Chebyshev filter has a linear phase characteristic. All other filters exhibit the unequalized Chebyshev phase characteristic.

Note that the filter in the transmitter inherently sets the following parameters which are specified as user constraints in Ref. [1]:

- Data Transition Time
- Minimum 3 dB Bandwidth Prior to Power Amplifier

### 2.3.4 Power Amplifiers

#### 2.3.4.1 Introduction

The power amplifiers are modeled as memoryless devices with a gain characteristic which may depend on the instantaneous value of the signal envelope and with an envelope-dependent phase shift between the input and output. The transmitter HPA characteristic therefore sets the following distortion parameters:

- AM-PM
- Data Transition Induced PM

There are three different characteristics built into the program: a linear amplifier, a measured TWT characteristic and a characteristic with constant AM-AM and AM-PM distortion. These models are discussed below. An important parameter for a nonlinear power amplifier is the operating point. Its definition is discussed at the end of this section.

#### 2.3.4.2 Linear Amplifier

The linear amplifier has a constant arbitrary gain and no phase

shift. The input power is automatically adjusted so that the output power agrees with the specified amplifier output power, viz., the output saturation power (dBW) minus the output backoff (dB). It is understood that the terms "output saturation power" and "output backoff" are meaningless for a linear amplifier; however, they are used in the above definition of output power in order to reach a closer agreement with the TWT amplifier operating point definition which is given below.

2.3.4.3 TWT Characteristic

The measured TWT characteristic corresponds to the Hughes 261H tube and is shown in Fig. 2.10. In order to provide more flexibility the model includes two parameters which allow one to adjust the scale on the gain and phase nonlinearity separately to meet the output saturation power and maximum AM-PM specifications.

The AM-PM distortion is defined as

$$\text{AM-PM} = \frac{dg(R)}{d[20\ \log_{10} R]} = \frac{\ln(10)}{20}\ \frac{Rdg(R)}{dR}\ \left[\frac{\text{deg}}{\text{dB}}\right]$$

The normalized AM-PM function is plotted in Fig. 2.11. Note that it peaks at approximately 8 dB input backoff. This means that the worst degradation due to AM-PM can be expected if the TWT input signal power is 8 dB below the saturation power.

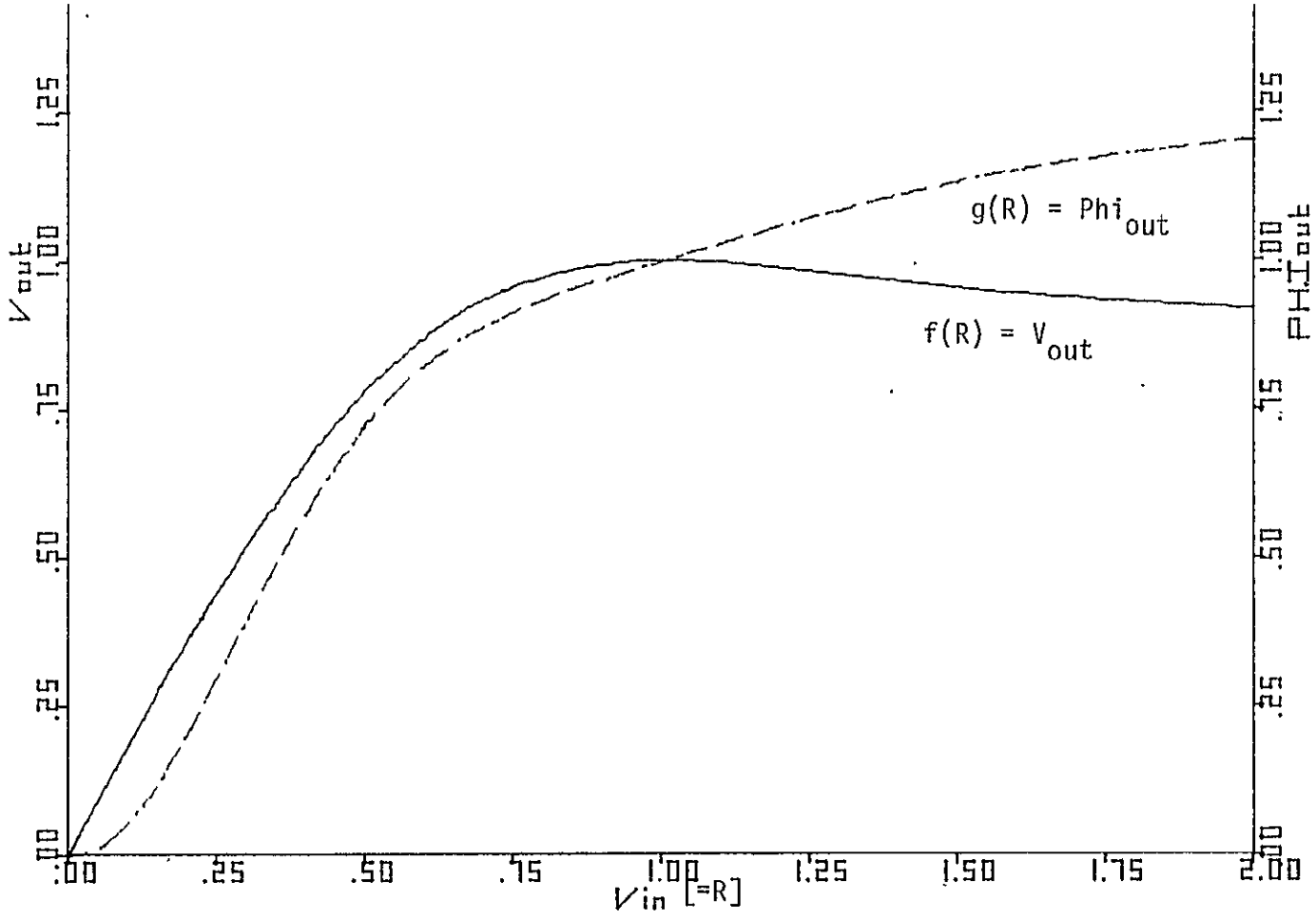


Figure 2.10. Normalized TWT AM-AM and AM-PM Characteristics.

2.3.4.4 Constant AM-AM, AM-PM Model

The AM-AM distortion is defined as

$$\text{AM-AM} = \frac{d[20 \log_{10} f(R)]}{d[20 \log_{10} R]} = \frac{R}{f(R)} \frac{df(R)}{dR} \left[\frac{dB}{dB}\right]$$

and the AM-PM distortion is

$$\text{AM-PM} = \frac{dg(R)}{d[20 \log_{10} R]} = \frac{\ln(10)}{20} \frac{Rdg(R)}{dR} \left[\frac{deg}{dB}\right]$$

Using

$$f(R) = R^{\text{AM-AM}}$$

$$g(R) = \begin{cases} \text{AM-PM } 20 \log_{10} R & R \geq \varepsilon \\ \text{AM-PM } 20 \log_{10} \varepsilon & R < \varepsilon \end{cases}$$

where $\varepsilon$ is some small (with respect to the r.m.s. signal) number we obtain a characteristic with a constant AM-AM and AM-PM value over all operating points. This model is implemented with AM-AM and AM-PM as parameters. A typical characteristic is plotted in Fig. 2.12. This model can also simulate a hard-limiter by setting AM-AM = AM-PM = 0.

As in the case of the linear amplifier the terms "output saturation power" and "output backoff" are not applicable to this characteristic. They are however used to define the output power in the same way as for the linear amplifier.

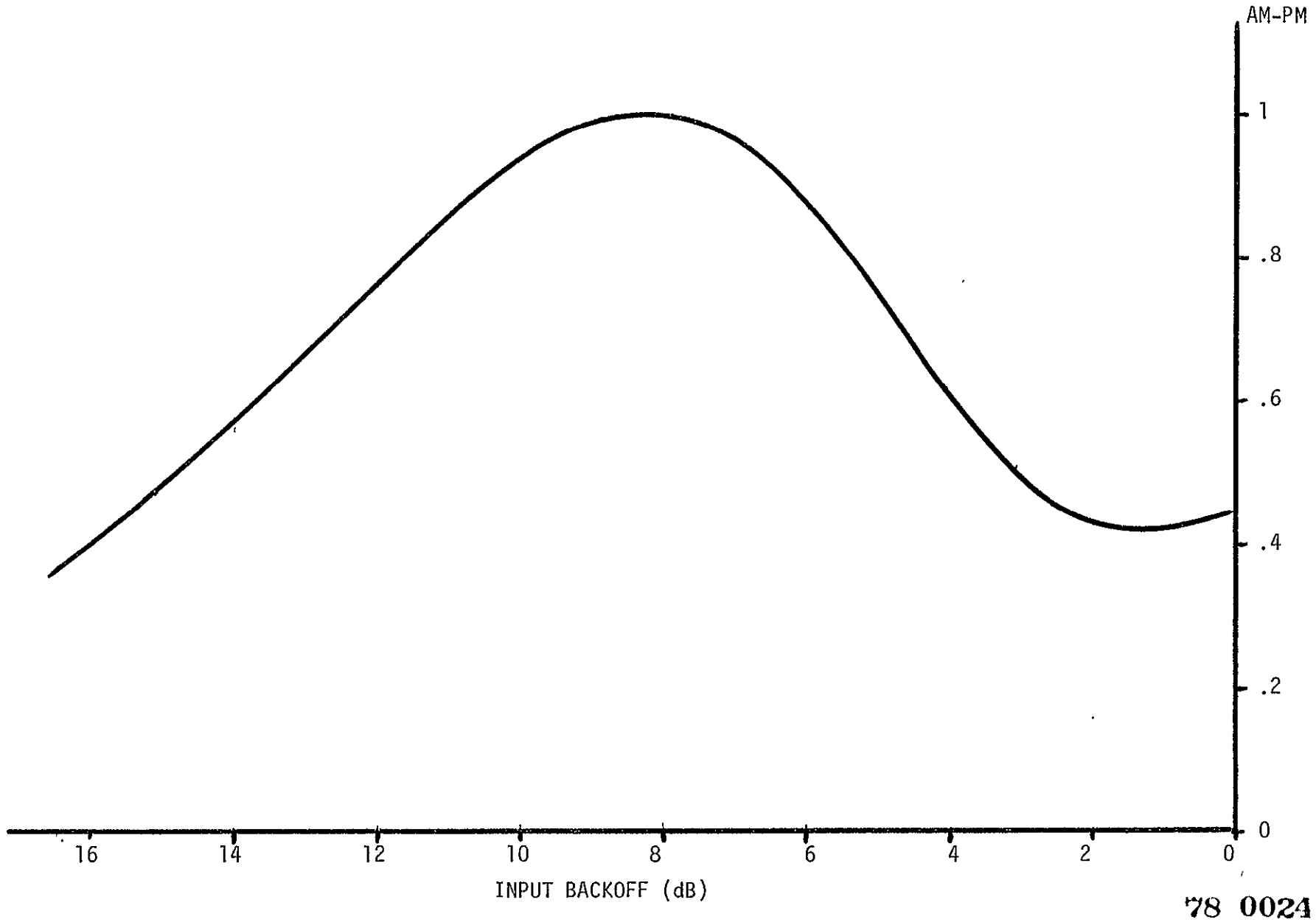


Figure 2.11. Normalized AM-PM Characteristic.

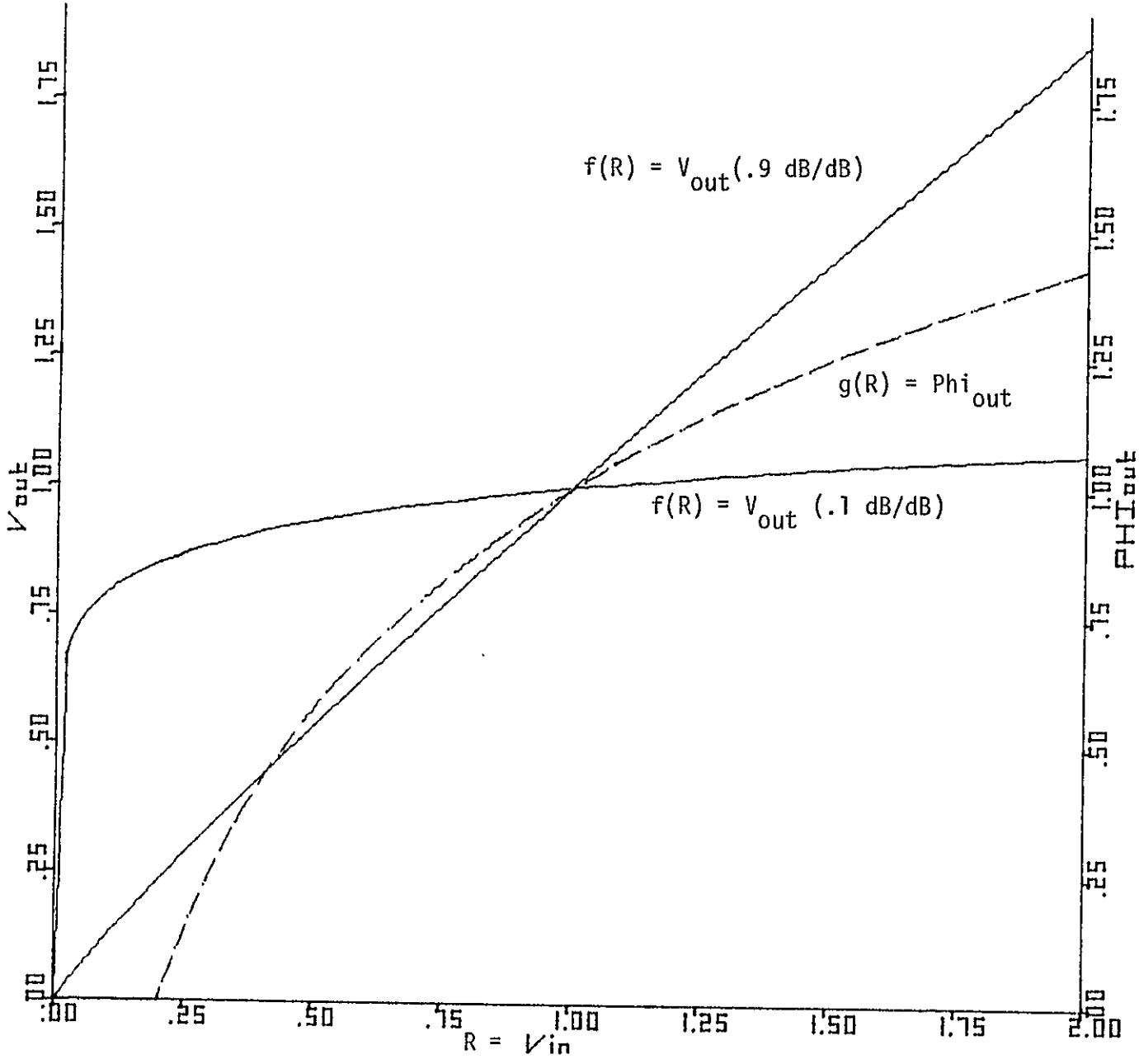


Figure 2.12. Normalized Characteristic for Constant AM-AM, AM-PM.

2.3.4.5 Definition of Operating Point

For the linear amplifier and the constant AM-AM, AM-PM model performance is insensitive to the amplifier operating point, viz., the power level of the signal into the amplifier. For the TWT model, however, it is an important parameter. Here the operating point is characterized by the input backoff, which is defined as the ratio of the input power (signal plus noise) to the input saturation power, where the input saturation power is the power of a CW input signal which produces the maximum output power. The input backoff is computed from the specified output backoff on the basis of a noise-free CW signal.

2.3.5 PN Despreader

The despreader implementation is shown in Fig. 2.13. For a four-phase signal, only one quadrature component (the higher-power channel for unbalanced QPSK signals) is used to find the PN epoch. Both PN sequences are then derived from the same PN generator.

2.3.6 Carrier Recovery

The carrier tracking loop is modeled as a Costas loop for BPSK signals and for PN-spread signals and as a two-channel Costas loop with hard-limiters (Fig. 2.14) for balanced and unbalanced QPSK signals. For PN-spread QPSK or UQPSK signals a single loop tracks the carrier in one of the quadrature channels and its phase estimate is used for the demodulation of both channels.

2.3.7 Data Clock Recovery

The data tracking loop implementation is shown in Fig. 2.15. The baseband input signal is hard-limited and multiplied with a delayed copy of itself. This produces a line in the spectrum which

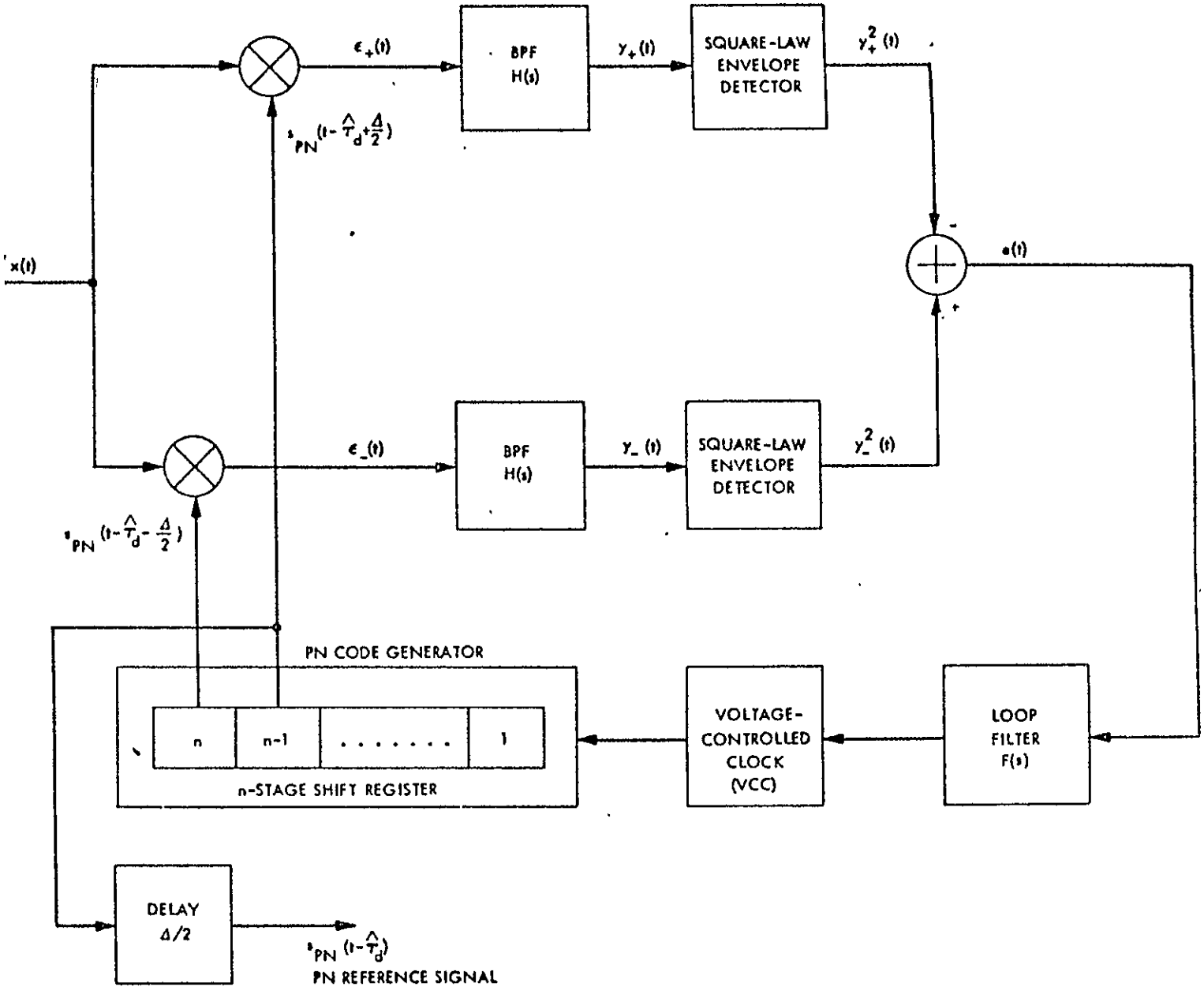


Figure 2.13. A Noncoherent "One Δ" Delay-Locked Loop

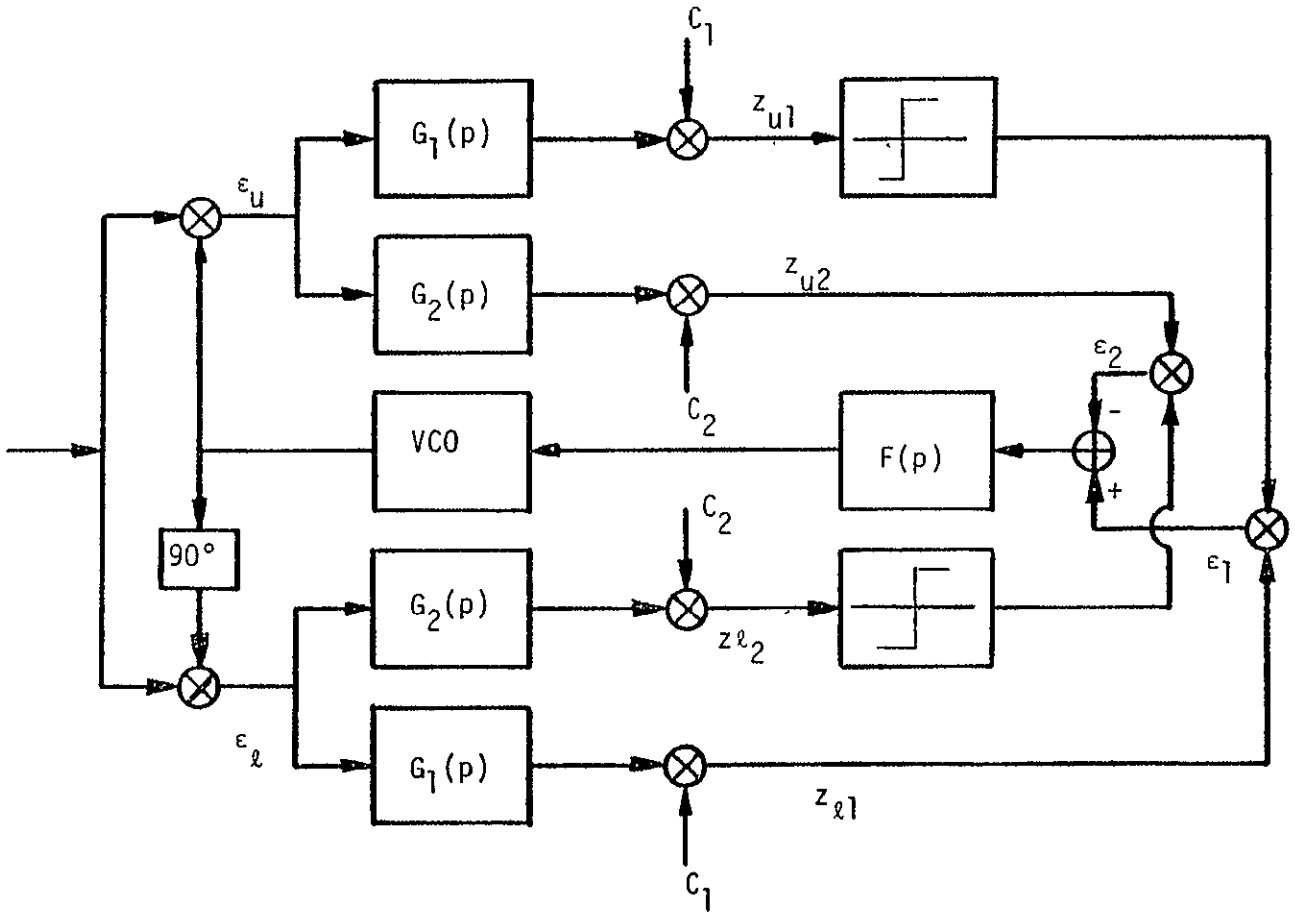


Figure 2.14. Two Channel Costas with Hard-Limiters.

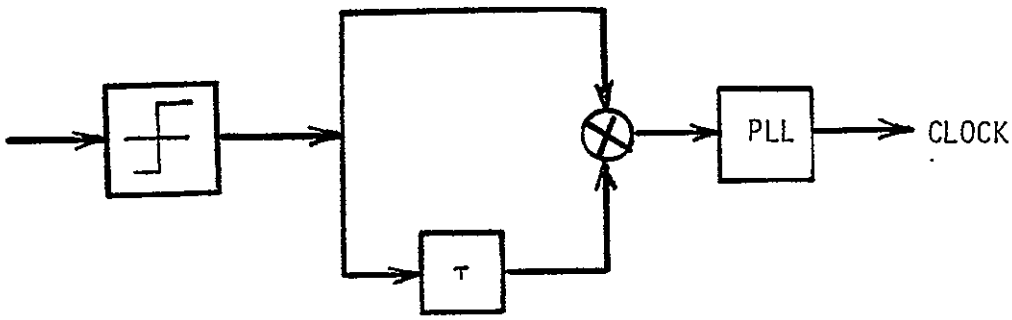


Figure 2.15. Data Clock Recovery Implementation.

is being tracked by a phase-locked loop. The delay $\tau$ can be selected; a typical value is half a bit time for NRZ symbols and one quarter of a bit time for biphase symbols. The resulting spectral line is at the data rate or twice the data rate, respectively. The loop bandwidth is set at 1/1000 of the data rate or 10 Hz, whichever is more.

### 2.3.8 Data Detector

The data detector is modeled as a hard-limiter for uncoded data and as a three-bit quantizer for convolutionally encoded data.

## 2.4 Definition and Modelling of User Constraints

### 2.4.1 Introduction

This section lists all the user constraint parameters specified in [1], Table 3-14, along with their official definition ([1], Appendix I) and the model used in LinCsim. An effort was made to find for every parameter the worst-case model meeting the specifications.

### 2.4.2 User Constraints

Modulator Phase Imbalance (BPSK Only)

Definition: The steady state phase difference between the phase separation of the BPSK modulated +1 and -1 data bits and 180 degrees.

Model:

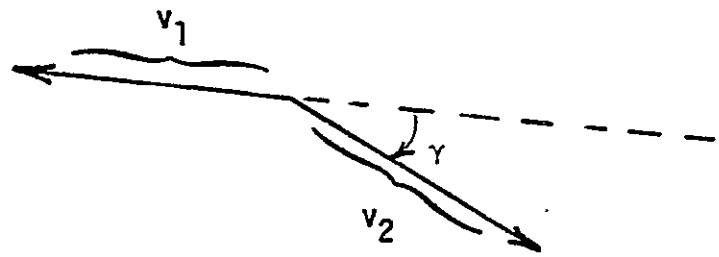


$\gamma$ = Phase Imbalance

Modulator Gain Imbalance (dB)

1. BPSK

Definition: 10 log $P_1/P_0$ = 20 log$[\frac{X+\Delta X}{X}]$ where $P_1$ is the power in an all 1's data pattern as measured at the modulator output, $P_0$ is the power in an all 0's data pattern as measured at the modulator output, X is the steady state amplitude gain of the modulator phase state one, $X+\Delta X$ is the steady state amplitude gain of modulator phase state two, and $\Delta X \geq 0$.

Model:

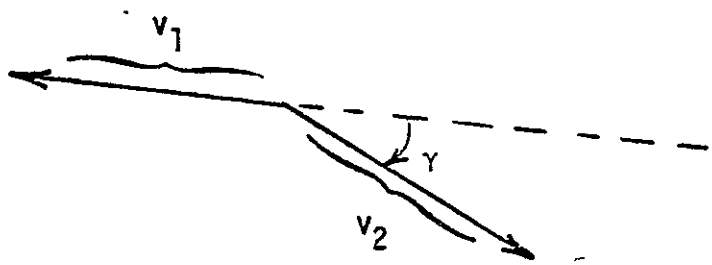


$|20 \log(v_1/v_2)|$ = modulator gain imbalance

$\frac{1}{2}[\max(v_1,v_2)]^2$ = design modulator output power

2. QPSK and UQPSK

Definition: $20 \log \left[\frac{X+(\Delta X_i)_{max}}{X}\right]$ where the four modulator phase states have steady state amplitude gains X, $X+\Delta X_1$, $X+\Delta X_2$ and $X+\Delta X_3$, and where $\Delta X_i \geq 0$.

Model:

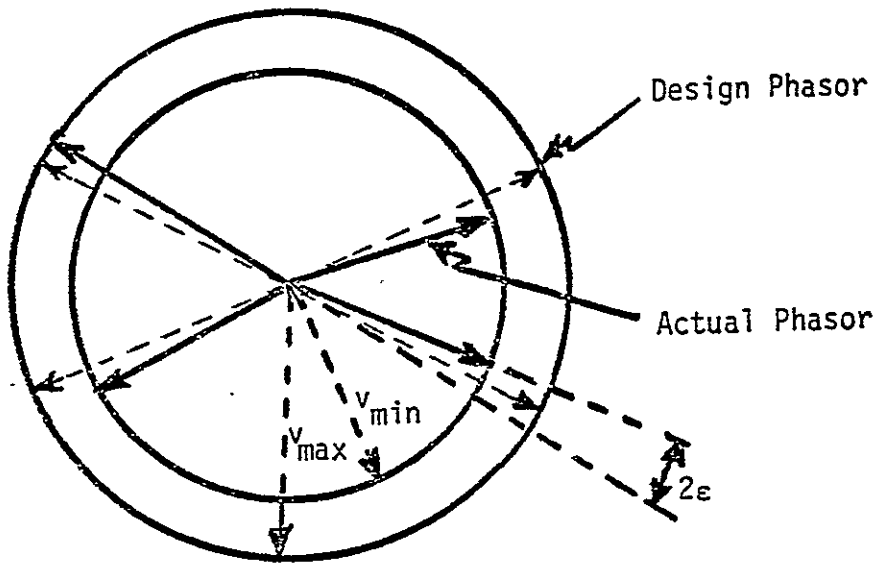


$20 \log(v_{max}/v_{min})$ = modulator gain imbalance

$v_{max}^2/2$ = design modulator output power

Relative Phase Between I and Q Channels

Definition: The difference in phase, as shown below, between the best fit orthogonal reference phase vectors and the actual phase vectors.

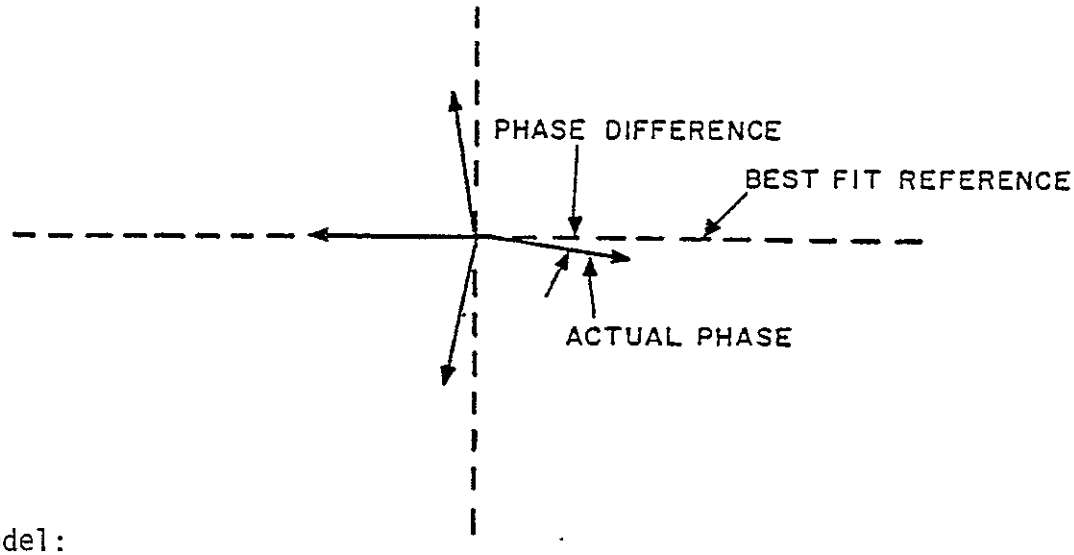


Model:

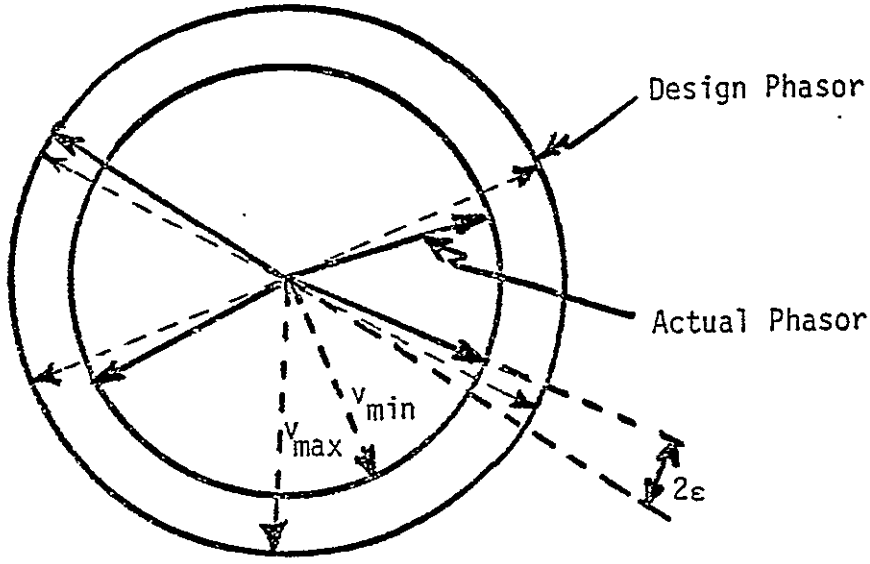


$\varepsilon$ = relative phase between I and Q channel

Data Asymmetry

Definition:

1. For an NRZ format signal:

$$\left[\frac{\text{length of long bit - length of short bit}}{\text{length of long bit + length of short bit}}\right] \times 100\%$$

2. For a bi-ø format signal, data asymmetry applies to both the entire bit as well as to each half symbol pulse.

   For data bits, data asymmetry is:

$$\left[\frac{\text{length of long bit - length of short bit}}{\text{length of long bit + length of short bit}}\right] \times 100\%$$

   For half symbol pulse, data asymmetry is:

   [length of long half symbol pulse - length of short half symbol pulse]/[length of long half symbol pulse + length of short half symbol pulse] x 100%

Model:

Each positive-going pulse transition is advanced by $\alpha T_s/2$, each negative going transition is retarded by $\alpha T_s/2$ with respect to a perfect clock, where $T_s$ = symbol time for NRZ, $T_s$ = 1/2 symbol time for Bi-ϕ data. Then

Length of long pulse: $T_s(1+\alpha)$

Length of short pulse: $T_s(1-\alpha)$

$$\text{Data Asymmetry} = \frac{T_s(1+\alpha)-T_s(1-\alpha)}{T_s(1+\alpha)+T_s(1-\alpha)} \cdot 100 = \alpha \cdot 100$$

Data Transition Time

Definition: The time required to switch from 90% of the initial data state to 90% of the final data state, illustrated as follows:

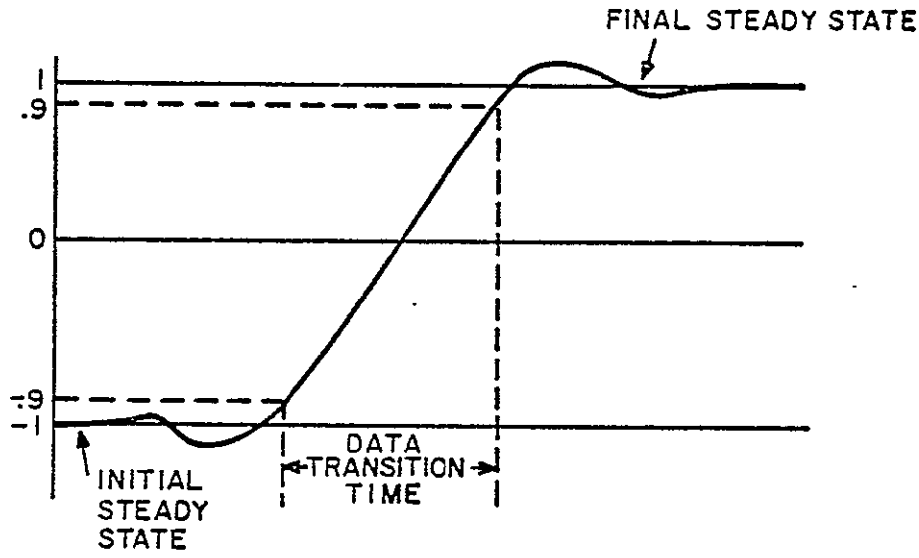


DATA TRANSITION TIME DEFINITION

Model: The data transition time is set by the pulse-shaping filter characteristic.

Phase Nonlinearity

Definition: The peak deviation of the phase from the best linear fit to the actual phase versus frequency relationship over the bandwidth of interest, illustrated as follows:

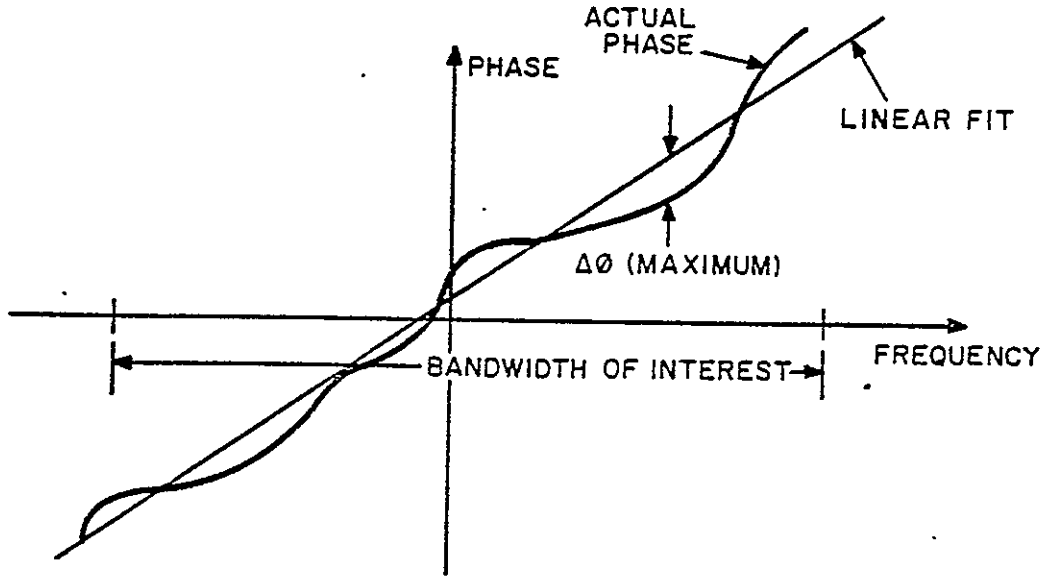


PHASE NONLINEARITY (ΔØ) DEFINITION

Model: The phase nonlinearity is modeled as a sinusoidal ripple within the specification bandwidth B. Outside, it flares out linearly as shown below. The ripple period is equal to the data rate, the amplitude $\phi_{max}$ is equal to the specified phase nonlinearity.

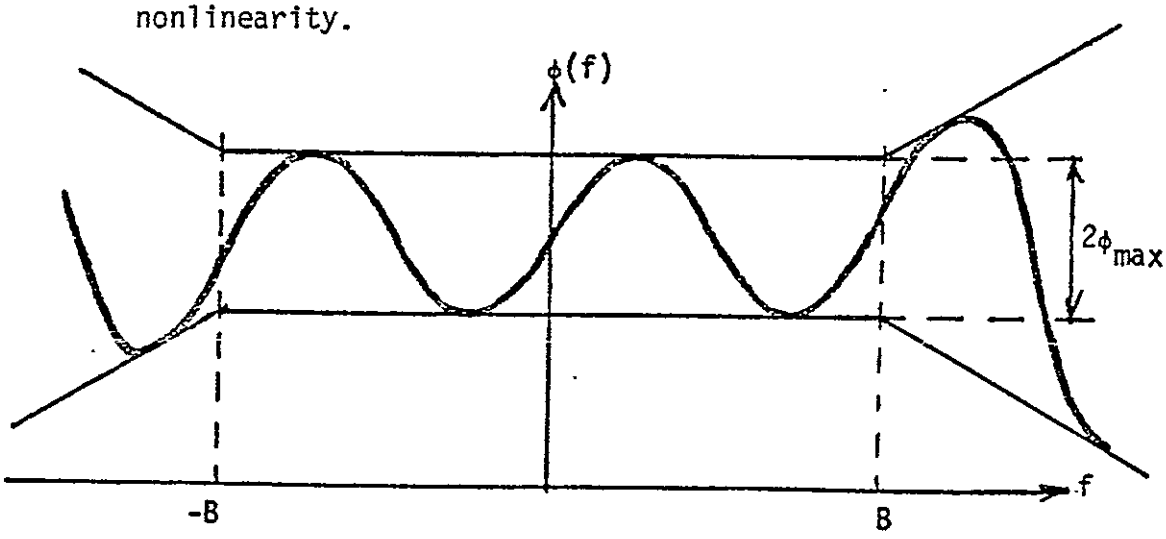

Gain Flatness

Definition: The peak deviation of the gain from the best horizontal fit to the actual gain versus frequency relationship over the bandwidth of interest, illustrated as follows:

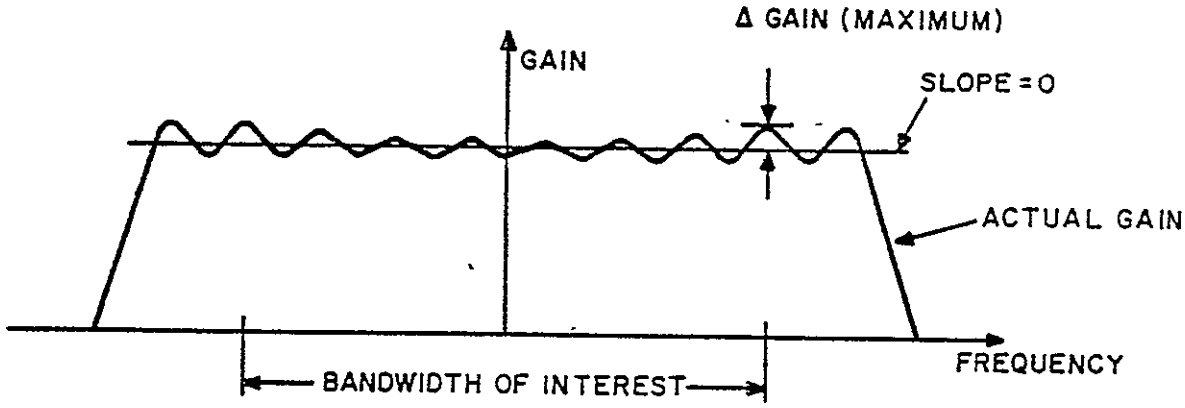


Model: If the specified gain slope is sufficiently large the logarithmic gain characteristic is modeled as a trapezoidal waveform with a peak-to-peak amplitude of twice the specified gain flatness $\Delta G$ with a slope equal to the gain slope G' specified. Outside of B it flares out. The ripple period is equal to the data rate. The resulting characteristic is illustrated in (a). If the gain slope is too small to obtain the above characteristic a triangular waveform is used with the same peak-to-peak amplitude and with the given gain slope. The period of this waveform is determined by these parameters. The phase is adjusted to assure that the positive and negative peaks are reached within $\pm$B. Outside of B the characteristic flares out again, see (b)

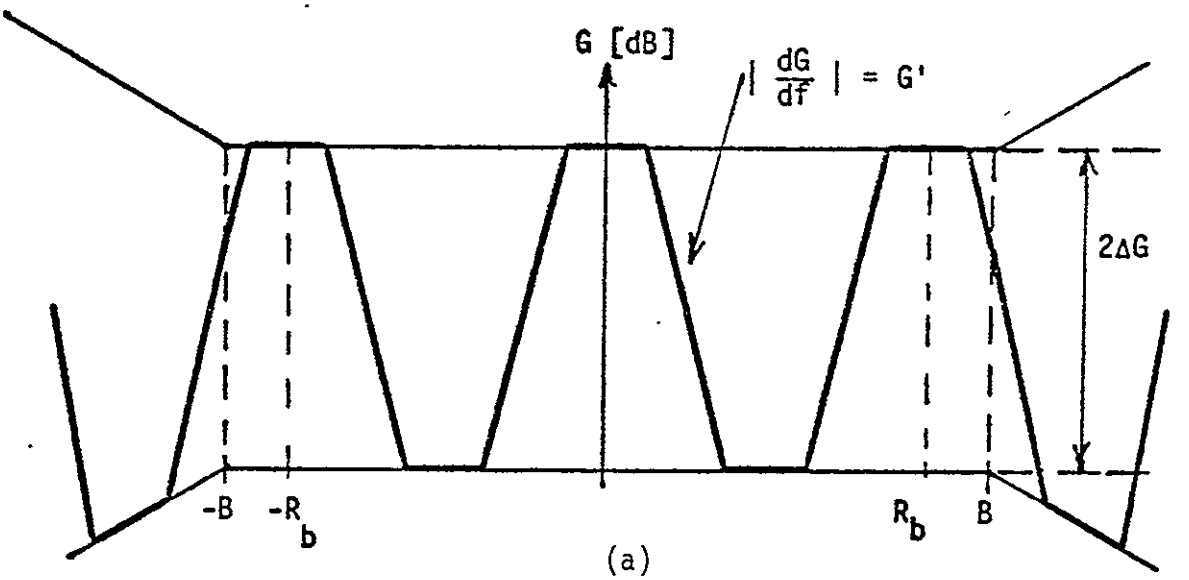


(a)

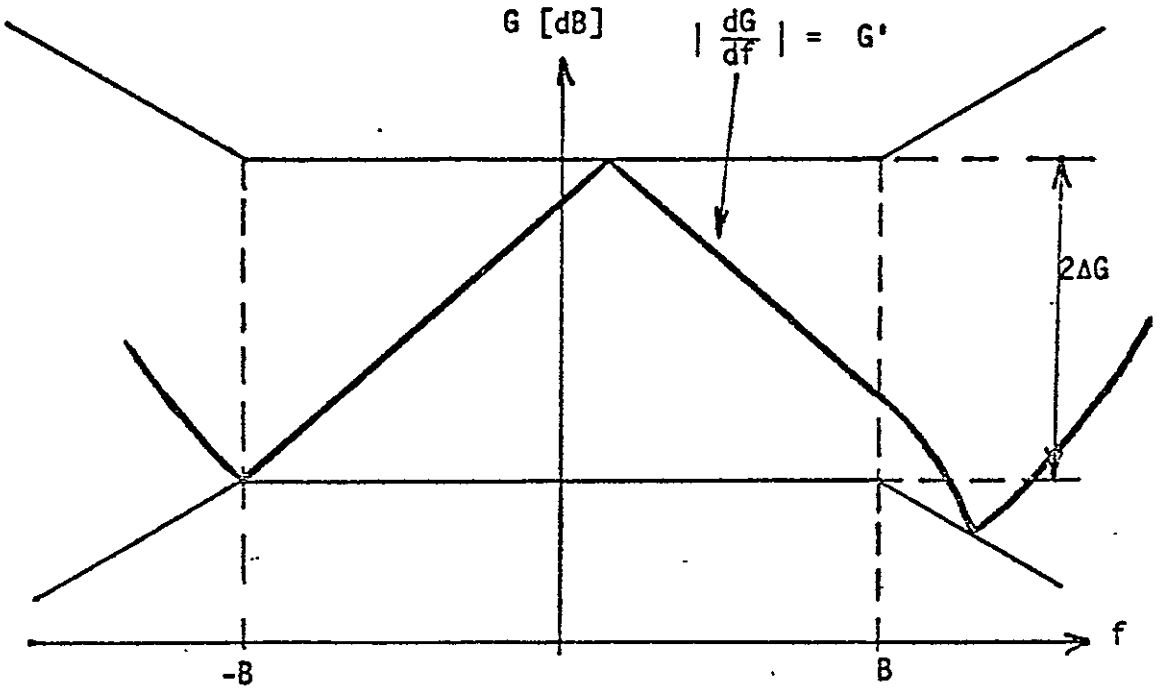


(b)

Gain Slope

Definition: The rate of change in gain versus frequency at any point within the bandwidth of interest, illustrated as follows:

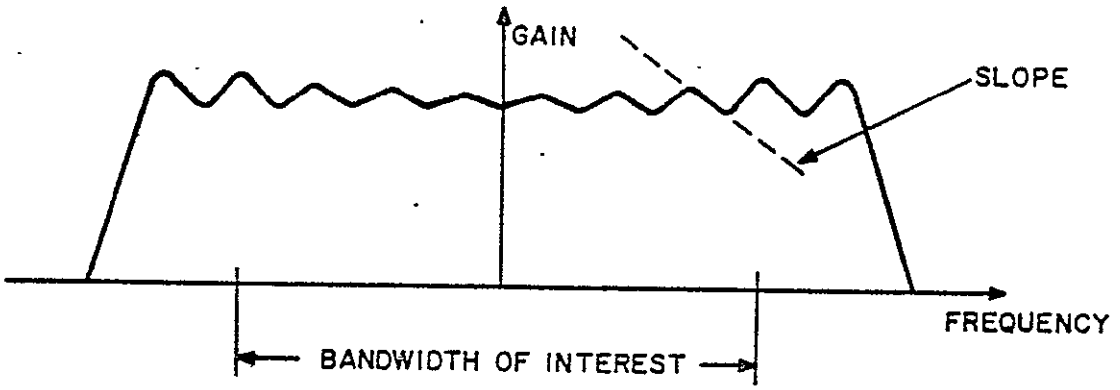


Model: If the specified gain slope is sufficiently large the logarithmic gain characteristic is modeled as a trapezoidal waveform with a peak-to-peak amplitude of twice the specified gain flatness $\Delta G$ with a slope equal to the gain slope G' specified. Outside of B it flares out. The ripple period is equal to the data rate. The resulting characteristic is illustrated in (a). If the gain slope is too small to obtain the above characteristic a triangular waveform is used with the same peak-to-peak amplitude and with the given gain slope. The period of this waveform is determined by these parameters. The phase is adjusted to assure that the positive and negative peaks are reached within $\pm B$. If the gain slope specified is too small, i.e., $G'B < \Delta G$ the slope is readjusted to $G' = \Delta G/B$. Outside of B the characteristic flares out again, see (b).

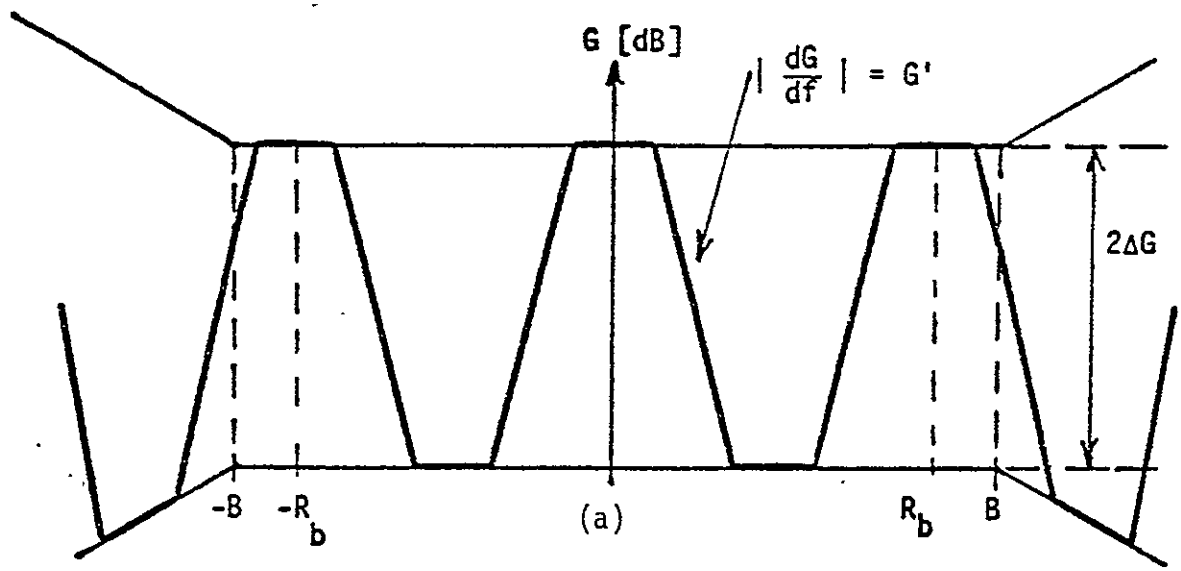
G [dB]
$\left|\frac{dG}{df}\right| = G'$
$2\Delta G$
-B
$-R_b$
$R_b$
B

(a)

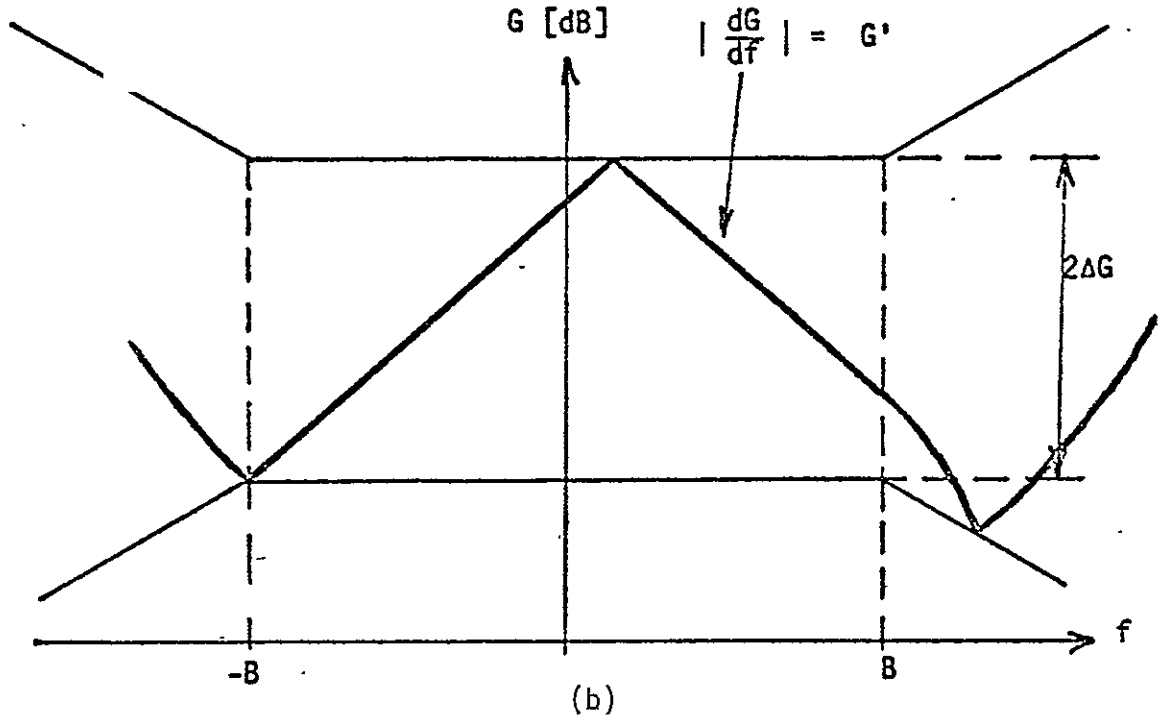
G [dB]
$\left|\frac{dG}{df}\right| = G'$
$2\Delta G$
f
-B
B

(b)

AM/PM

Definition: AM/PM = worst case $\frac{d\phi_{out}}{dP_{in}}$ over the range of operating points where $P_{in}$ = RF power input to power amplitier, in dB and $\phi_{out}$ = RF phase output from power amplifier, in degrees.

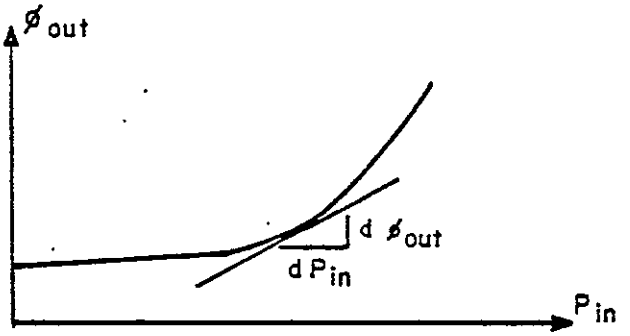


Model: The envelope-dependent phase shift is given by

$$g(R) = \begin{cases} \text{AM/PM } 20 \log_{10}(R) & R \geq \varepsilon \\ \text{AM/PM } 20 \log_{10}(\varepsilon) & R < \varepsilon \end{cases}$$

where

R = RF input envelope (V)

$\varepsilon$ = some small voltage (with respect to r.m.s. signal)

This results in a constant value for the AM/PM.

Data Transition Induced PM

Definition: Phase variation at the power amplifier output which is correlated with the modulation on the carrier. This phase variation results from the combined effects of bandlimiting followed by AM/PM conversion.

Model: The data transition induced PM is determined by the choice of type and bandwidth of the pulse shaping filter together with the selected value of transmitter AM/PM.

PN Chip Jitter

Definition: Let $\varepsilon T$ be the error in seconds between the actual chip transition time and the correct transition, when T is the chip period and $\varepsilon$ is a random variable. Then PN chip jitter is the square root of the variance of $\varepsilon$ multiplied by 100 percent.

PN chip jitter is measured as the rms phase error in a baseband bandwidth of 1 MHz using a high gain second-order PN Code Tracking Loop with a damping factor of 0.707 and a two-sided noise bandwidth ($2B_L$) of 0.2 Hz. This user constraint is based upon zero TDRSS forward link PN jitter.

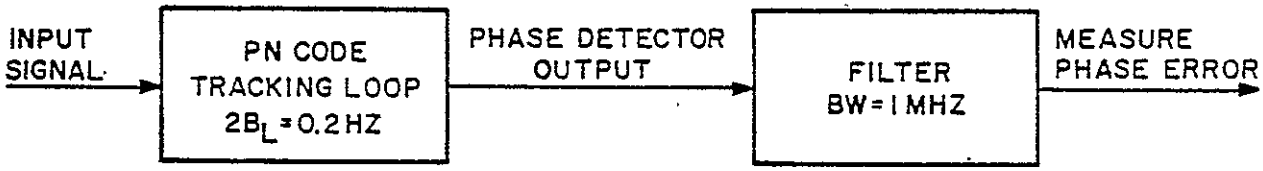


Model: This parameter describes the random variation of the PN clock phase. A Gaussian distribution is assumed and the rms value is set to one third of the peak value specified.

Minimum 3 dB Bandwidth Prior to Power Amplifier

Definition: (No official definition available.)

Model: This is the 3 dB bandwidth of the pulse-shaping filter.

Data Bit Jitter

Definition: User spacecraft peak clock frequency jitter and peak jitter rate (sinusoidal or $3\sigma$ random) as percent of the symbol clock rate.

Model: This parameter describes the random variation of the data clock phase. A Gaussian distribution is assumed. Note that this definition deviates from the definition above.

Spurious PM

Definition: Consider a carrier

$$\sin[\omega_c t+\phi(t)]$$

$\phi(t)$ = PM spurs + phase noise.

-PM spurs are discrete phase modulated components on the carrier.

-Phase noise is random phase modulation.

Then each PM spur can be written as

$$B_i \sin(\omega_i t)$$

and the resulting rms spurious PM will be

$$\text{Spurious PM} = \sqrt{\sum_i \frac{B_i^2}{2}}$$

where the sum is taken over all i for which $\omega_i$ is within the specified frequency range.

Spurious PM can be determined by measuring the power in each spur and calculating the rms value for these powers.

Model: This parameter is not modelled presently.

Short Term EIRP Stability for KSA Acquisition Sequence No. 1.

Definition: The short-term EIRP stability is determined by measuring the peak-to-peak variations in signal EIRP in dB and dividing by the specified averaging periods in seconds.

Model: This parameter has no effect on the bit error performance and is therefore not modelled.

Spurious Outputs

Definition: The sum of the power in all spurs within the specified bandwidth measured relative to the total signal power. (dBc indicates dB below total signal power). Data bandwidth is the bandwidth between the first nulls of the signal. That is, two times the symbol rate for NRZ data and four times the symbol rate for Bi-ø formatted data. The channel bandwidth is 6 MHz for MA; 10 MHz for SSA, S-band Shuttle, and S-band IF service; and 225 MHz for KSA, Ku-band Shuttle, and Ku-band IF service.

Model: This parameter is not modelled presently.

Frequency Stability (Peak)

Definition: The peak instantaneous carrier frequency deviation from the nominal carrier frequency ($\Delta f$) normalized to the nominal carrier frequency as observed over the specified time interval of interest. This includes frequency deviation due to all sources including deviations induced by environmental changes. (This parameter only applies to the non-coherent modes of operation.)

Model: This parameter has no effect on the bit error performance and is therefore not modelled.

Incidental AM

Definition: Consider an ideal RF signal of the form:

$$A \cos[\omega_c t+\phi(t)]$$

Then a signal with amplitude modulation $m_i$ at frequencies $\omega_i$ with phase $\phi_i$ will be of the form:

$$A[1 + \sum_i m_i \cos(\omega_i t+\phi_i)]\cos[\omega_c t+\phi(t)]$$

The peak of the amplitude modulation will then occur when all of the incidental AM components line up. Therefore, the peak incidental AM will be:

$$\sum_i m_i \times 100\%$$

Model: This parameter has little effect on the bit error performance and is therefore not modelled.

Axial Ratio

Definition: For circularly polarized antennas, the electrical field vector usually produced describes an ellipse instead of a circle. The axial ratio is a measure of ellipticity and is the ratio of the minor axis of the ellipse to the major axis.

Model: This parameter has little effect on the bit error performance and is therefore not modelled.

Phase Noise

Definition: Phase noise is the random component of the phase modulation on the carrier. If the spectrum of the phase noise is taken as $S_{\phi}(f)$, then the rms phase from $f_1$ to $f_2$ is:

$$\text{Phase Noise} = \sqrt{\int_{f_1}^{f_2} S_{\phi}(f)df}$$

Phase nosie can be determined by measuring the power in each frequency band and then subtracting the power in the spurs within that band.

Phase noise values for the coherent turnaround mode assume no phase noise on the signal received by the user and therefore represent the phase noise added by the user. Values indicated for the noncoherent mode represent total output phase noise of the user.

Model: The phase noise is modelled as a Gaussian random process with a flat spectrum in each of the frequency bands specified.

I/Q Data Skew

Definition: Relative time delay of the data transitions between I and Q channels measured as a percent of a bit time. This parameter is determined by data, clock, and modulator characteristics.

Model: This parameter applies to balanced staggered QPSK only. It defines the relative time delay between the pulse center in the one channel and the pulse transition in the other channel. Due to the ground station hardware implementation this parameter has a negligible effect on the performance of an unspread link and no effect on a PN spread link.

Permissible EIRP Variation

Definition: Range over which the user EIRP measured along the user/TDRS line-of-sight may vary without requiring user reconfiguration. Performance is determined from user transmitter power variation, transmit antenna pattern, worst case user orientation, and maximum variation in range between the user and TDRS over the duration of a pass.

Model: This parameter has no effect on the bit error performance and is therefore not modelled.

Permissible Rate of EIRP Variation

Definition: The time derivative of EIRP.

Model: This parameter has no effect on the bit error performance and is therefore not modelled.

Maximum User EIRP

Definition: (No official definition available.)

Model: This parameter has no effect on the bit error performance and is therefore not modelled.

Frequency Error of 8.5 MHz Subcarrier

Definition: Difference between subcarrier frequency and 8.5 MHz.

Model: The frequency error itself has no effect on the bit error performance and is therefore not modelled. The effect of the loop stress in the receiver is modelled through the resulting static phase offset.

Subcarrier Phase Noise

Definition: Phase noise on the 8.5 MHz subcarrier (see phase noise definition).

Model: The subcarrier phase noise is modelled as a Gaussian random process whose power is concentrated outside the subcarrier tracking loop bandwidth but considerably below the data rate (worst-case assumption).

I/Q PN Skew

Definition: Relative time delay of the chip transitions between I and Q channels measured as a percent of a chip time.

Model: Relative time delay between the chip center in one channel and the chip transition in the other channel of a SQPN signal.

PN Asymmetry

Definition: PN chip asymmetry is defined as:

$$\left[\frac{\text{length of long chip - length of short chip}}{\text{length of long chip + length of short chip}}\right] \times 100\%$$

Model: Each positive going chip transition is advanced by $\alpha T_c/2$, each negative going transition is retarded by $\alpha T_c/2$ with respect to a perfect clock, where $T_c$ = chip time. Then

$$\text{PN Asymmetry} = \frac{T_c(1+\alpha)-T_c(1-\alpha)}{T_c(1+\alpha)+T_c(1-\alpha)} \times 100 = \alpha \cdot 100.$$

REFERENCE

[1] Tracking and Data Relay Satellite System (TDRSS) Users' Guide, Revision 3, STDN No. 101.2, Goddard Space Flight Center, Greenbelt, MD, January, 1978.

## 3.0 LinCsim PERFORMANCE PREDICTION

### 3.1 Introduction

The Shuttle/TDRSS link simulation software package (LinCsim) has been used to predict the Shuttle/TDRSS S-band return link bit error rate performance based on current link budgets user constraint values and TDRS/ground station hardware data. The results of this effort are presented in this section.

### 3.2 Performance Prediction for Shuttle S-band Return Link

This section presents the sensitivity of the Shuttle S-band return link BER performance to variations of the user constraint values based on current link budgets, nominal user constraint value estimates and TDRS/ground station hardware data. This simulation is based on the link models presented in Chapter 2 and on the system parameters listed in Table 2.3.

The link characteristics assumed are summarized in Table 3.1. The nominal values of the user constraints are listed in Table 3.2. They agree with the expected Shuttle values obtained from JSC. The link budget is reproduced in Table 3.3. It is based on the budgets contained in Ref. 1 with some updates obtained from Dr. Kwei Tu. Table 3.4 lists the user constraints whose effect on performance was studied.

The results are shown in two different forms. The BER curves show the bit error probability as a function of Shuttle-to-TDRS link carrier-to-noise ratio (CNR) variation around the nominal link budget of Table 3.3. The horizontal distance between the bit error rate curve and the design point shown represents

Table 3.1. Shuttle S-band Return Link Characteristics Used for LinCsim

| | |
|---|---|
| Data Rate | 192 Kbps |
| Data Format | BPSK, Biphase, Unspread |
| Coding | Rate 1/3 Convolutional Code |
| Carrier | Noncoherent with Forward Link |
| Design Error Rate | $10^{-4}$ |

Table 3.2. Nominal User Constraint Values Used for LinCsim

| | |
|---|---|
| Data Bit Jitter ($3\sigma$) | .6% |
| Modulator Phase Imbalance | 11° |
| Modulator Gain Imbalance | .1 dB |
| Data Asymmetry | 3.8% |
| Phase Nonlinearity | 3° |
| Gain Flatness | .4 dB peak |
| Gain Slope | .1 dB/MHz |
| AM/PM | 14°/dB |
| 3 dB Bandwidth | 100 MHz |
| Phase Noise | |
| 1 Hz - 10 Hz | 0° |
| 10 Hz - 100 Hz | 1° |
| 100 Hz - 1 kHz | 10° |
| 1 kHz - 6 MHz | 1° |

Table 3.3. Shuttle S-Band Return Link Power Budget.

| | |
|---|---|
| **Shuttle-to-TDRS Link** | |
| Shuttle EIRP | 16.7 dBW |
| Space Loss | 192.1 dB |
| Polarization Loss | .5 dB |
| TDRS G/T | 9.55 dB/°K |
| **TDRS-to-Ground Link** | |
| TDRS TWT max Output Power | 13.4 dBW |
| TWT Output Backoff | 2 dB |
| SSA Power Allocation | -10 dB |
| TDRS Hardware Losses | 2.46 dB |
| TDRS Antenna Gain | 45.9 dB |
| Pointing Loss | .65 dB |
| Space Loss | 207.7 dB |
| Polarization Loss | .1 dB |
| Atmospheric Loss | .8 dB |
| Ground Station G/T | 40.3 dB/°K |

Table 3.4. Parameters Studied.

Modulator Gain Imbalance

Modulator Phase Imbalance

Data Asymmetry

Data Bit Jitter

Data Static Timing Offset

XTR AM/AM

XTR AM/PM

Static Phase Error

XTR Gain Slope

XTR Gain Flatness

XTR Phase Nonlinearity

Phase Noise R.M.S.

the margin in carrier-to-noise ratio which can be allocated to the various subsystems for hardware degradations. The sensitivity curves show the increase in Shuttle-to-TDRSS CNR needed to offset the performance degradation (relative to the nominal performance) due to the variation of a single parameter at the design error rate of $10^{-4}$.

The error rate curve in Fig. 3.1 represents the BER performance of a Shuttle transponder transmitting a perfect signal (i.e. all user constraints are set to zero). The CNR loss shown (.9 dB) can be attributed to the TDRS and the ground station. This BER curve is reproduced on all other BER plots and labeled "Perfect User." The horizontal distance between this curve and one of the other BER curves represents the CNR loss due to the combined effect of all the user constraints. For the nominal conditions this loss amounts to .75 dB.

Fig. 3.20 shows that by far the biggest contribution of degradation comes from the phase noise which is specified as 10° rms in the 0 to 270 Hz frequency range. As a worst-case assumption this noise power was concentrated in the 100-270 Hz range (i.e. outside the tracking loop bandwidth). A more accurate performance prediction could be made if the noise power inside and outside the tracking loop bandwidth were known separately.

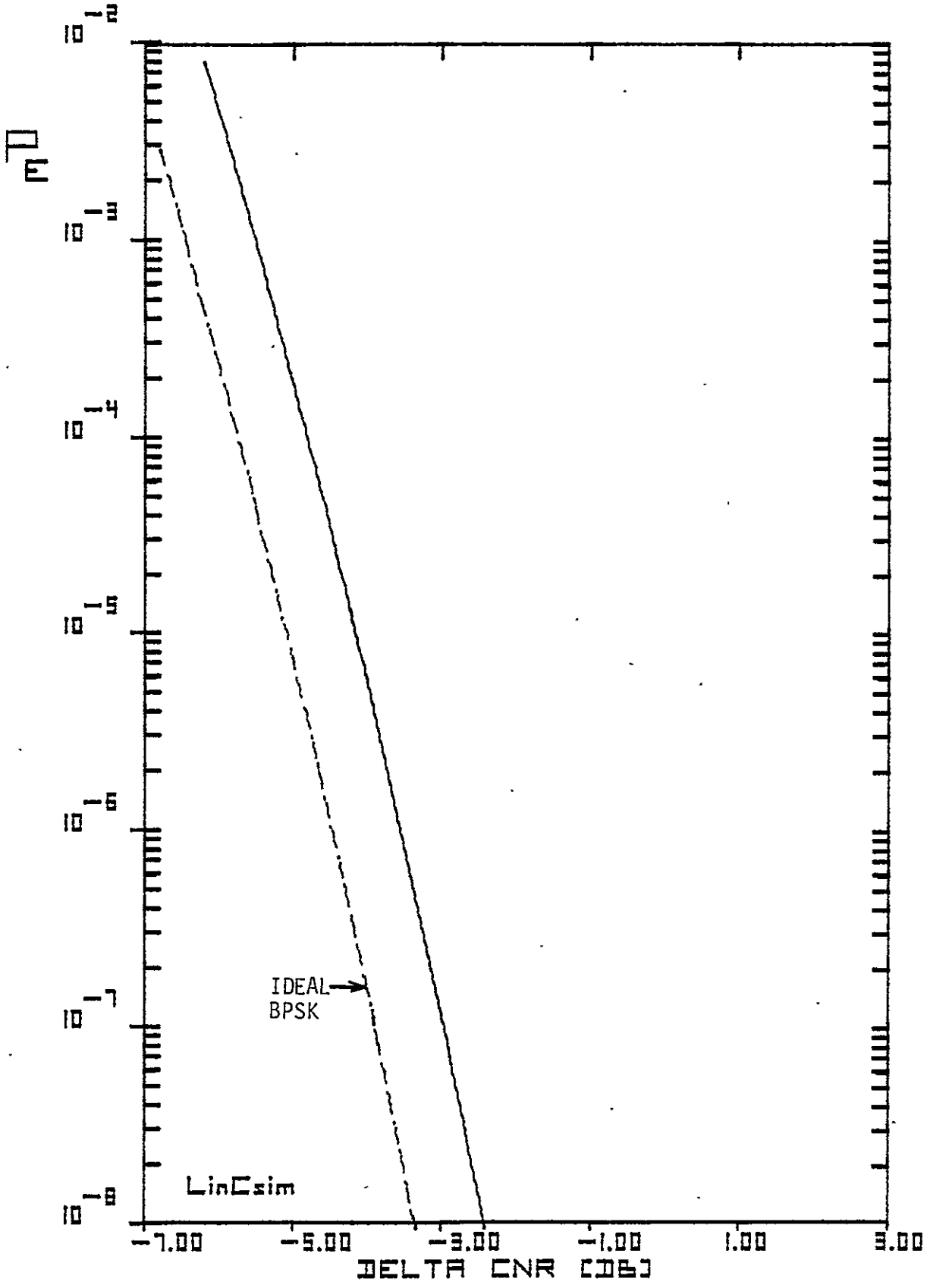


Figure 3.1.BER Plot for Perfect Shuttle Transmitter.

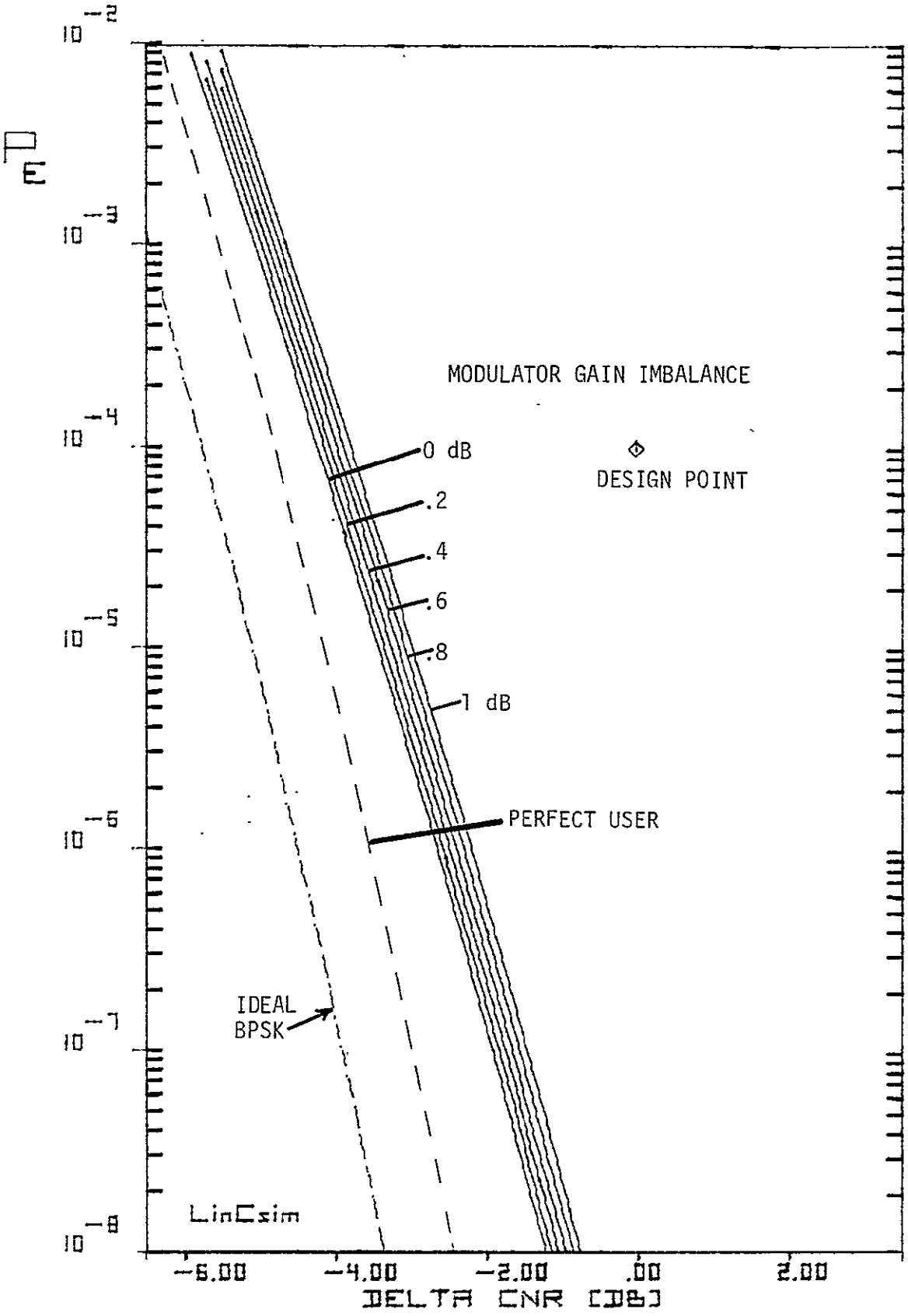


Figure 3.2. BER Plot for Gain Imbalance.

79 0050

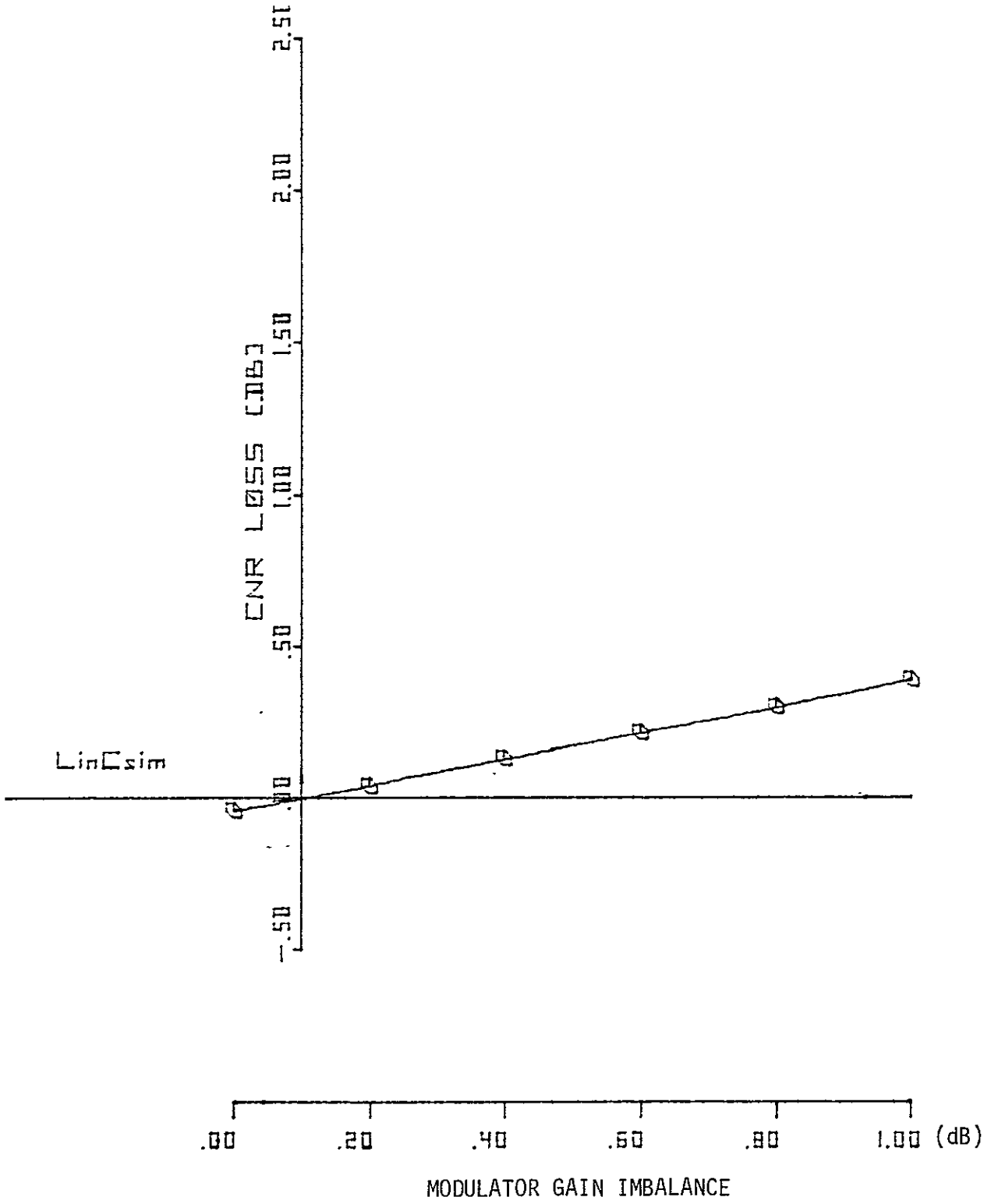


Figure 3.3. Sensitivity Curve.

79 0051

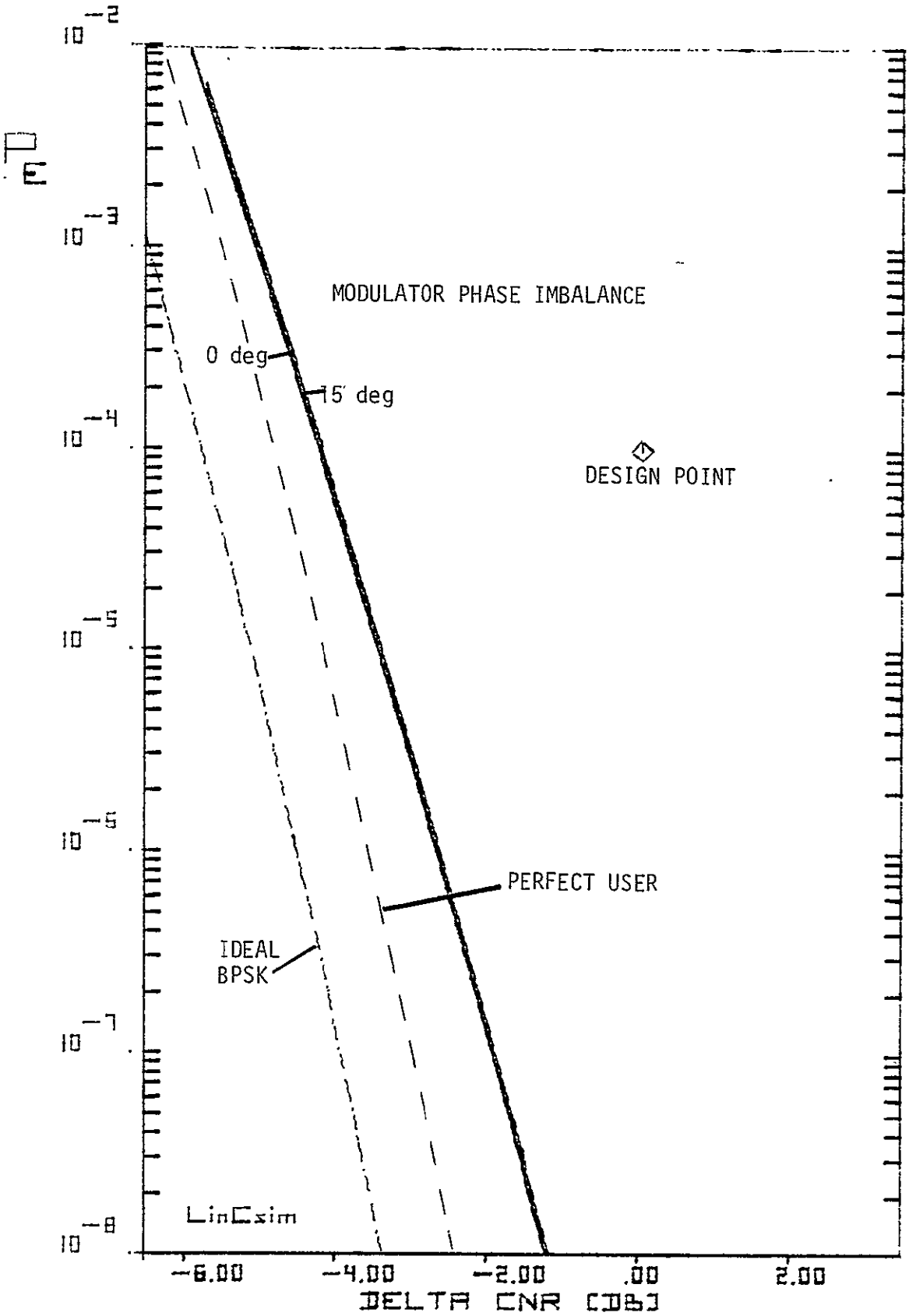


Figure 3.4.BER Plot for Phase Imbalance.

79 0052

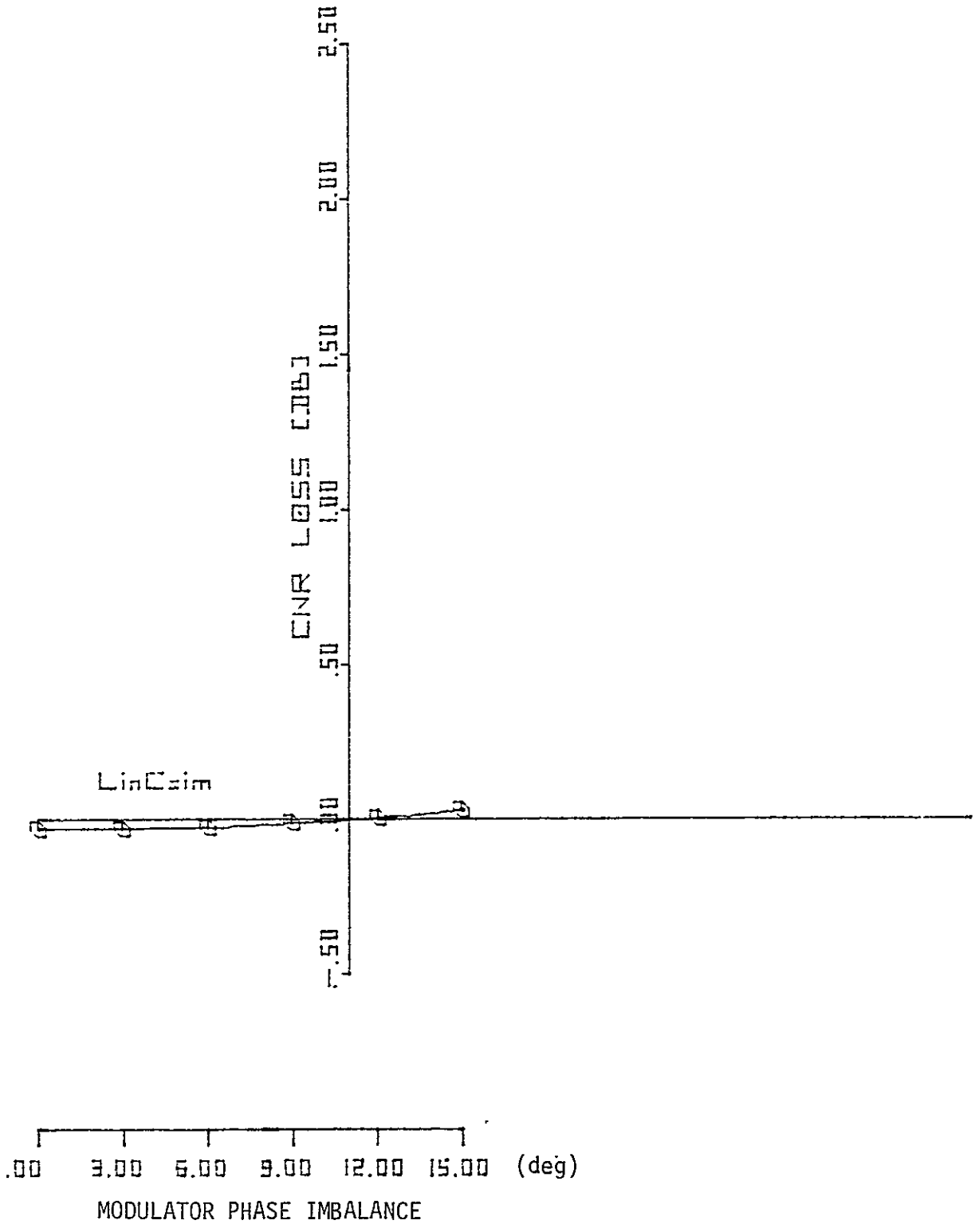


Figure 3.5 Sensitivity Curve.

79 0053

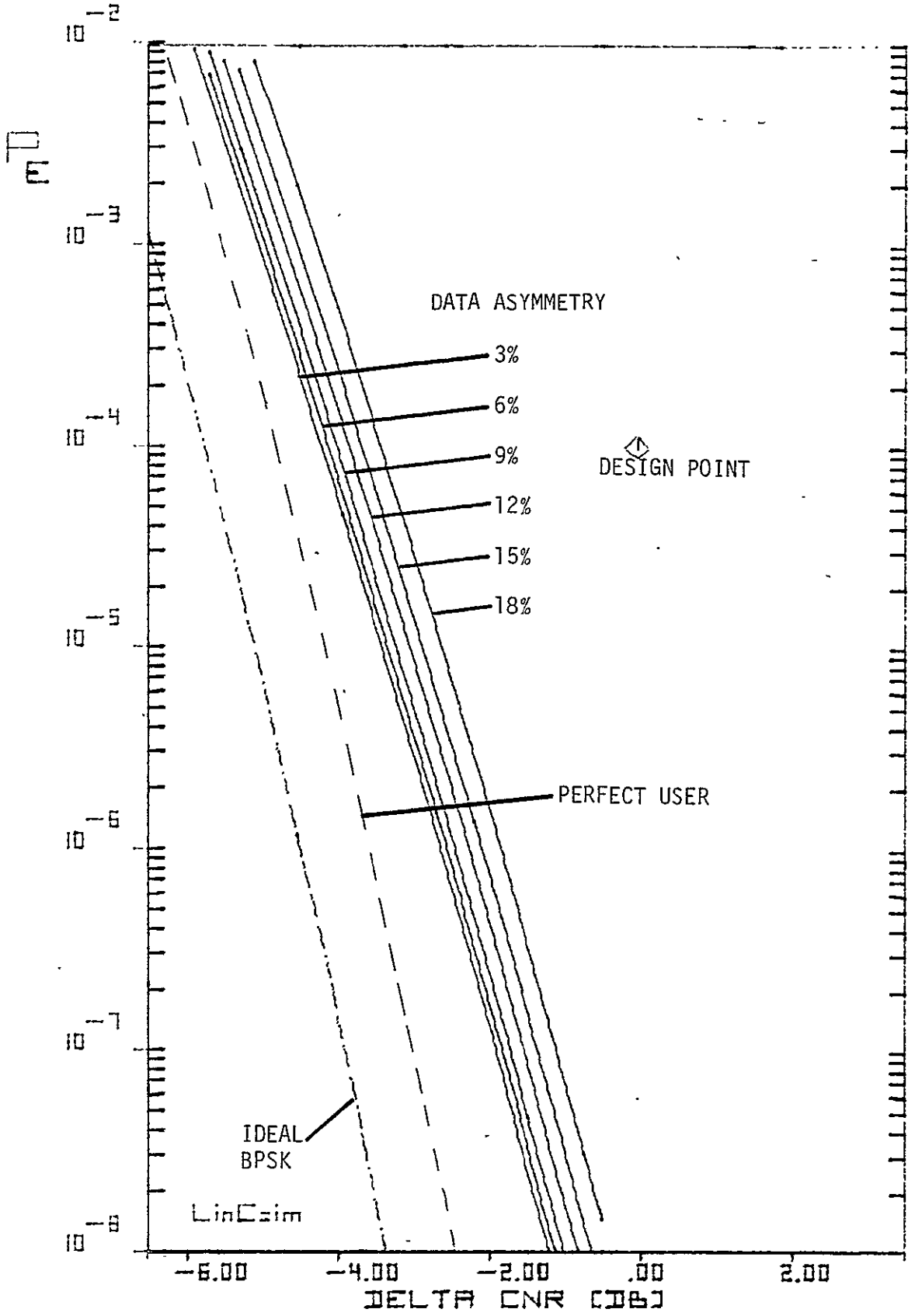


Figure 3.6. BER Plot for Data Asymmetry.

79 0054

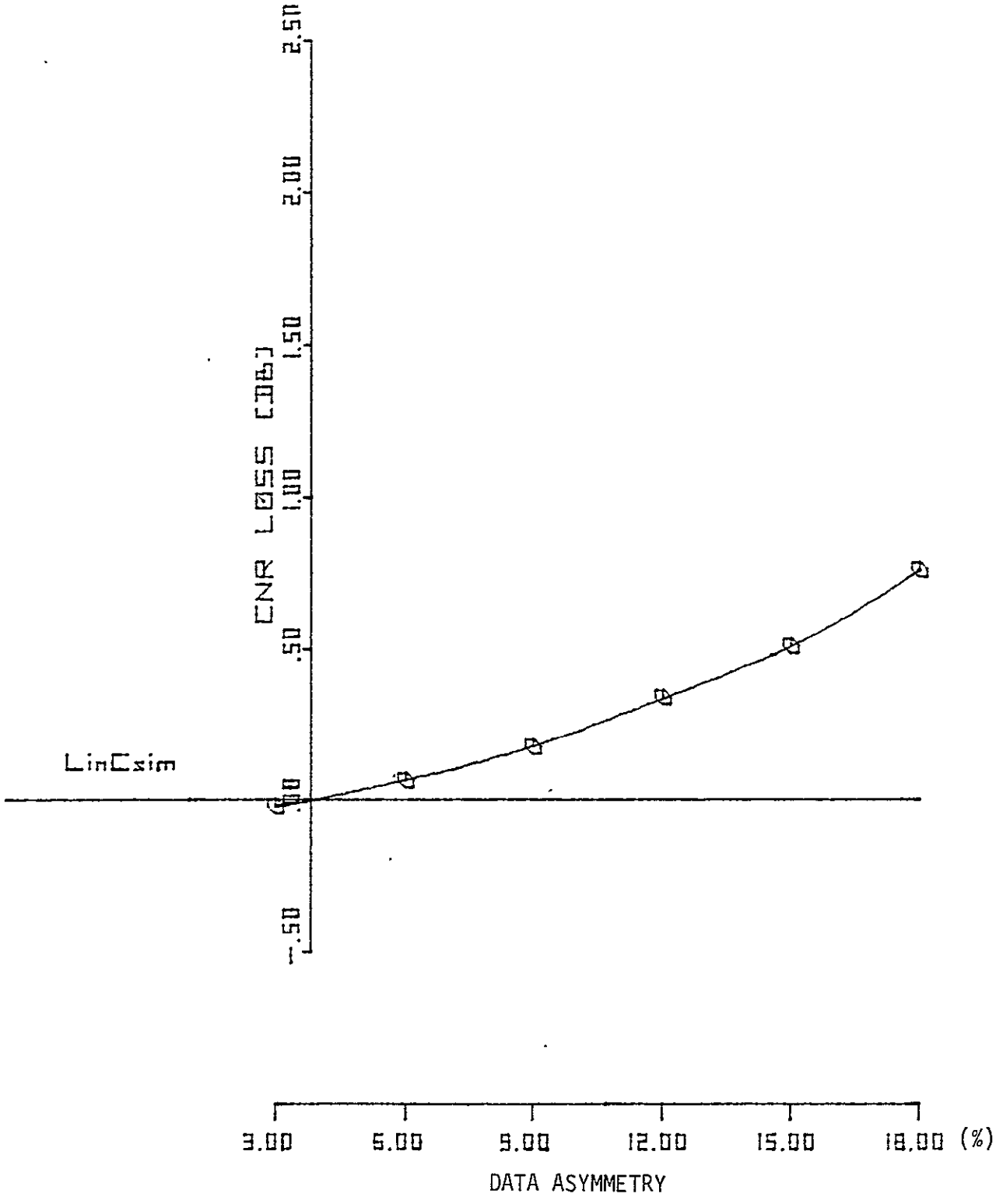


Figure 3,7.Sensitivity Curve.

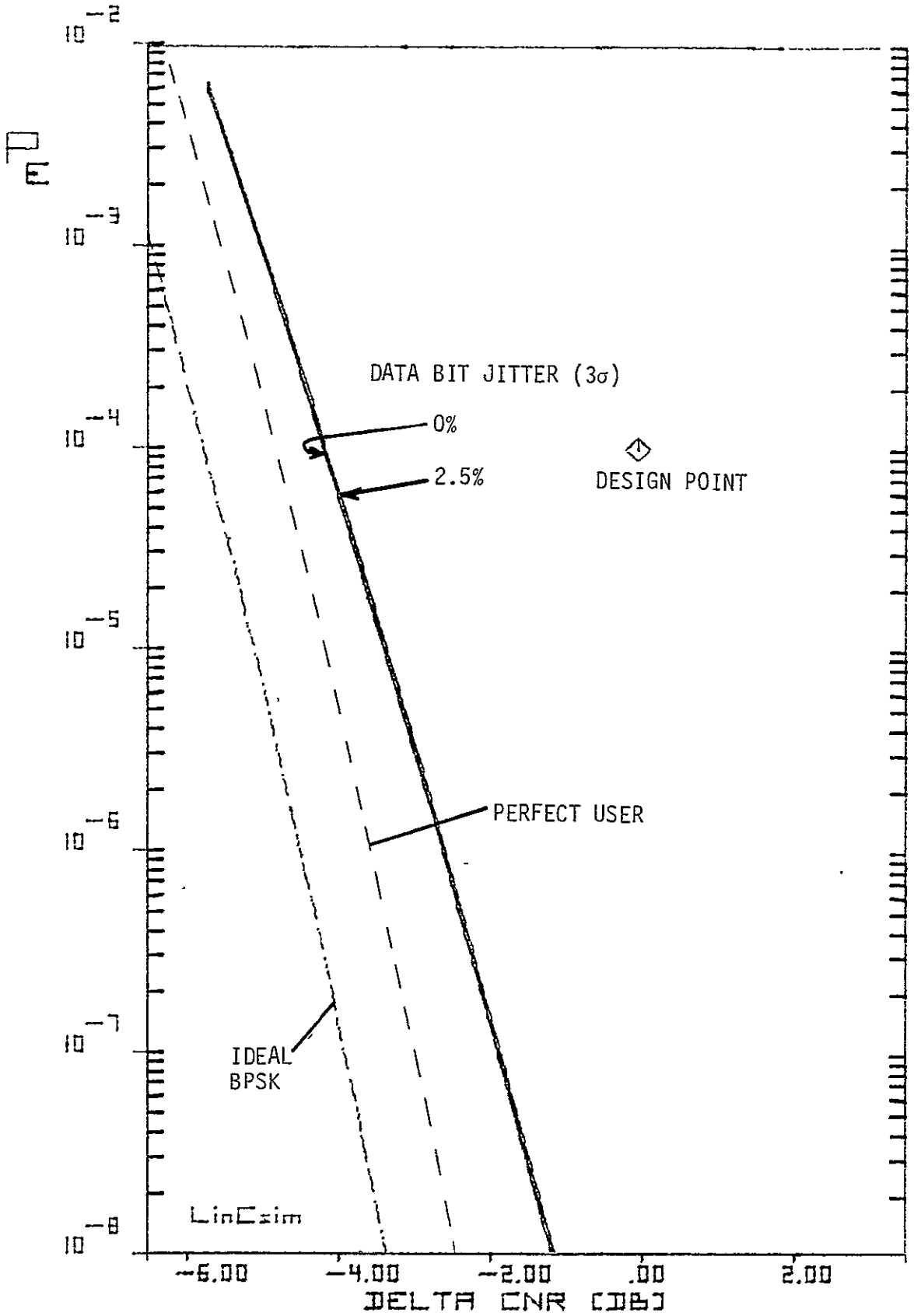


Figure 3.8. BER Plot for Bit Jitter.

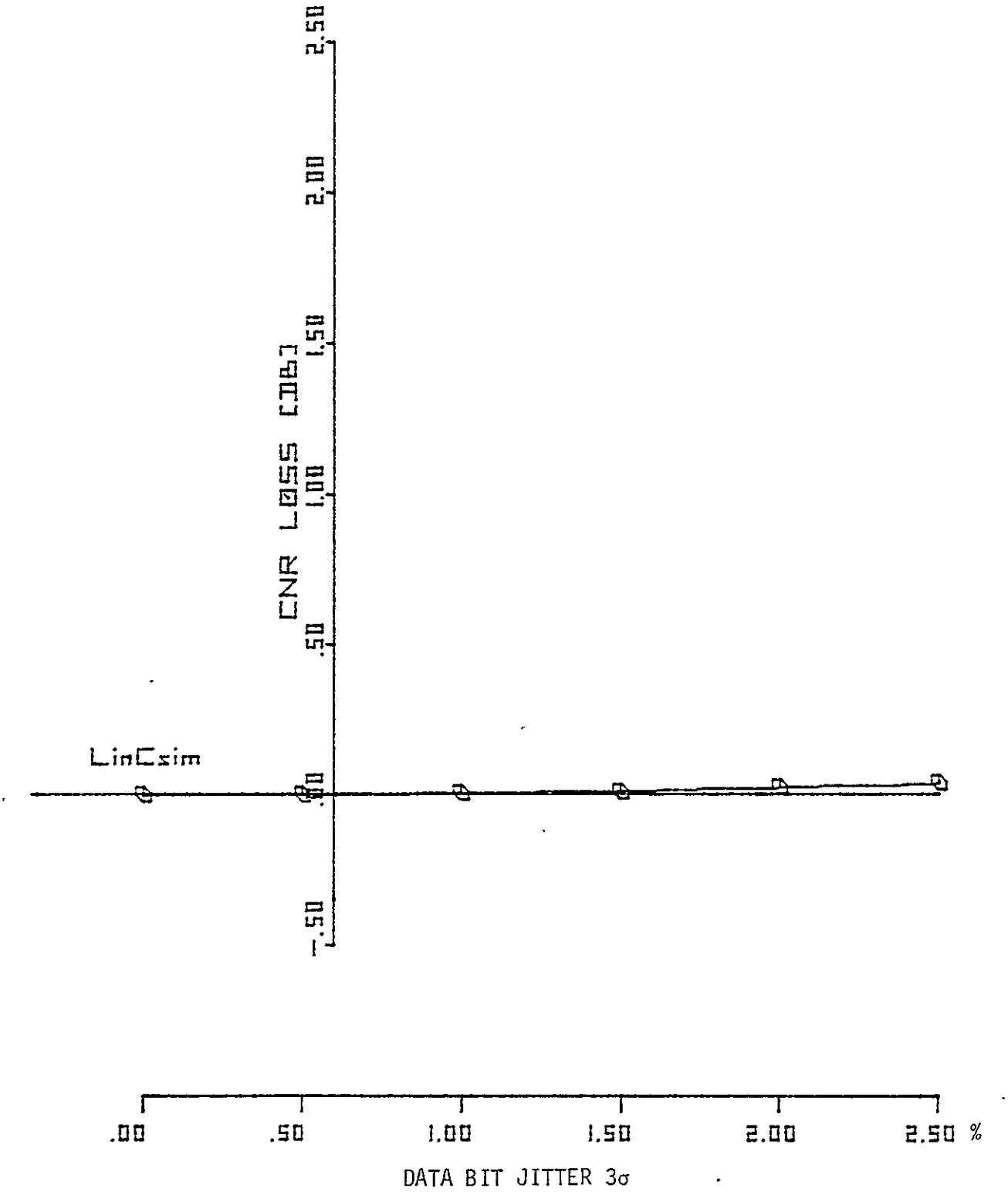


Figure 3.9 .Sensitivity Curve.

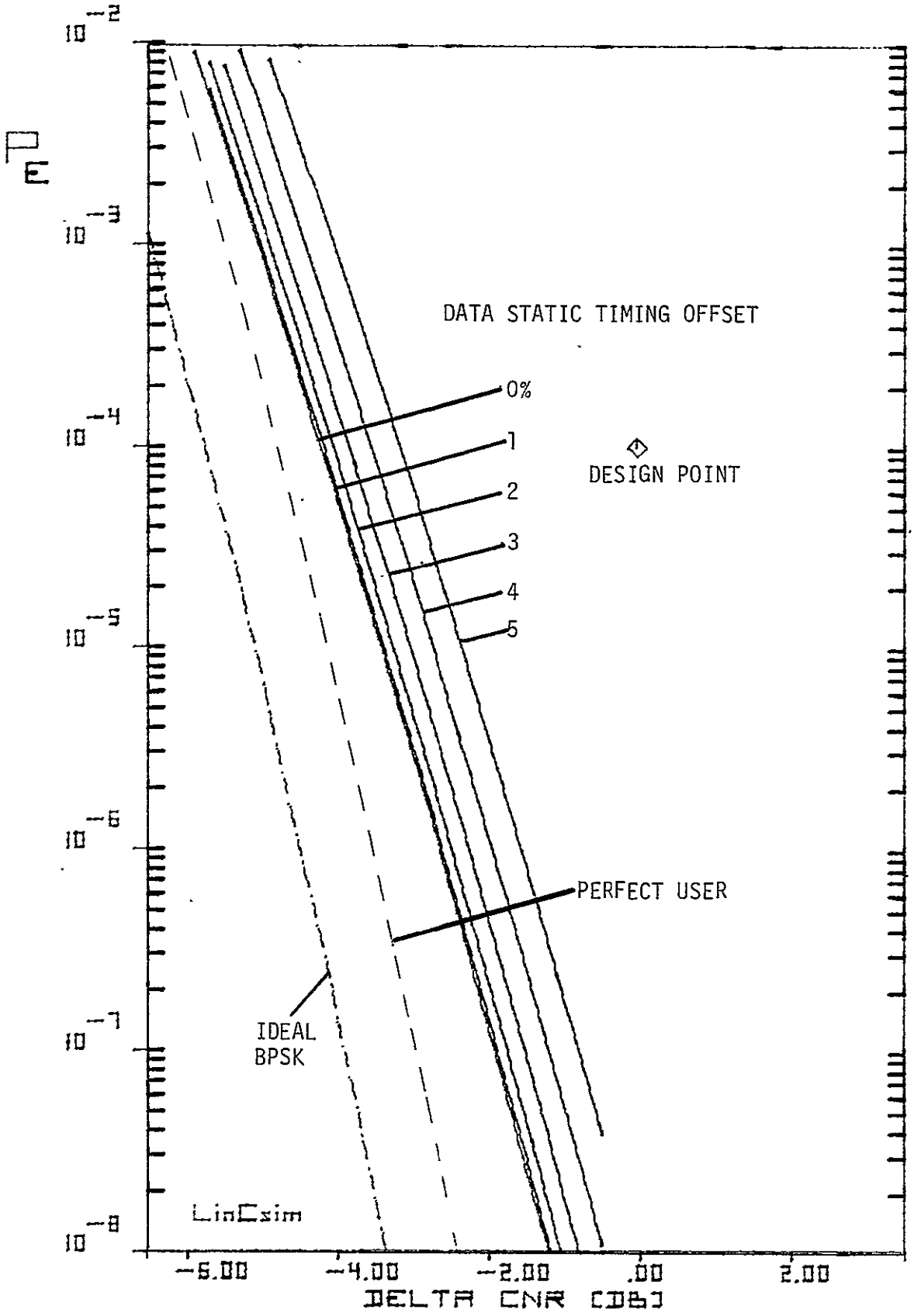


Figure 3.10 BER Plot for Timing Offset.

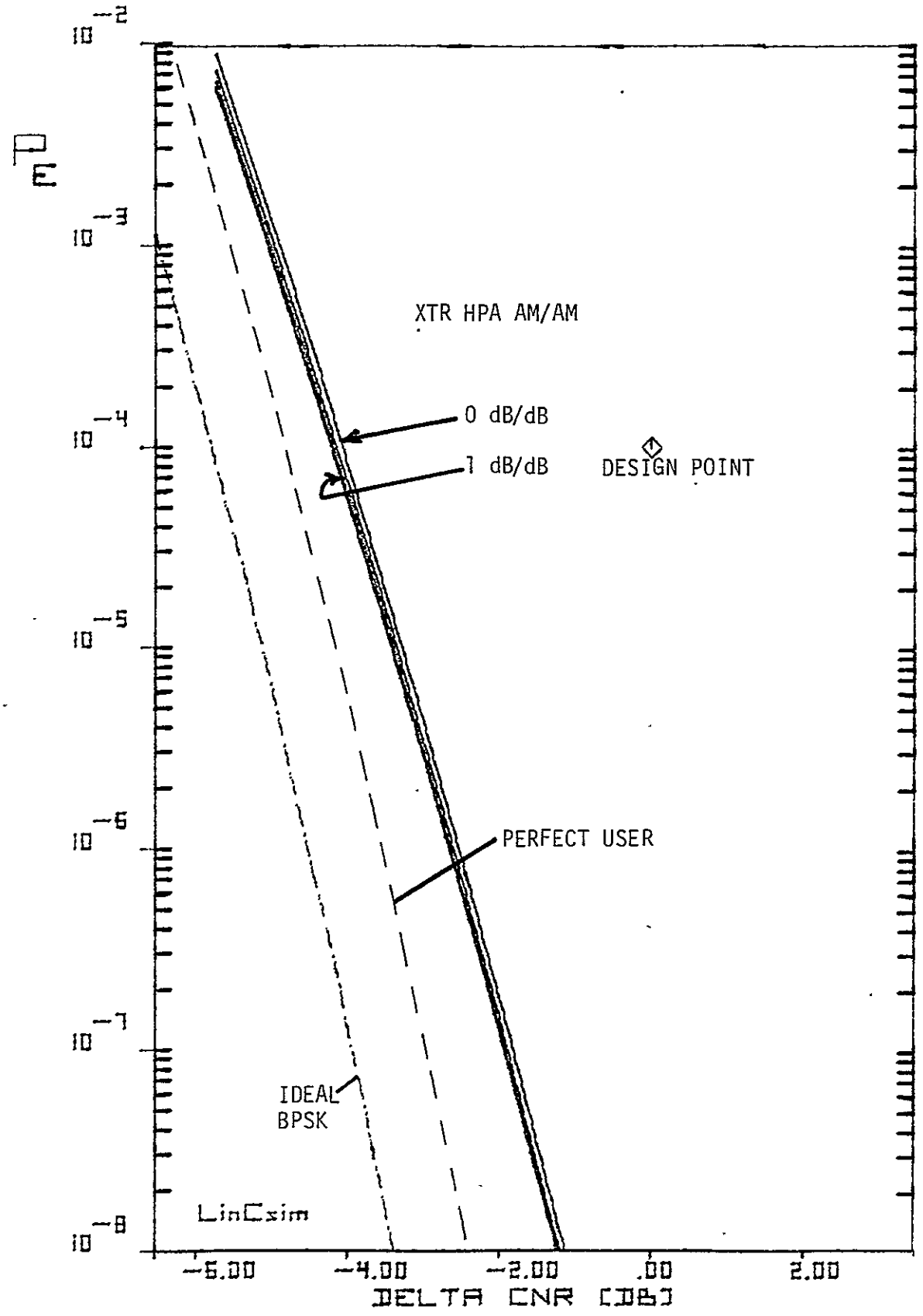


Figure 3.11.BER Plot for AM/AM.

C-2

79 0059

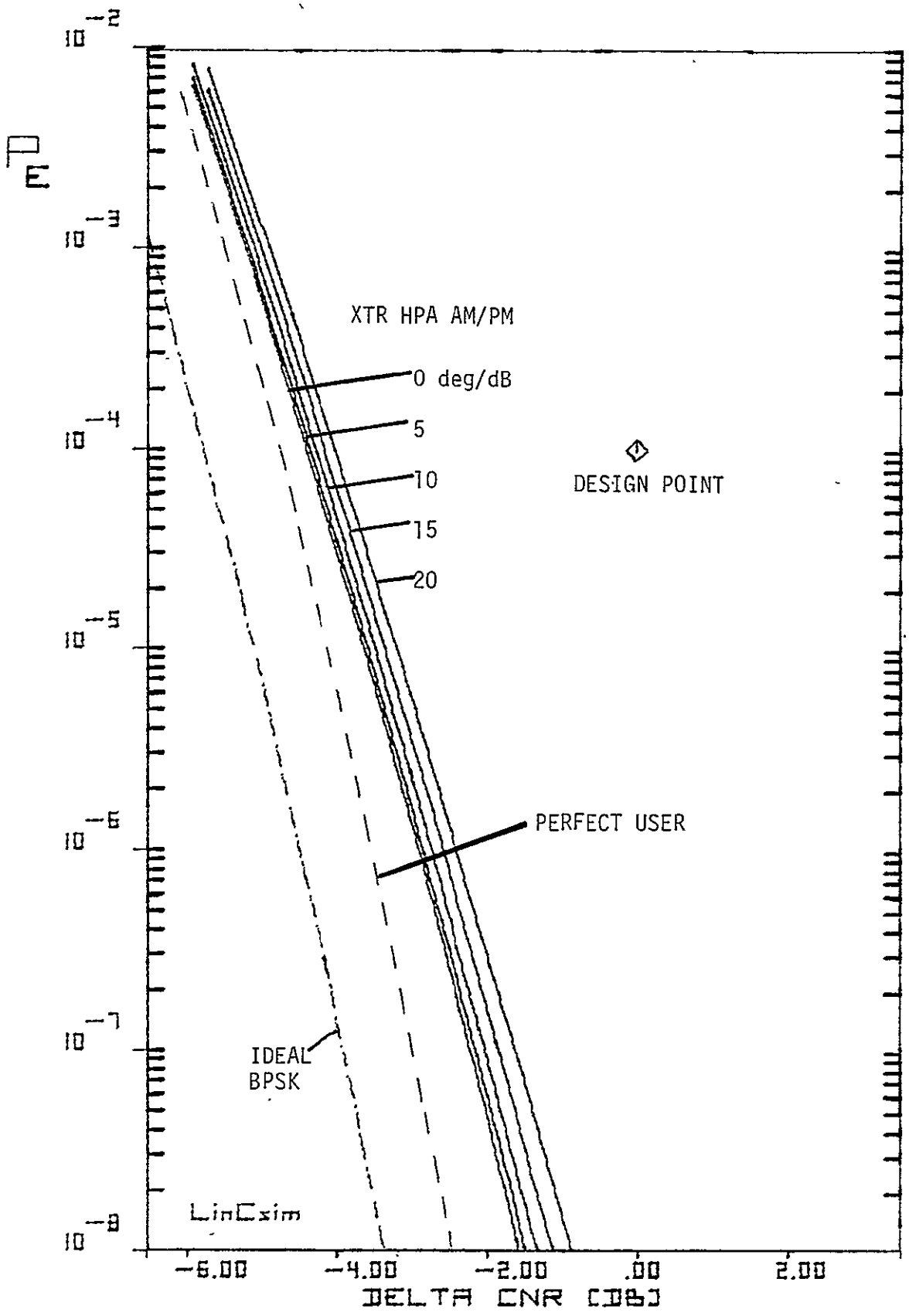


Figure 3.1.2. BER Plot for AM/PM

79 0060

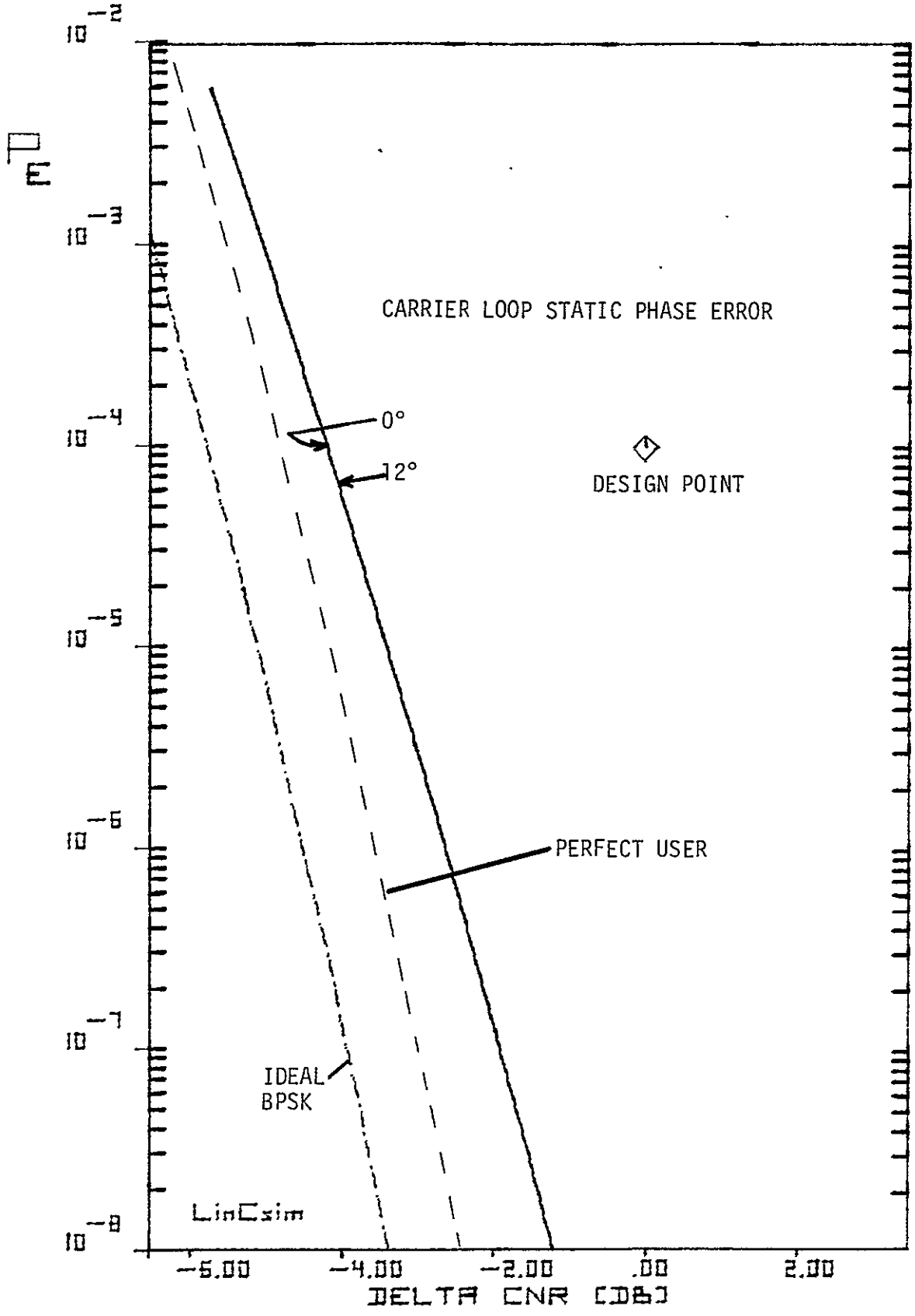


Figure 3.13.BER Plot for Static Phase Error.

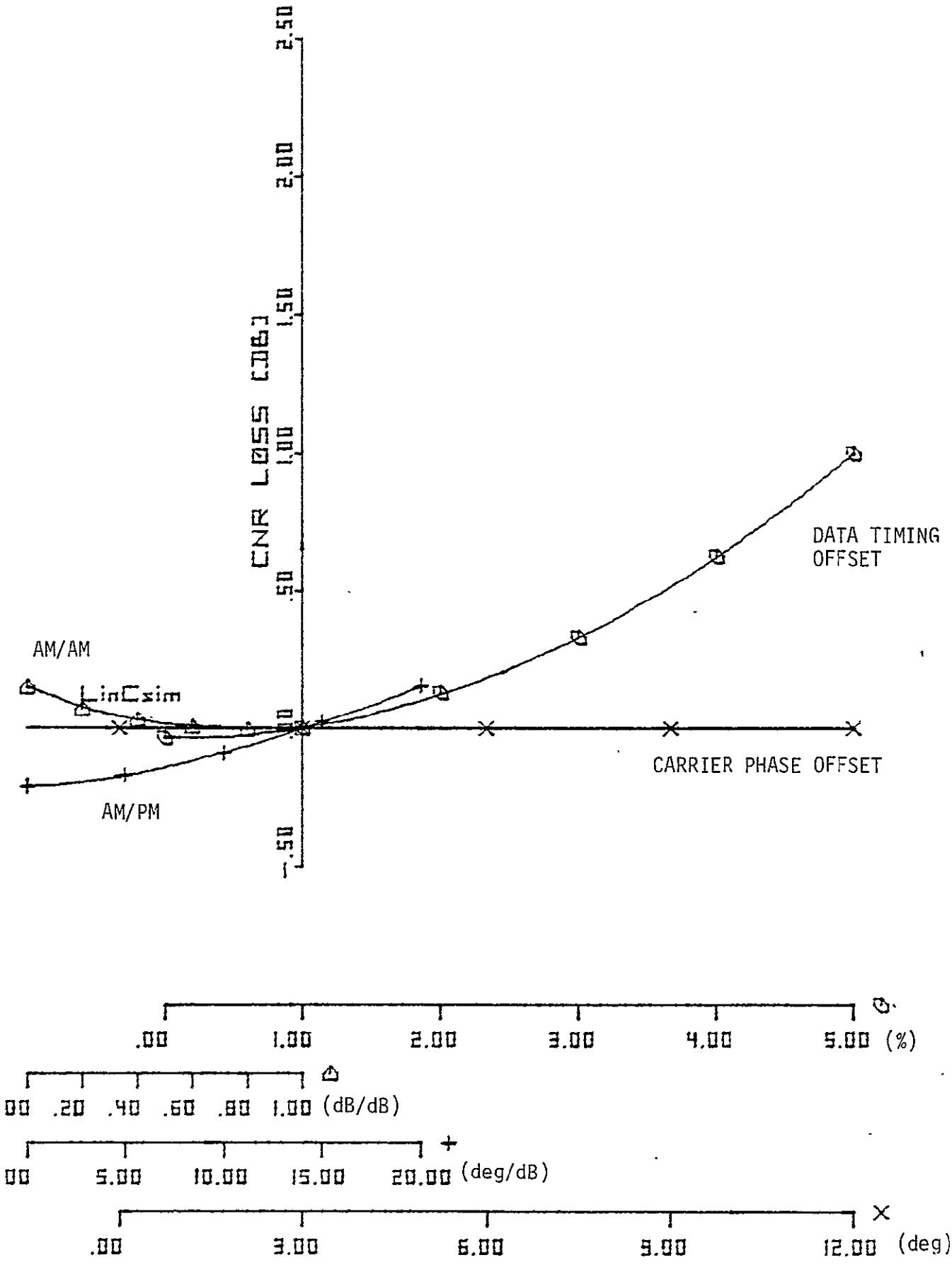


Figure 3.14. Sensitivity Curves.

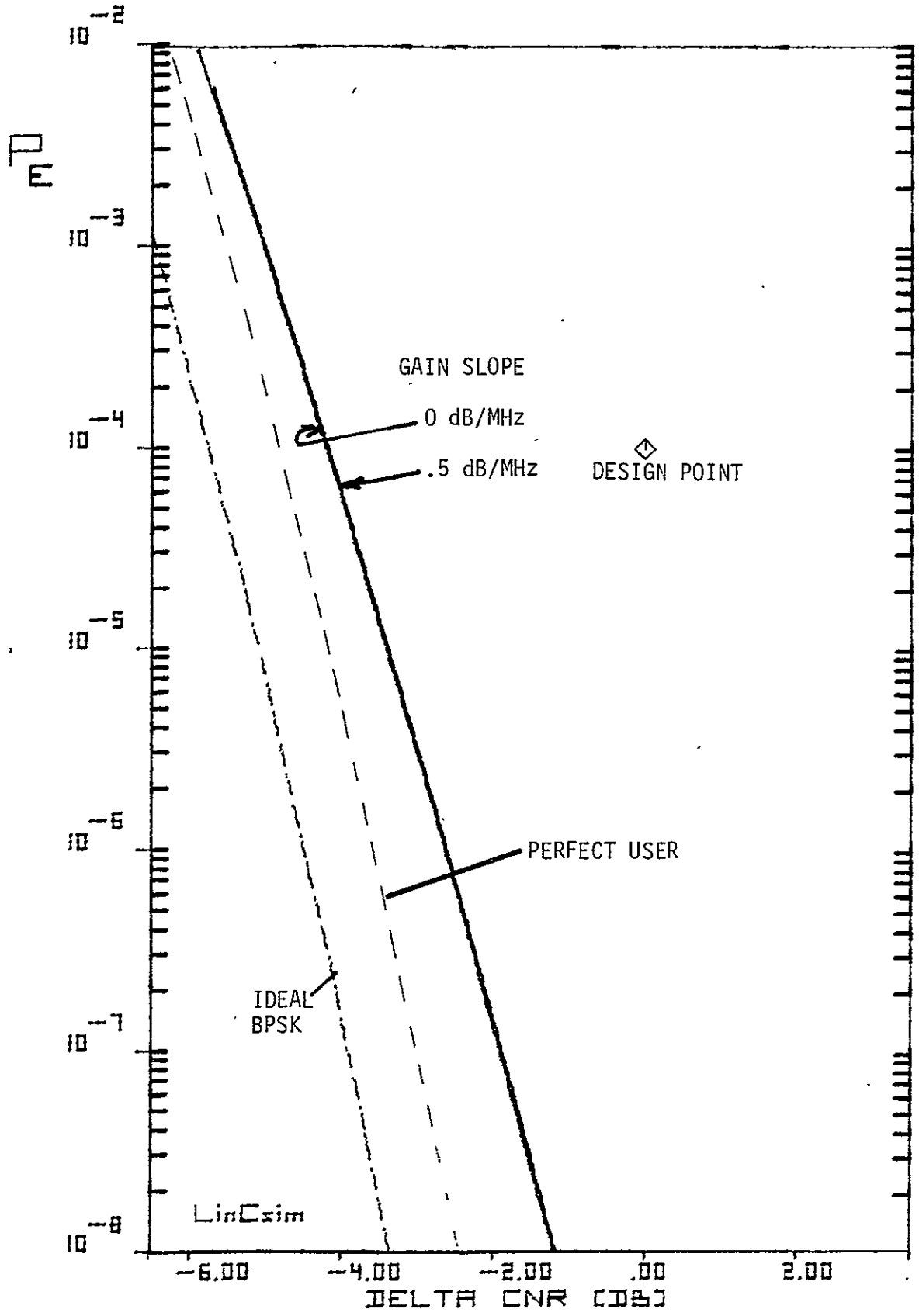


Figure 3.15. BER Plot for Gain Slope.

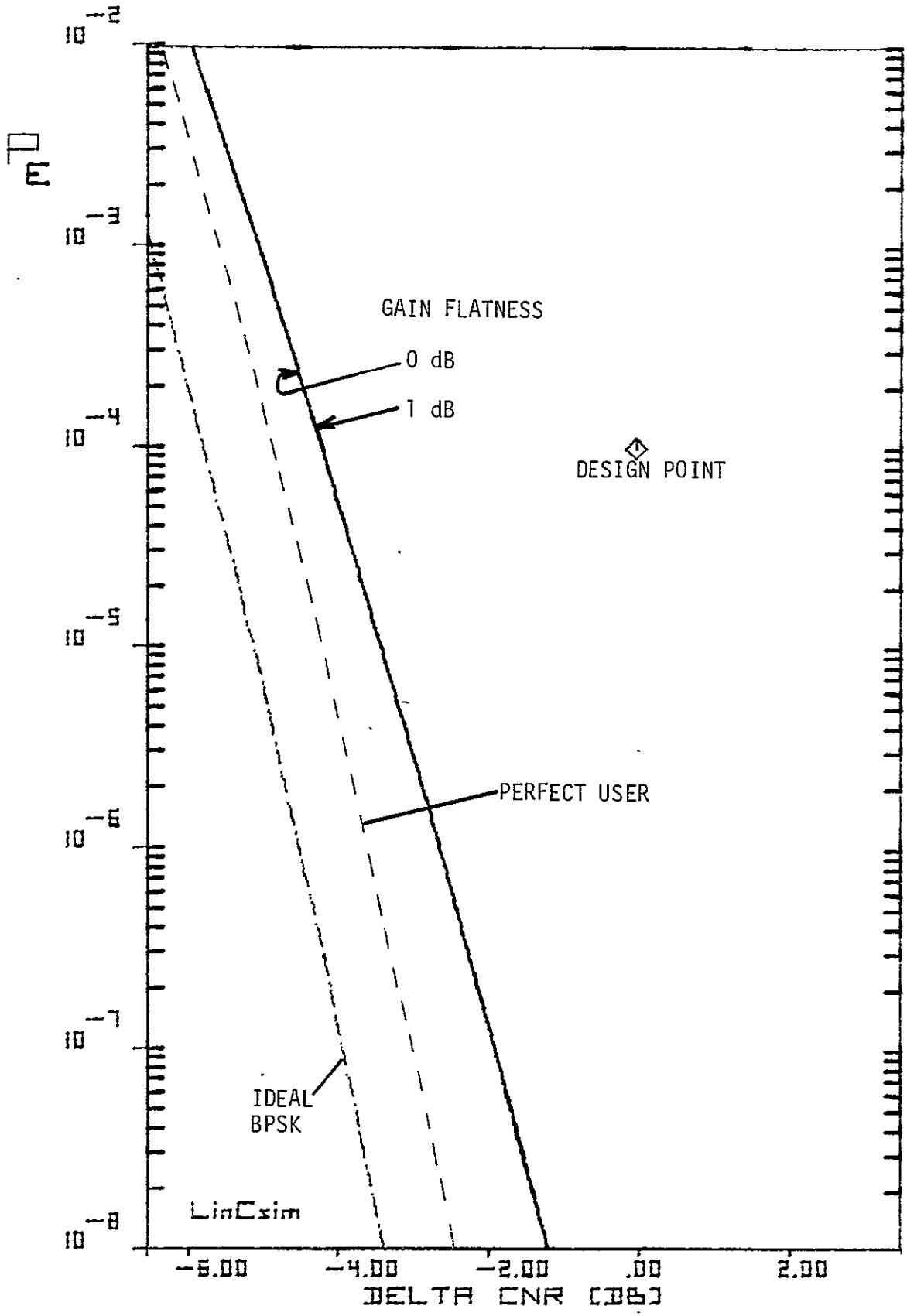


Figure 3.16.BER Plot for Gain Flatness.

79 0064

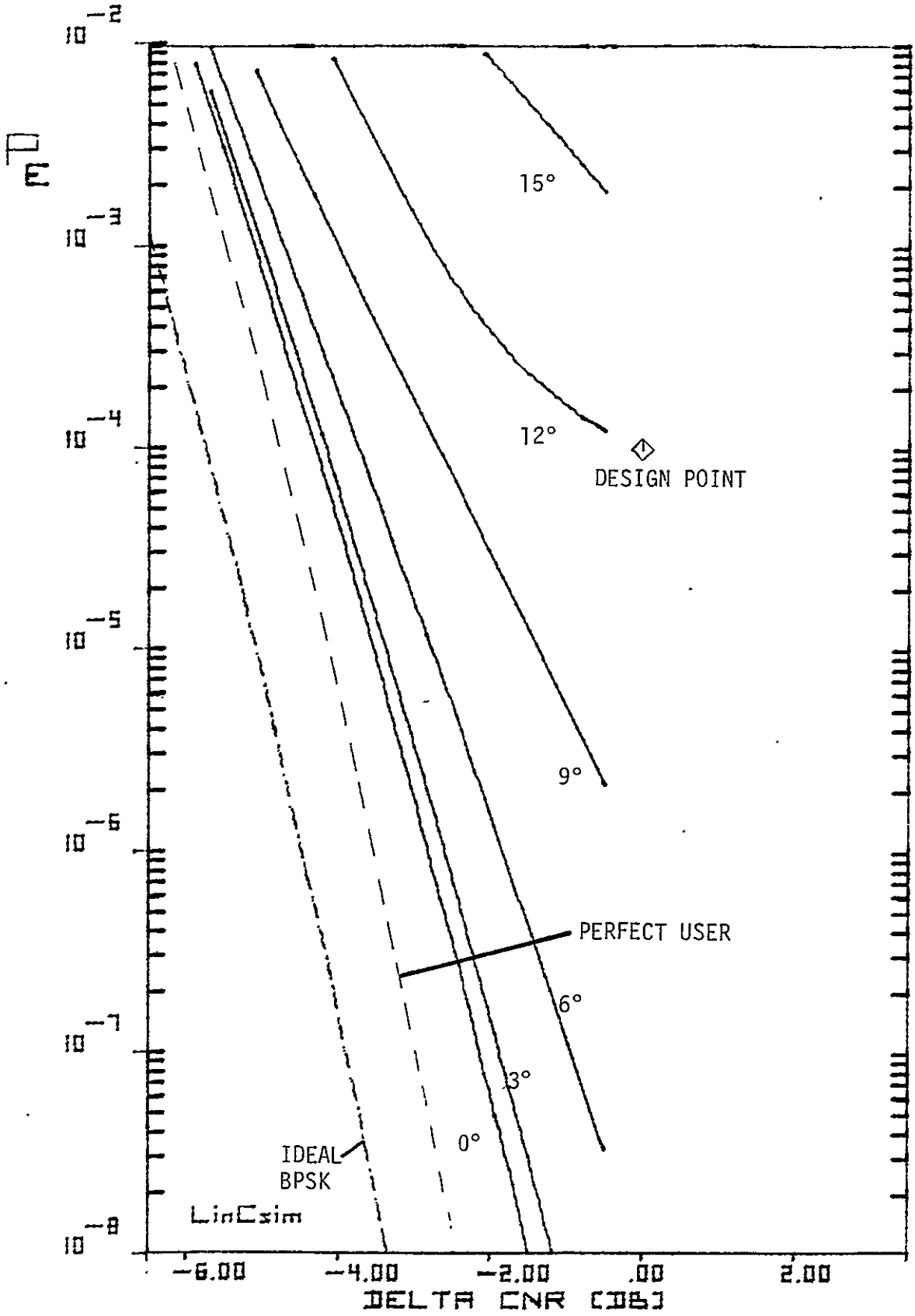


Figure 3.17.BER Plot for Phase Nonlinearity.

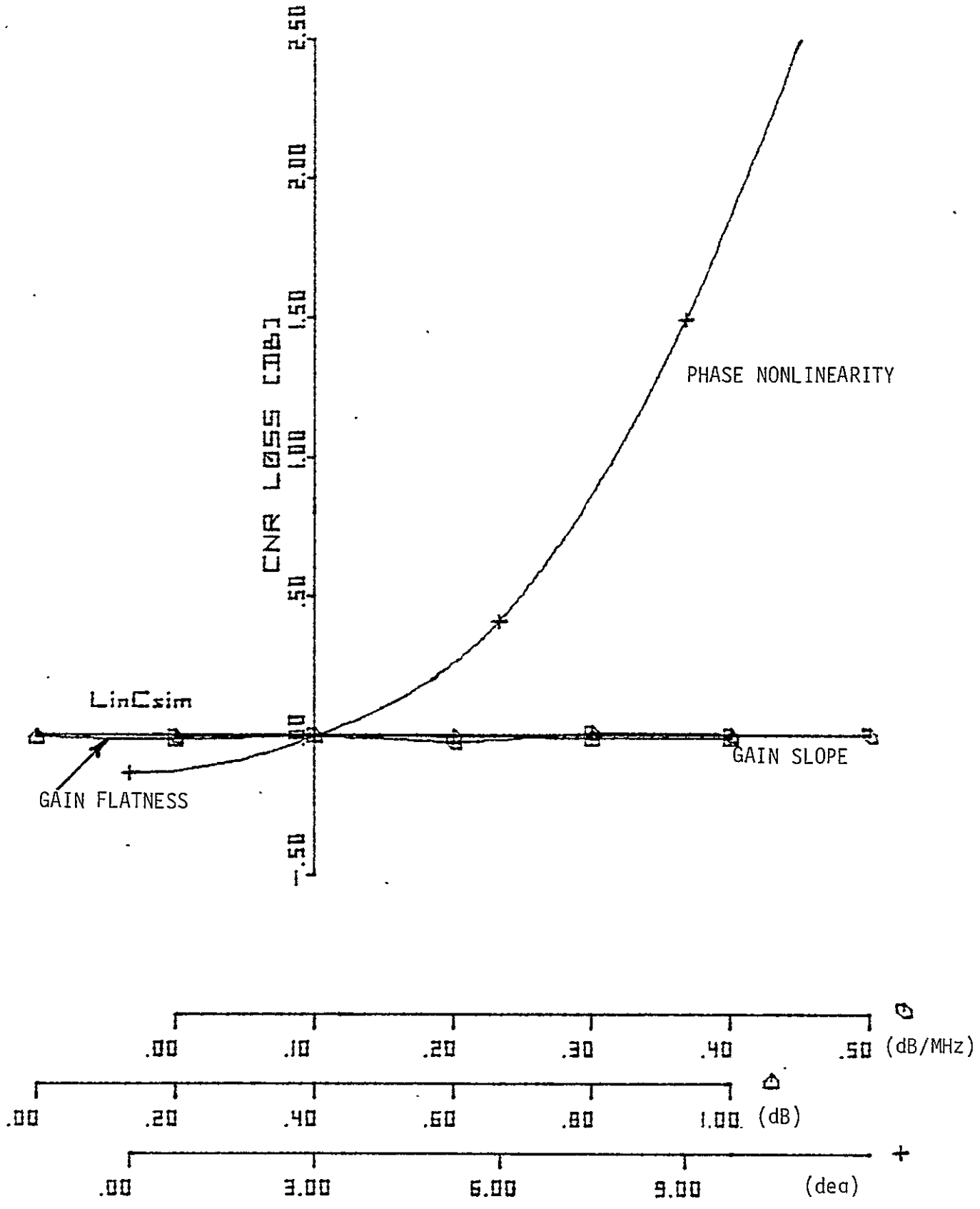


Figure 3.18. Sensitivity Curves.

79 0066

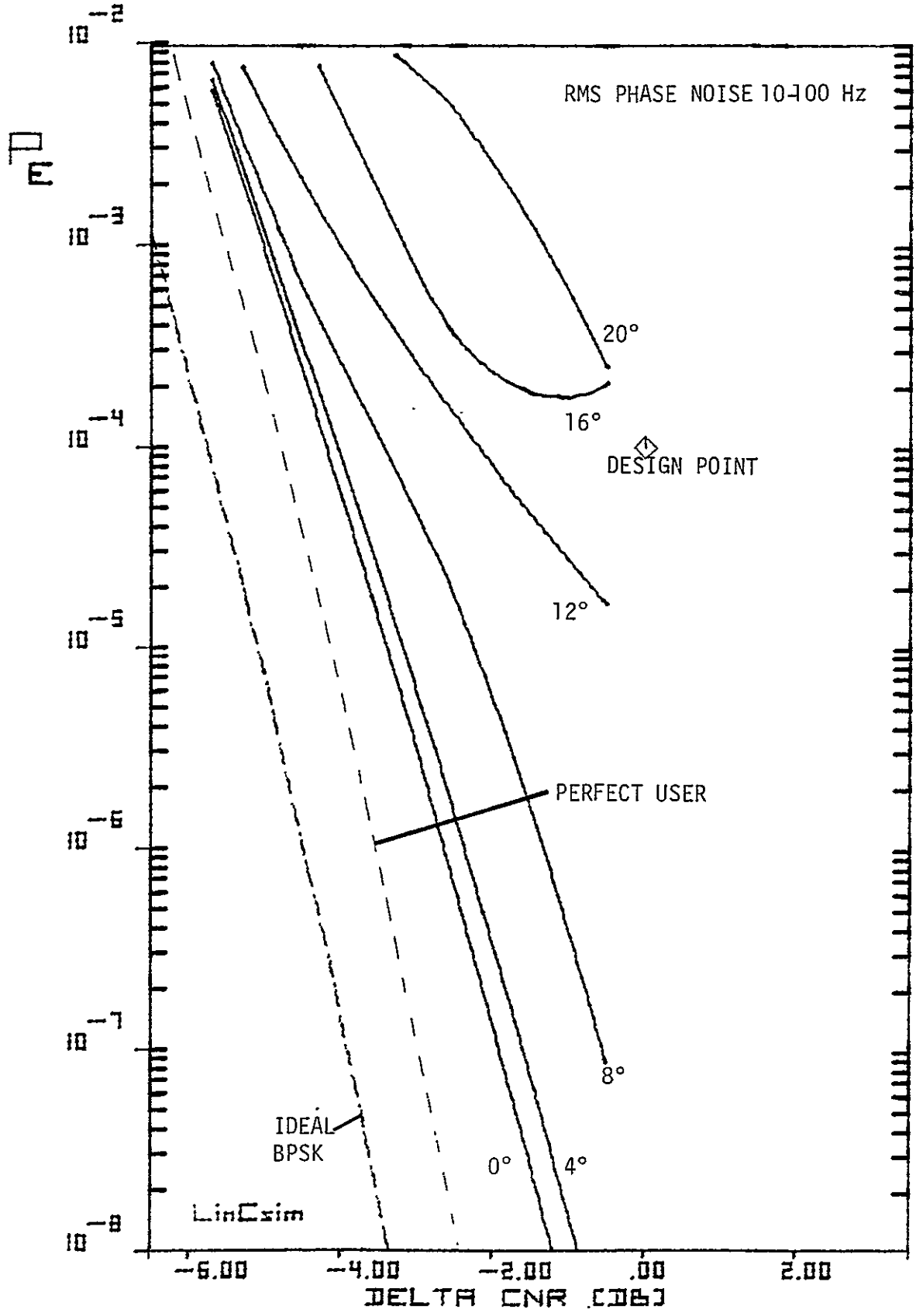


Figure 3.19.BER Plot for Low Frequency Phase Noise.

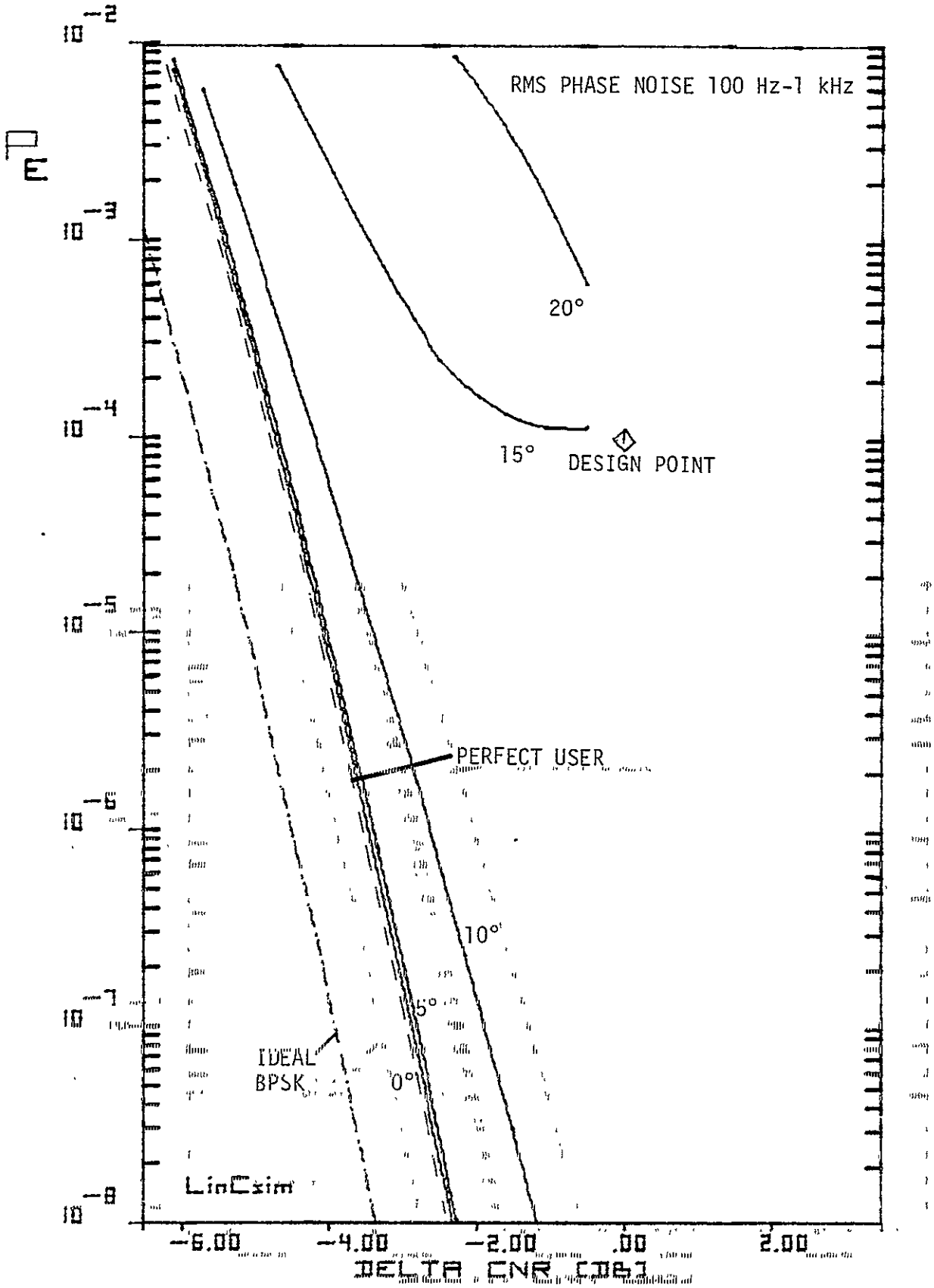


Figure 3-20. BER Plot for Medium Frequency Phase Noise.

79 0068

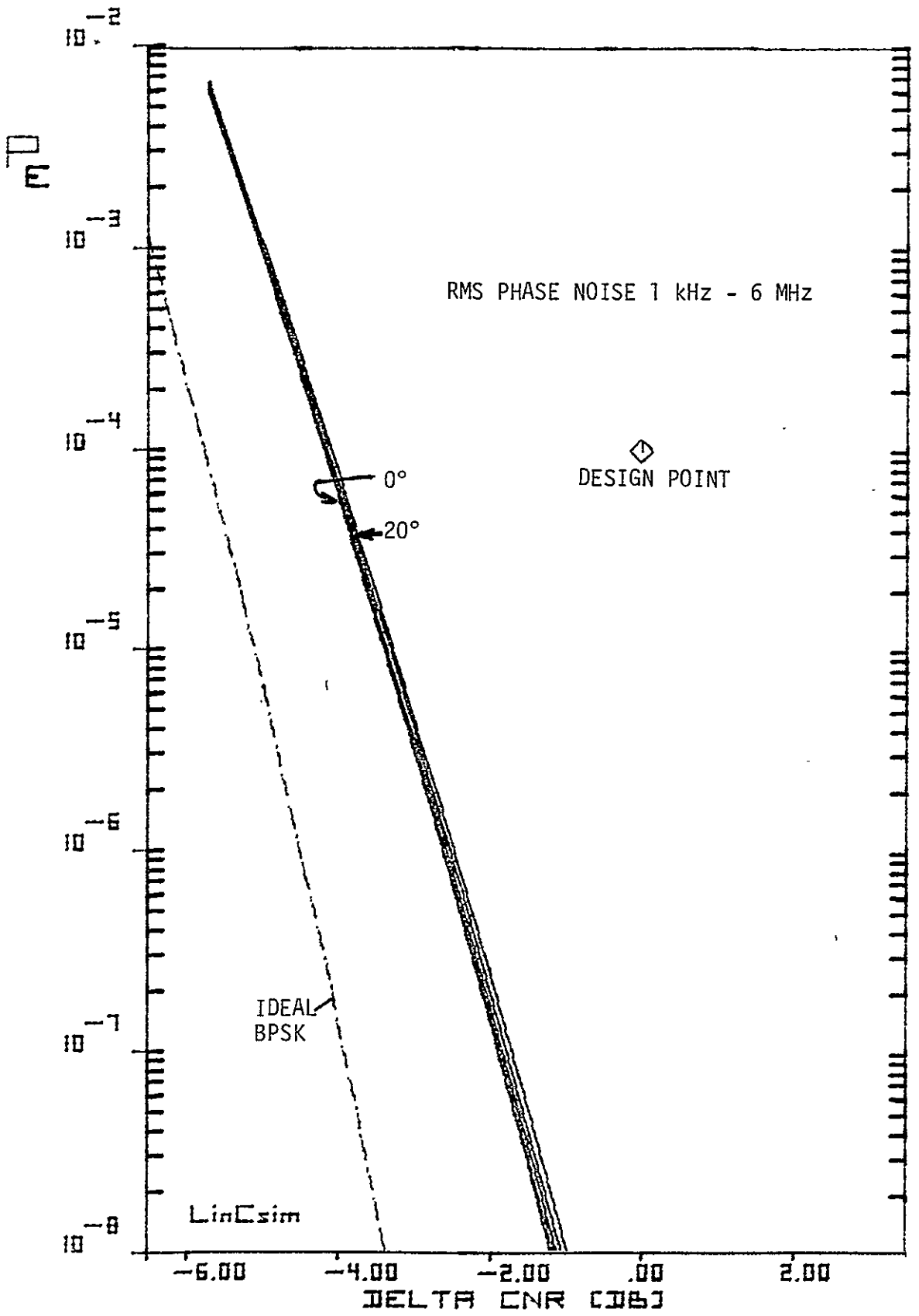


Figure 3.21.BER Plot for High Frequency Noise.

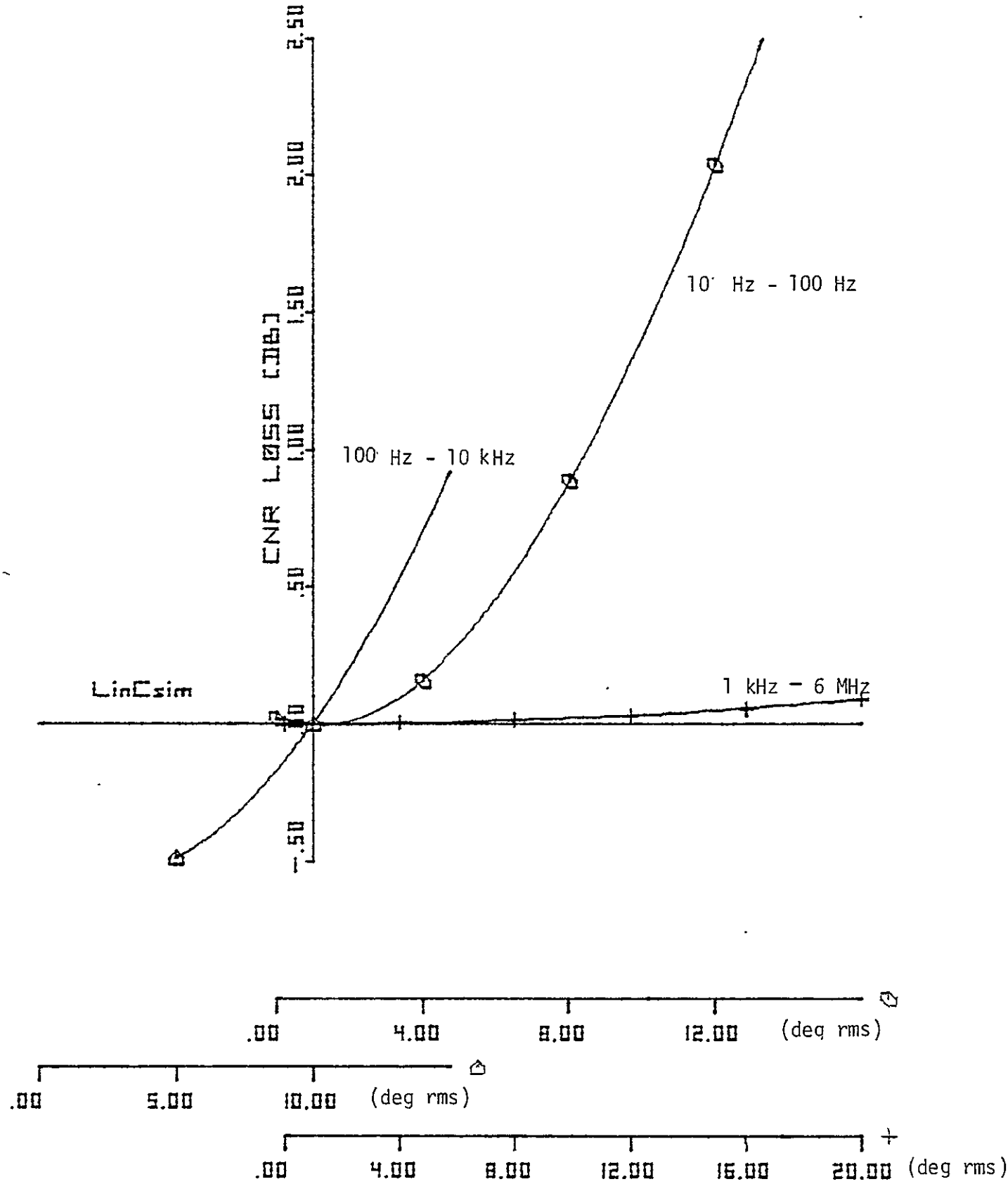


Figure 3.22. Sensitivity Curves for Phase Noise.

79 0070

REFERENCE

[1] Tracking and Data Relay Satellite System (TDRSS) Users' Guide, Revision 3, STDN No. 101.2, Goddard Space Flight Center, Greenbelt, MD, January, 1978.

## 4.0 ATTACHED SPACELAB PAYLOAD BIT JITTER PERFORMANCE

### 4.1 Introduction

In this section the problem of bit jitter on the attached spacelab payload link is studied and the effect on the bit error rate performance is predicted. The analysis also includes the effect of data asymmetry. The results show that the limiting level of acceptable clock jitter at the output of the attached spacelab payload is determined by the sensitivity of the Viterbi decoder to imperfect pulses at the ground station receiver. In Section 4.2 we introduce the mathematical model we have adopted for our analysis. We also present in this section the model we have selected for clock jitter, bit jitter and data asymmetry. Based on laboratory measurements, we have determined the shape of the possible data sequences out of the attached spacelab into the Ku-band Space Shuttle equipment. These various pulse shapes are also presented in Section 4.2. In Section 4.3 we derive an expression for the bit error rate at the spacelab Ku-band transmitter interface due to imperfect timing. We then show that for the available SNR the effect of an acceptable level of clock jitter at the ground receiver has a negligible impact on the overall link performance even for a biased sampling time of $\pm$12.5% in the Shuttle repeater. (This figure for the maximum bias was given to LinCom by JSC personnel. Note, however, that this does not agree with the description in [3]. According to this source the worst-case sampling point is 5 nsec from the transition. At the highest data rate of 50 Mbits/sec this is equivalent to 25% of the bit-

time. Hence the maximum bias would also be 25%.) The coded link bit jitter performance is analyzed in Section 4.4. We show in this section how a completely soft Viterbi decoder significantly ameliorates the effect of imperfect pulses at the output of the Ku-band transmitter. Finally, in Section 4.5 we summarize the results and present some conclusions on the effect of clock and bit jitter on the overall system performance.

## 4.2 System Model, Clock Jitter and Data Asymmetry

The mathematical system model we have adopted for our analysis is as shown in Figure 4.1. Notice that although this is a simplified model of the overall system it allows us to accurately represent the various sources of link performance degradation. It is assumed first that the data flow from the attached spacelab payload to the Ku-band Shuttle transmitter is at baseband. The shape of the pulses carrying the data has been determined from laboratory measurement (4.2) and for the purpose of our analysis they will be assumed to be as shown for a typical case in Figure 4.3a Other typical pulse sequences are shown in Figure 4.3b. The clock information entering into the Ku-band transmitter is assumed to be emanating from an imperfect oscillator. The phase detector output $\varepsilon(t)$ of the clock regenerator circuit will then be a random process whose statistics depend on the oscillator phase noise characteristic. If we now sample this process $\varepsilon(t)$ at times $t^*$ and $t^*+\overline{T}$ where $\overline{T}$ is the inverse of the symbol rate, then we obtain two random variables $\varepsilon(t^*)$ and $\varepsilon(t^*+\overline{T})$. Pictorially we have the following situation:

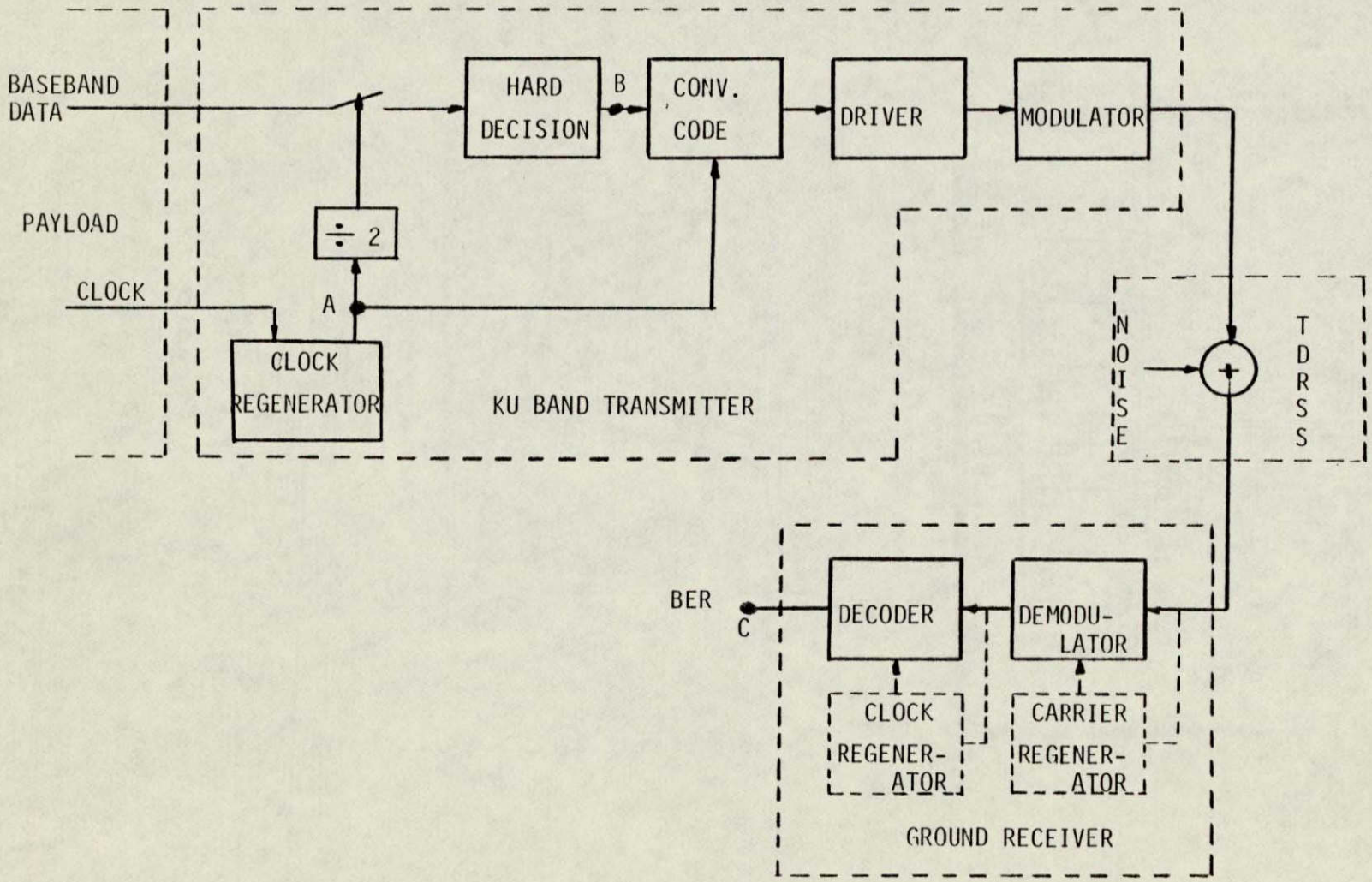


Figure 4.1. MATHEMATICAL SYSTEM BLOCK DIAGRAM

Figure 4.2. HRM Clock Analysis.

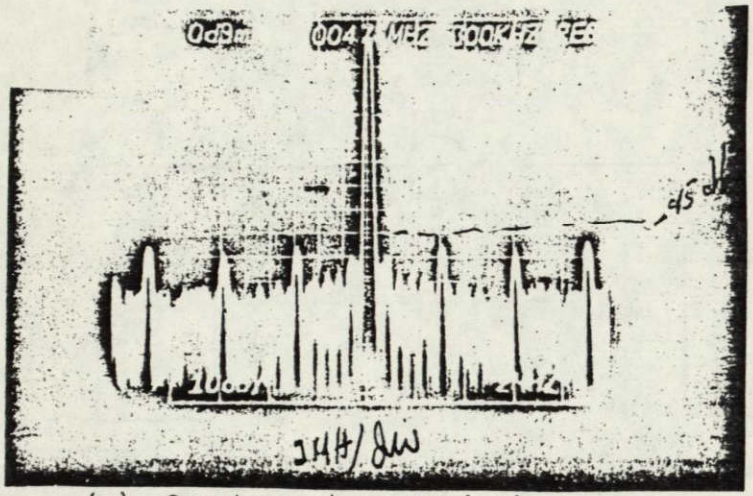


(a) Spectrum characteristic

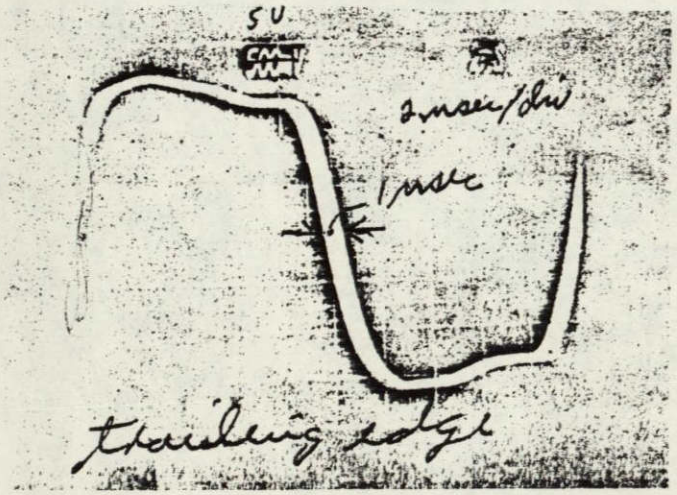


(b) Pulse shape characteristic. Trailing edge.

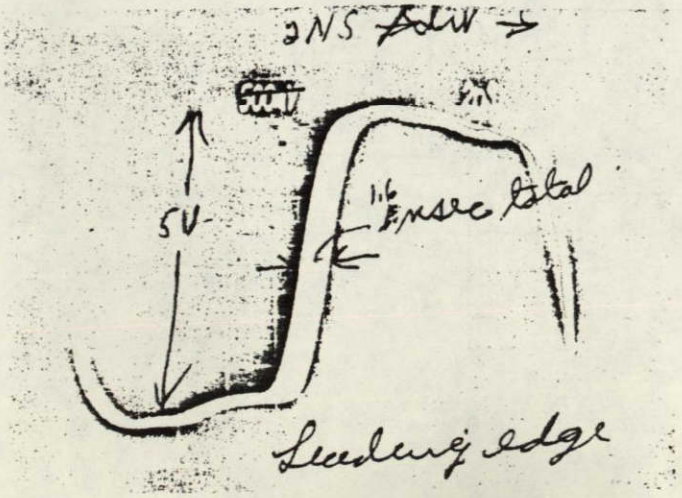


(c) Pulse Characteristic. Leading edge

78 0539

Figure 4.3a. NORMALIZED PULSE SHAPE CHARACTERISTIC

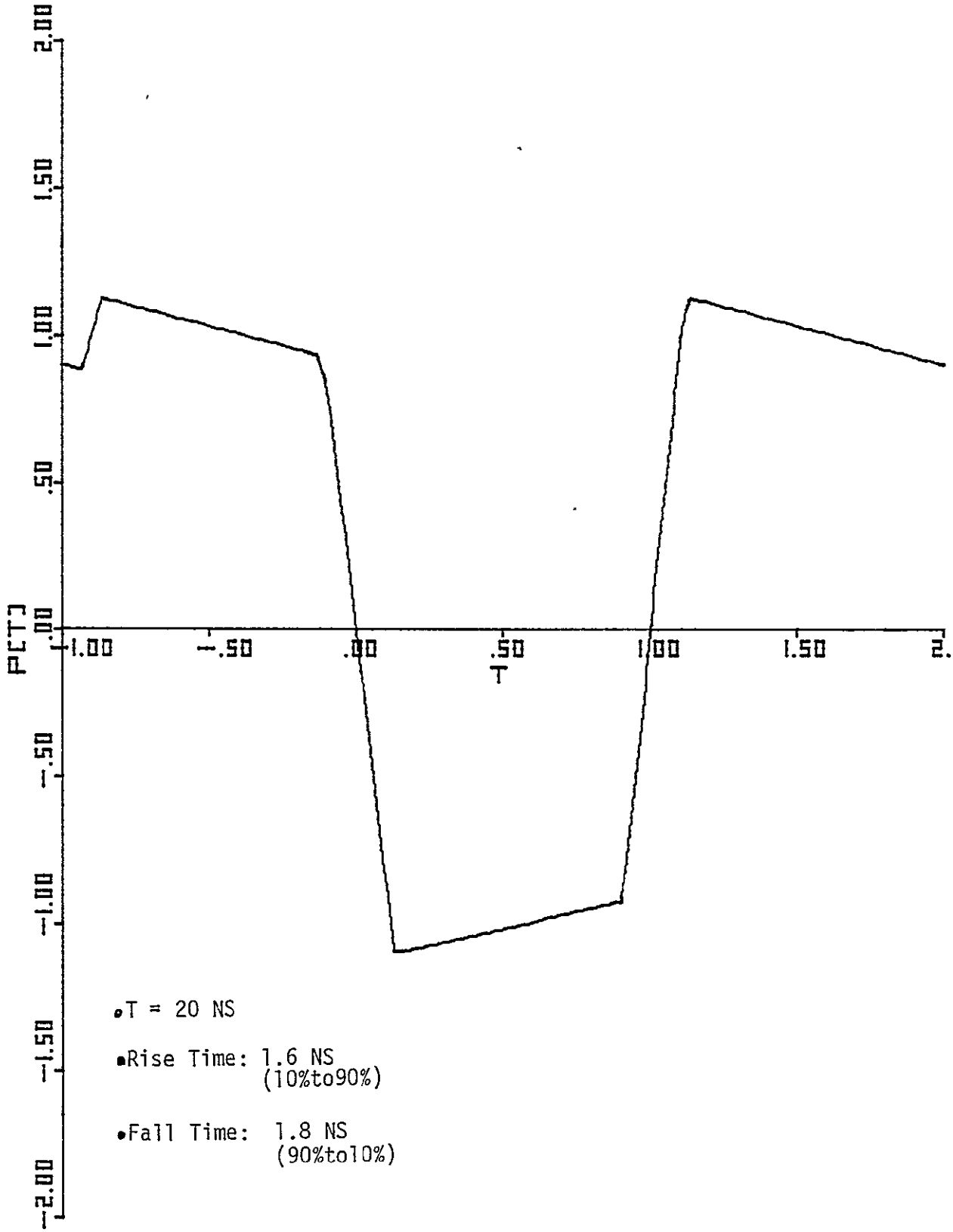


- T = 20 NS
- Rise Time: 1.6 NS (10%to90%)
- Fall Time: 1.8 NS (90%to10%)

78 0195

Figure 4.3b. TYPICAL INPUT PULSE SHAPES

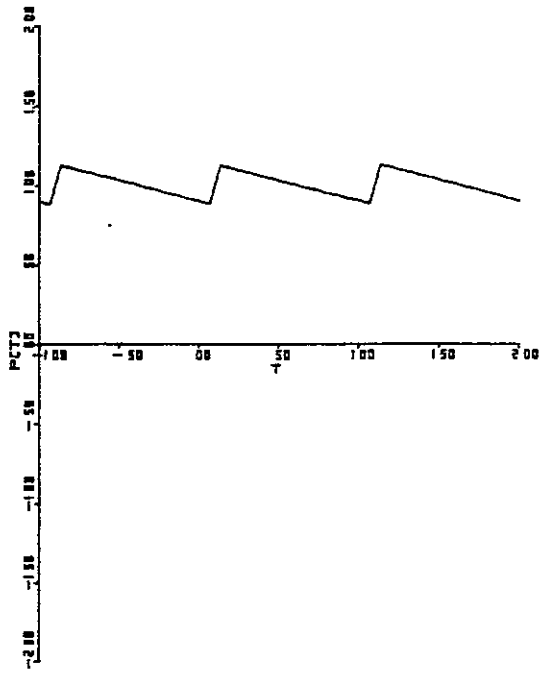

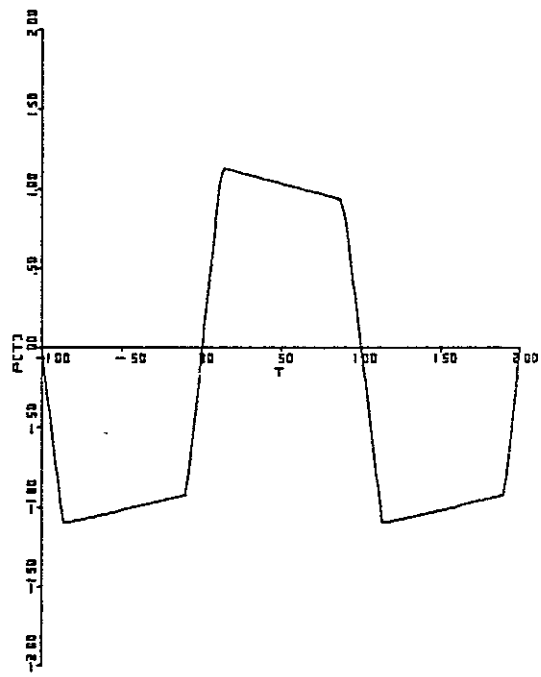

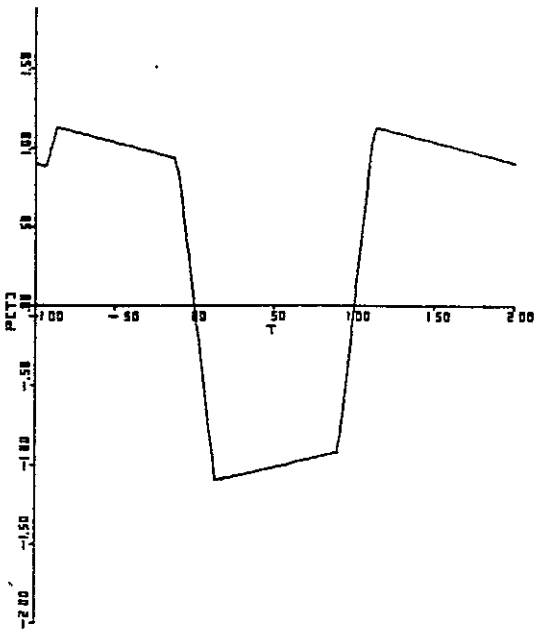

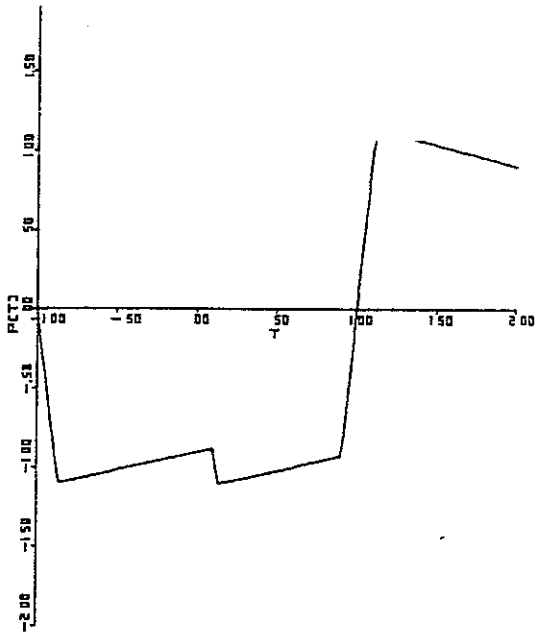

78 0196

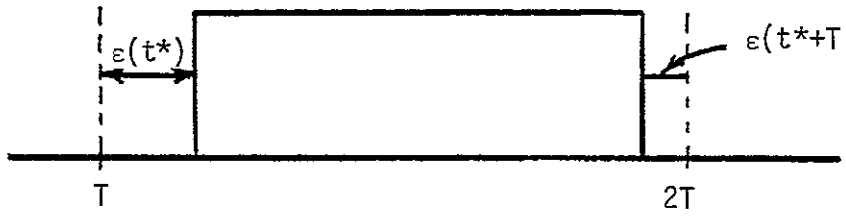


We shall assume that $\varepsilon(t^*)$ and $\varepsilon(t^*+\overline{T})$ are jointly Gaussian correlated random variables and such that

$$\sigma^2 = \mathrm{Var}[\varepsilon(t^*)] = \mathrm{Var}[\varepsilon(t^*+\overline{T})] \qquad (1)$$

We now define two new random varibles

$$T_{ck} = \frac{\varepsilon(t^*)+\varepsilon(t^*+\overline{T})+\overline{T}}{2\overline{T}} \qquad (2)$$

and

$$T_b = \frac{\varepsilon(t^*+\overline{T})-\varepsilon(t^*)+\overline{T}}{\overline{T}} \qquad (3)$$

It is clear then that the $T_{ck}$ and $T_b$ are two independent Gaussian random variables

$$T_{ck} \sim \mathcal{N}(1/2,\sigma_{ck}^2) \qquad (4)$$

$$T_b \sim \mathcal{N}(1,\sigma_b^2) \qquad (5)$$

we refer in what follows to

$$\sigma_{ck} = \sqrt{\frac{\sigma^2}{2\overline{T}^2}}\,[1+\gamma] \qquad (6)$$

as clock jitter and

$$\sigma_b = \sqrt{\frac{2\sigma^2}{\overline{T}^2}}\,(1-\gamma) \qquad (7)$$

as bit jitter and where $\gamma$ is the correlation coefficient between $\varepsilon(t)$ and $\varepsilon(t^*+\overline{T})$. Notice that sampling instant of the imperfect pulse entering to the Ku-band transmitter from the attached spacelab payload will be governed by the random variable $T_{ck}$.

The output of the convolutional encoder is fed into a driver which we assume introduces data asymmetry. The model for data asymmetry we have adopted for our analysis is described in [1] and is such that a positive going transition occurs early and a negative going transition occurs late relative to the nominal transition time instants. Data asymmetry is then defined as the difference in length between the shortest and longest pulses in the sequence divided by their sum. For our model we get then

$$\eta = \frac{\overline{T}(1+2\delta)-\overline{T}(1-2\delta)}{\overline{T}(1+2\delta)+\overline{T}(1-2\delta)} = 2\delta \qquad (8)$$

where $\delta$ represents the fractional (relative to the nominal symbol duration $\overline{T}$) increase in positive pulse length due to a single adjacent negative pulse.

4.3 BER at the Spacelab Ku-Band Transmitter Interface

For this part of the analysis we can concentrate on the mathematical model of Figure 4.4. The input NRZ pulses into the Ku-band transmitter are sampled at random instants of time governed by the random variable $t_s$ where $t_s = \mathcal{N}(\overline{T}, \overline{T}^2\sigma_{ck}^2)$. Since the clock signal is synchronous with the NRZ data, for the purpose of our analysis we can assume that, the NRZ pulses are of perfect duration T. The probability of error at A conditioned on a sampling instant $t_s$ and an input sequence S is

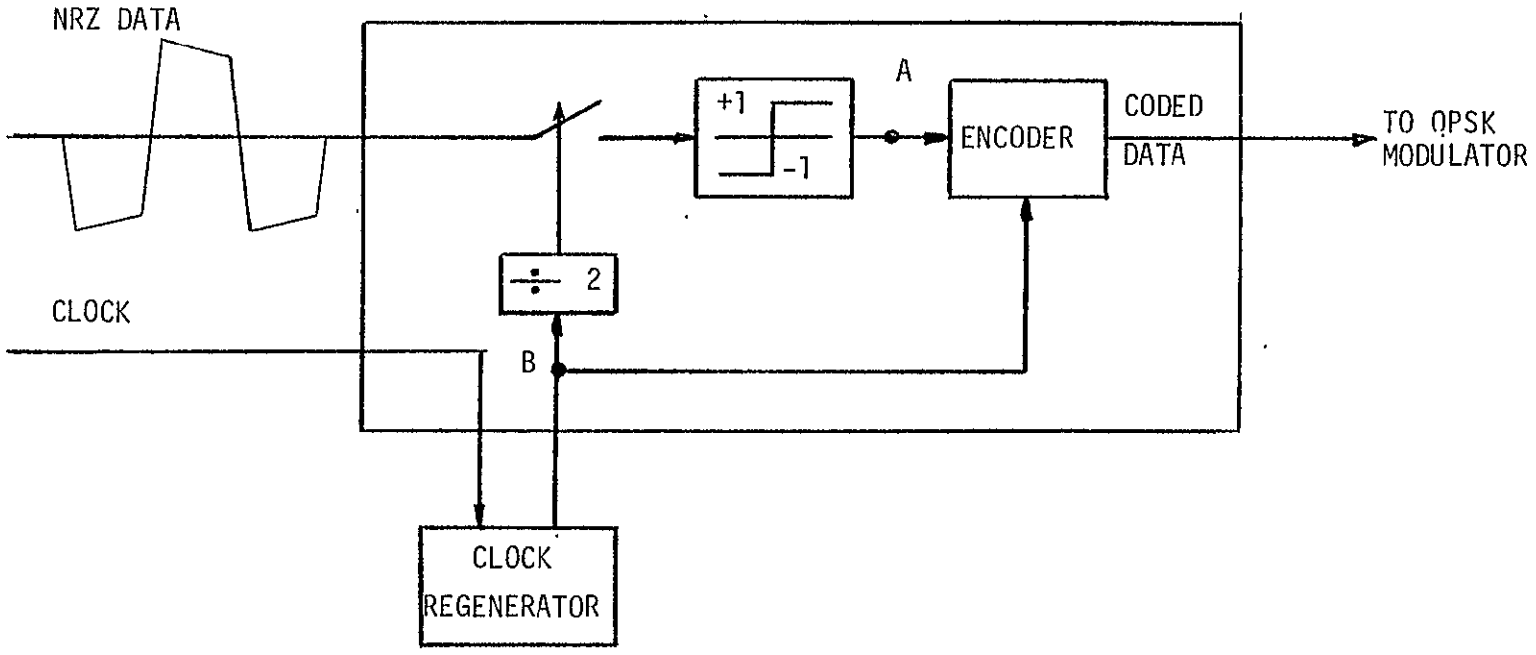


Figure 4.4. BASEBAND SPACELAB/SHUTTLE INTERFACE

$$P_e(t,S) = \frac{1}{2}\,\mathrm{erfc}\left\{\frac{p(t_s/T,S)}{\sqrt{2}\,\sigma_n}\right\} \qquad (9)$$

where $\sigma_n^2$ is the power of the noise entering into the Ku-band Shuttle transmitter from the attached spacelab payload $p(t,S)$ is the pulse shape input function which at any given instant of time is a function of at most three consecutive data bits. The relationship between $p(t_s,S)$ and $P(t,S)$ as given in Figure 4.3 is

$$P(\alpha,S) = \frac{p(\alpha=t/T,S)}{A} \qquad (10)$$

We can obtain the unconditional bit error probability by averaging (9) over all possible sequences S of length three and the random variable $t_s$, we then have

$$P_e = \frac{1}{8}\sum_S \frac{1}{2} \int_{-\infty}^{\infty} \mathrm{erfc}\left\{\frac{p(t_s/T,S)}{\sqrt{2}\,\sigma_n}\right\} f(t_s)dt_s$$

$$= \frac{1}{8}\sum_S \frac{1}{2} \int_{-\infty}^{\infty} \mathrm{erfc}\left\{\rho\,\frac{P(T'_{ck},S)}{\sqrt{2}}\right\} f(T'_{ck})dT'_{ck} \qquad (11)$$

where $\rho^2$ is the signal to noise ratio at the interface and given by

$$\rho^2 = \frac{A^2}{\sigma_n^2} \qquad (12)$$

and $T'_{ck} = \mathcal{N}(1/2,\sigma_{ck}^2/4)$.

When the sampling instant is biased by some $T_{bias}$, then $T'_{ck}$ has to be replaced in (11) by $T'_{ck}+T_{bias}$, where $T_{bias}$ is also normalized to be between 0 and 1. The relationship in (11) has been programmed and the result of this computation is shown in Figure 4.5.

Figure 4.5. BER PERFORMANCE AT KU BAND ENCODER INPUT (A)

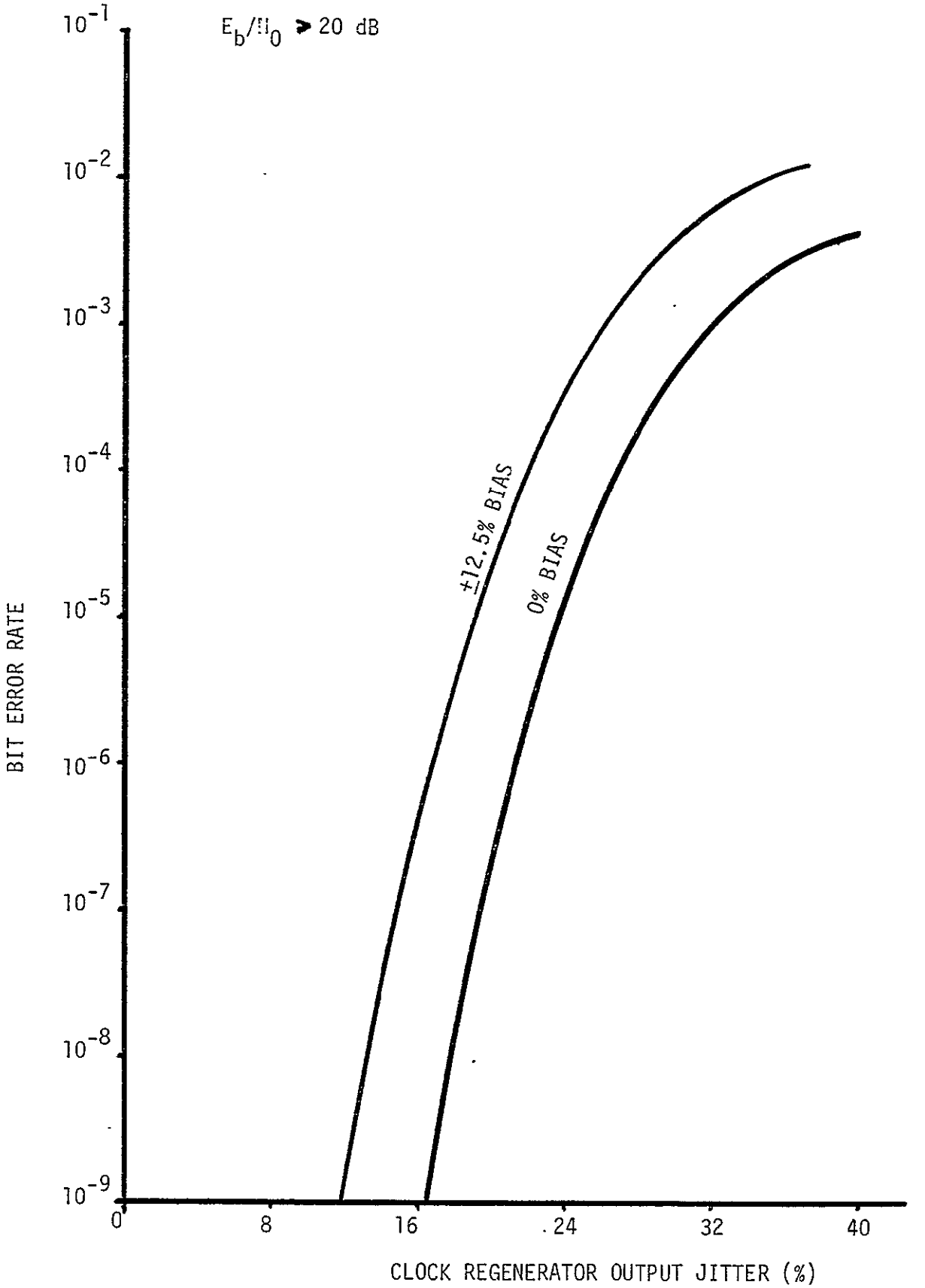


78 2138

## 4.4 Coded Link Bit Jitter Performance

We are interested now in the bit jitter performance between points C and D of Figure 4.1. We shall assume here without any significant loss of accuracy in the final answer that the receiver is implemented as an ideal integrate and dump detector followed by a completely soft Viterbi decoder. We shall also assume that the timing at the receiver is perfect.

Lets assume now that a codeword $\underline{c} = (c_1, c_2, \ldots, c_N)$ where $c_i = \pm 1$ is transmitted out of the Space Shuttle Ku-band transmitter. We model the channel as an ideal AWGN channel, we then have that the decoder input signal

$$\underline{r} = \underline{x}(\underline{c}) + \underline{n} \tag{13}$$

where

$$\underline{r} = (r_1, r_2, \ldots, r_N) \tag{14}$$

$$\underline{x}(\underline{c}) = (x_1(\underline{c}), x_2(\underline{c}), \ldots, x_N(\underline{c})) \tag{15}$$

$$\underline{n} = (n_1, n_2, \ldots, n_N) \tag{16}$$

lets define now for simplicity of notation

$$t_{ij} = \varepsilon[(j-1)\overline{T}] \tag{17}$$

$$t_{fj} = \varepsilon[j\overline{T}] + \overline{T} \tag{18}$$

then it is possible to show after some algebraic manipulation that

$$x_j(\underline{c}) = \frac{\sqrt{\epsilon_j}}{\overline{T}} \{c_{j-1}(t_{ij}+c_{j-1}\delta\overline{T})u(t_{ij}+c_{j-1}\delta\overline{T}) + c_j[(j-1)\overline{T}+t_{fj}+c_j\delta\overline{T}]$$

$$\cdot u(\overline{T}-t_{fj}-c_j\delta T) + c_j j\overline{T}[1-u(\overline{T}-t_{fj}-(j\delta\overline{T})]$$

$$- c_j[(j-1)\overline{T}+t_{ij}+c_{j-1}\delta\overline{T}]u(t_{ij}+c_{j-1}\delta\overline{T}) - c_j(j-1)\overline{T}$$

$$\cdot[1-u(t_{ij}+c_{j-1}\delta\overline{T})] + c_{j+1}(\overline{T}-t_{fj}-c_j\delta\overline{T})u(\overline{T}-t_{fj}-c_j\delta\overline{T})\} \quad (19)$$

If we now define as we did before

$$T_{ck}^{(j)} = (t_{ij}+t_{fj})/2\overline{T} \quad (20)$$

and

$$T_b^{(j)} = (t_{fi}-t_{ij})/\overline{T} \quad (21)$$

then from (17),(18),(20) & (21) it is possible to argue that $T_{ck}^{(k)}$ is a slow varying random variable and such that

$$T_{ck}^{(j)} = T_{ck}^{(\ell)} = \tau_{ck} \quad (22)$$

and that $T_b^{(j)}$ is a fast varying random variable such that

$$E\{T_b^j T_b^\ell\} = E\{T_b^j\}E\{T_b^\ell\} \quad \text{for } \ell \neq j \quad (23)$$

We then set

$$\tau_{bj} = T_b^{(j)} \quad (24)$$

This allows us to rewrite (19) as follows

$$x_j(\underline{c}) = \sqrt{\varepsilon_s}(c_{j-1}-c_j)(\tau_{ck}-\tau_{bj}+c_{j-1}\delta)u(\tau_{ck}-\tau_{bj}+c_{j-1}\delta)$$

$$+ c_j(\tau_{ck}+\tau_{bj}+c_j\delta)u(1-\tau_{ck}-\tau_{bj}-c_j\delta) + c_j[1-u(1-\tau_{ck}-\tau_{bj}-c_j\delta)]$$

$$+ c_{j+1}(1-\tau_{ck}-\tau_{bj}-c_j\delta)u(1-\tau_{ck}-\tau_{bj}-c_j\delta)$$

$$= x_j(c_{j-1},c_j,c_{j+1},\tau_{ck},\tau_{bj}) \tag{25}$$

In what follows and in order to avoid any boundary condition problems we let

$$c_0 = c_{N+1} = 1 \tag{26}$$

Lets assume now the decoder picks the codeword $\hat{\underline{c}}$ of the dimension N and $\underline{c}$ is the correct one, then the probability of an error even is

$$P_d(\tau_{ck},\underline{\tau}_b) = \frac{1}{2}\operatorname{erfc}\left\{\frac{\|\underline{x}(\underline{c})-\underline{x}(\underline{c})\|}{2\sqrt{N_0}}\right\} \tag{27}$$

where d is the Hamming distance between $\underline{c}$ and $\hat{\underline{c}}$,

$$\underline{\tau}_b = (\tau_{b1},\tau_{b2},\ldots,\tau_{bN}) \tag{28}$$

and $\|\underline{x}(\underline{c})-\underline{x}(\underline{c})\|$ is the Euclidean norm given by

$$\|\underline{x}(\underline{c})-\underline{x}(\underline{c})\|^2 = \sum_{j=1}^{N}[x_j(c_{j-1},c_j,c_{j+1},\tau_{ck},\tau_{bj})-x_j(c_{j-1},c_j,c_{j+1},\tau_{ck},\tau_{bj})]^2 \tag{29}$$

We now let the correct code word be the all 1's code word, then

$$x_j(c_{j-1},c_j,c_{j+1},\tau_{ck},\tau_{bj}) = \sqrt{\varepsilon_s} \tag{30}$$

so that (24) reduces to

$$\|\underline{x}(\underline{1})-\underline{x}(\underline{c})\|^2 = \varepsilon_s \sum_{j=1}^{N} [1-x_j'(\hat{c}_{j-1},c_j,\hat{c}_{j+1},\tau_{ck},\tau_{bj})]^2 \tag{31}$$

We can now rewrite (27) as

$$P_d(\tau_{ck},\underline{\tau}_b) = \frac{1}{2}\operatorname{erfc}\left\{\sqrt{\rho_s}\,\frac{1}{2}\sqrt{\sum_{j=1}^{N}[1-x_j'(c_{j-1},c_j,c_{j+1},\tau_{ck},\tau_{bj})]^2}\right\} \tag{32}$$

In order to obtain the unconditional probability of an error event we need to average (32) over $\tau_{ck}$ and $\underline{\tau}_b$ as

$$P_d = E_{\tau_{ck}}\{E_{\underline{\tau}_b}\{P_d(\tau_{ck},\underline{\tau}_b)|\tau_{ck}\}\} \tag{33}$$

The conditional expectation in (33) is in general very hard to find whenever N is larger than three. We notice on the other hand that the expression inside the square root in (32) is a sum of independent random variables and for the K=7 rate 1/2 code we are interested in N is always larger or equal to 18. This allows us to use a central limit argument to write

$$E_{\underline{\tau}_b}\{P_d(\tau_{ck},\underline{\tau}_b)|\tau_{ck}\} = \int_{-\infty}^{\infty} \frac{e^{-[y-\mu(\tau_{ck})]^2/2\sigma^2(\tau_{ck})}}{\sqrt{2\pi\sigma^2(\tau_{ck})}} f(y)dy \tag{34}$$

where

$$\mu(\tau_{ck}) = \sum_{j=1}^{N} E_{\tau_{bj}}\{[1-x_j'(c_{j-1},c_j,c_{j+1},\tau_{ck},\tau_{bj}]^2\} \tag{35}$$

$$\sigma^2(\tau_{ck}) = \sum_{j=1}^{N} E_{\tau_{bj}}\{[1-x'_j(c_{j-1},c_j,c_{j+1},\tau_{ck},\tau_{bj})]^4\}$$

$$- \sum_{j=1}^{N} E^2_{\tau_{bj}}\{[1-x'_j(c_{j-1},c_j,c_{j+1},\tau_{ck},\tau_{bj})]^2\} \qquad (36)$$

$$f(y) = \frac{1}{2}\,\mathrm{erfc}\left\{\frac{\rho_s}{2}\sqrt{y}\right\} \qquad (37)$$

The bit error can be found from the probability of an error event as given in (33) and the transfer function bound [2]. This approach is very tedious and usually computationally impractical. We can then get a very good approximation to the bit error probability by computing first the probability of an error event for all those paths which are at distance $d_{free}$* [2] from the correct path. Lets assume there are n such paths, we then find $\rho_s^*$ such that

$$\frac{1}{n}\sum_{i=1}^{n} P_{d_{fi}} = \frac{1}{2}\,\mathrm{erfc}\{\sqrt{d_f}\;\rho_s^*\} \qquad (38)$$

or in terms of an equivalent bit energy to noise spectral density ratio

$$\rho_b^* = \frac{\sqrt{2}\,\mathrm{erfc}^{-1}\left\{\frac{2}{n}\sum_{i=1}^{n} P_{d_{fi}}\right\}}{\sqrt{d_f}} \qquad (39)$$

We then set the bit error probability to be the one that corresponds to the decoding of a jitter and data asymmetry free signal transmitted over a channel with an $\mathcal{E}_b/N_0 = \rho_b^*$. This approach has been programmed and the result of this computations are shown in Figures 4.6, 4.7, and 4.8. The clock and bit jitter parameters in these curves are defined with respect to the Shuttle Ku-band transmitter clock regenerator phase detector output and the cycle duration time $\overline{T}$ of the clock signal out of the attached spacelab payload.

*In what follows we let $d_{free}=d_f$.

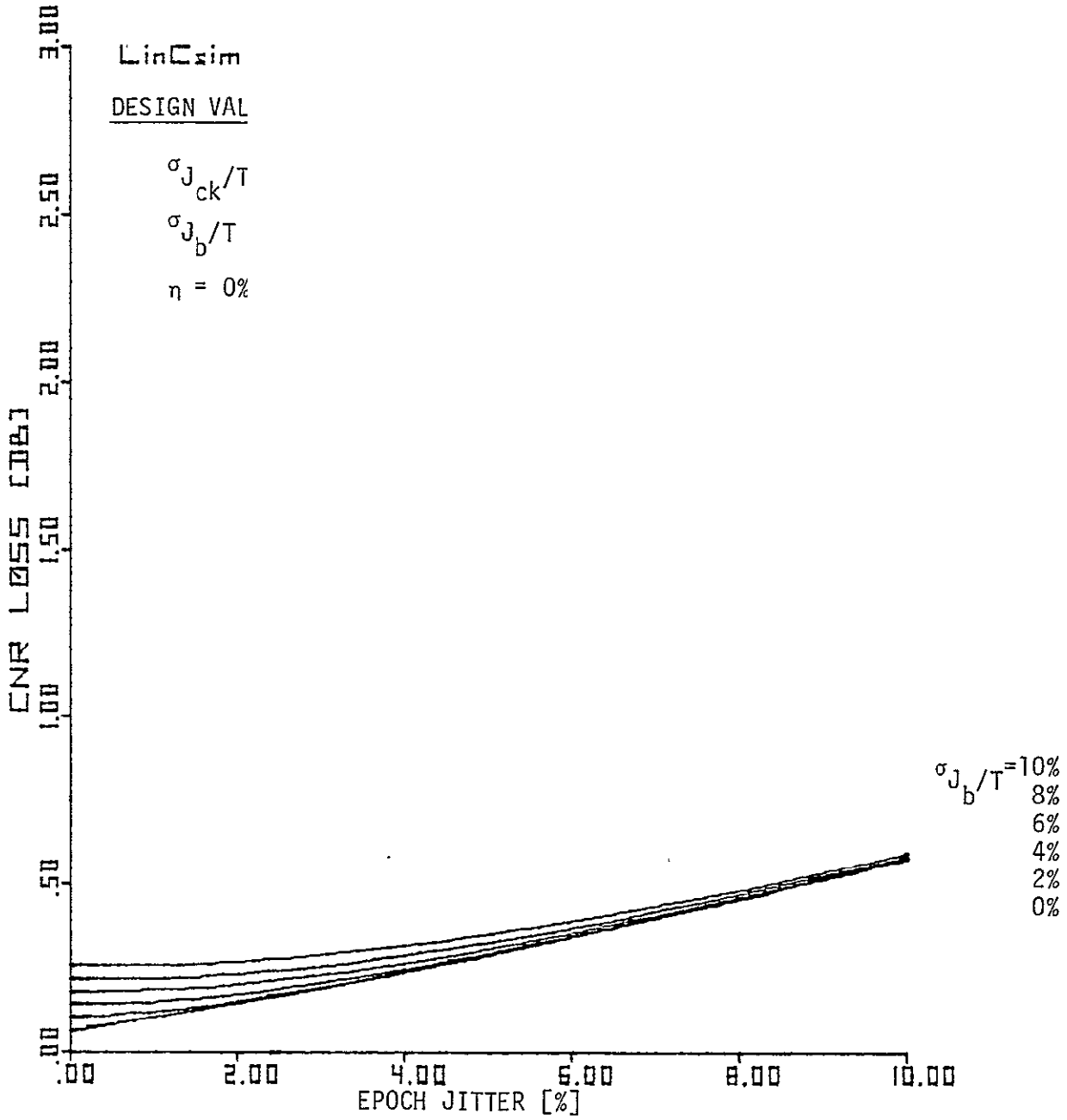


CODED LINK. CNR LOSS VS CLOCK JITTER FOR FIXED BIT JITTER, DATA ASYMMETRY: $\eta$ = 0% AND BER = $10^{-5}$.

Figure 4.6. Sensitivity Curve for Clock Jitter.

78 0266

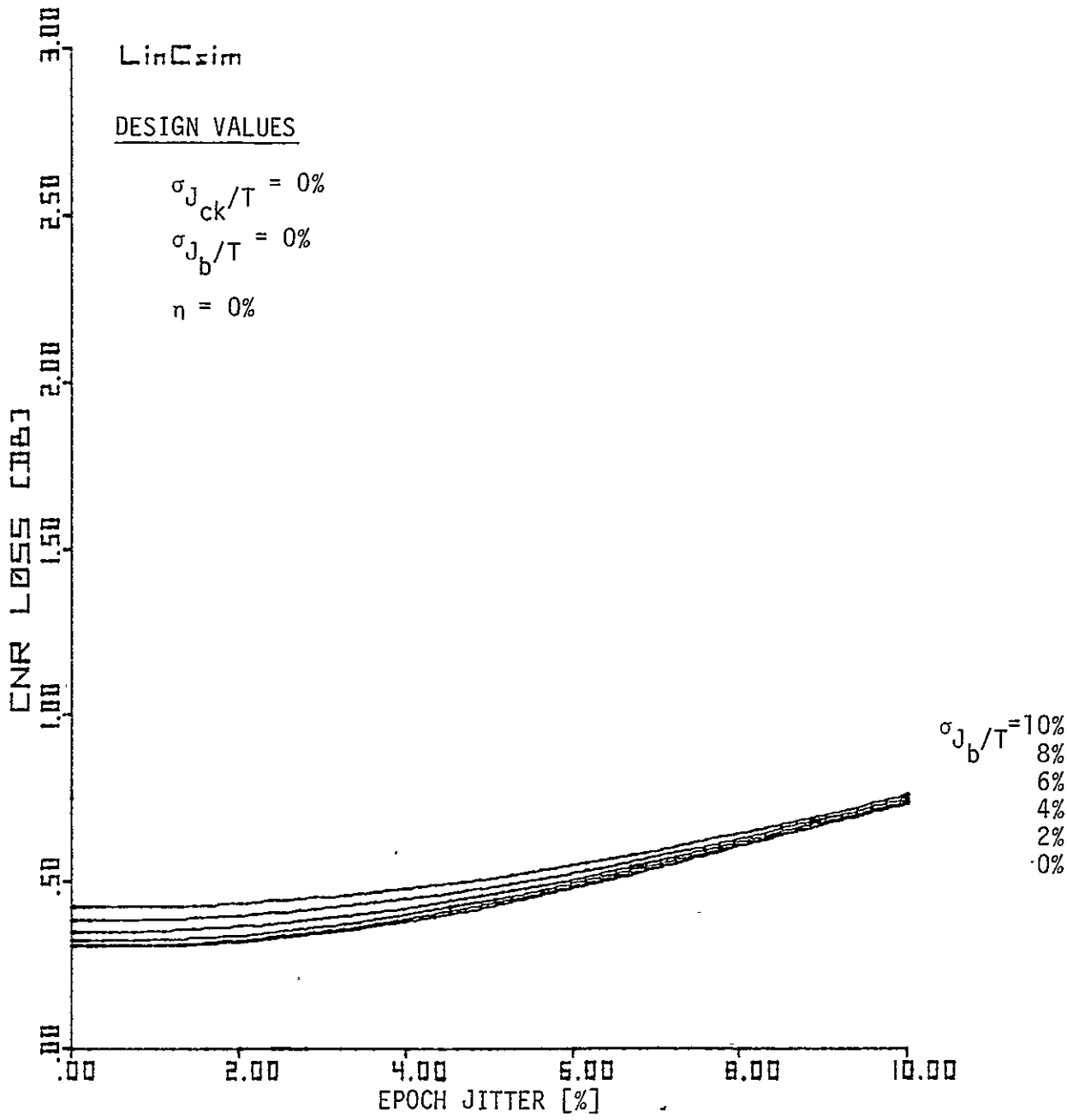


CODED LINK CNR. LOSS VS CLOCK JITTER FOR FIXED BIT JITTER, DATA ASYMMETRY: η = 5% AND BER = $10^{-5}$.

Figure 4.7. Sensitivity Curve for Clock Jitter.

78 0265

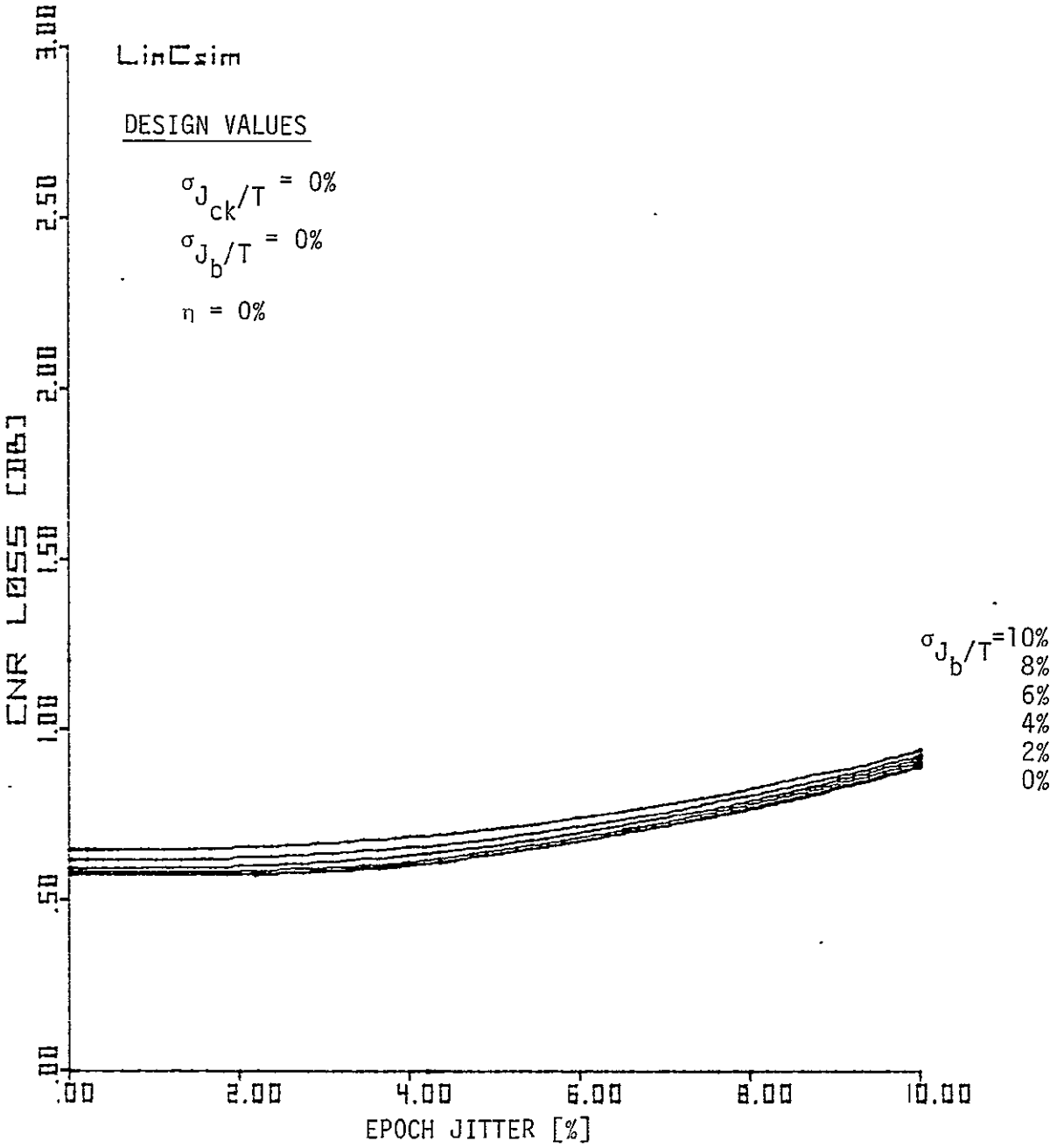


CODED LINK. CNR LOSS VS CLOCK JITTER FOR FIXED BIT JITTER, DATA ASYMMETRY: $\sigma$ = 10% AND BER = $10^{-5}$.

Figure 4.8. Sensitivity Curve for Clock Jitter.

78 0264

## 4.5 Summary and Conclusions

We have analyzed here the bit and clock jitter performance of the attached spacelab payload. We have first shown that the effect of an imperfect sampler at the spacelab Ku-band transmitter interface does not impose any measurable loss in performance for rms clock jitter levels less than 10%. On the other hand we have also shown that for a jitter-free link the required $E_b/N_0$ to maintain a BER of $10^{-5}$ with 10% of data asymmetry is 4.72 dB. This implies a $\Delta$CNR degradation of 0.52 dB with respect to the 4.2 dB of $E_b/N_0$ required for an ideal coded channel to achieve a BER of $10^{-5}$. In Table 1 we show the additional $\Delta$CNR (with resepct to 4.72 dB) required due to the presence of jitter*.

Table 1.

| $\Delta$CNR | Bit Jitter |
|---|---|
| dB | % |
| 0.1 | 5.70 |
| 0.2 | 8.01 |
| 0.3 | 9.75 |
| 0.4 | 11.10 |
| 0.5 | 12.48 |

It is very important to observe that for the levels of the jitter shown in Table 1, the BER at the SL-Ku-band transmitter interface, remains below $10^{-9}$. Its effect on the BER at the above mentioned system interface can therefore be ignored.

## Appendix

In this appendix we attempt to predict the SL HDM return

*The numbers shown in Table 1 correspond to worst case jitter for both epoch and duration jitter.

link performance based on the clock pulse shape characteristic and the spectrum characteristic shown in Figure 4.2, which has been provided to us by Sid Novosad. From Figure 4.2 we have estimated* that the $C/N_0$ present at the HRM clock output is approximately

$$C/N_0 = 104 \text{ dB-Hz.}$$

For this level of $C/N_0$ we have concluded* that the jitter observed in Figure 4.2b originates mostly from thermal effects. If we now assume that the Shuttle clock regenerator loop bandwidth is 10 KHz, it is possible to predict that the jitter at the scrubber output, including non-thermal effects, will be less than 2%. For this jitter level, the overall performance degradation taking into account the 0.52 ΔCNR due to 10% of data asymmetry will be

$$\Delta CNR = \underbrace{0.52 \text{ dB}}_{\substack{\text{Data} \\ \text{Asymmetry}}} + \underbrace{0.01 \text{ dB}}_{\text{Jitter}}$$

$$= 0.53 \text{ dB}$$

*Within the accuracy that this picture allows.

## REFERENCES

[1] Simon, M. K., Tu, K., and Batson, B., IEEE Transactions on Communications, Vol. COM-26, No. 11, November, 1977.

[2] Viterbi, A. J., and Omura, J. K., Digital Communications and Coding, McGraw-Hill, New York, 1979 (to appear).

[3] Cager, R. H., LaFlame, D. T., and Parode, L. C., "Orbiter Ku-Band Integrated Radar and Communications Subsystem," IEEE Transactions on Communications, Vol. COM-26, No. 11, November, 1977.

## 5.0 SHUTTLE PAYLOAD BENT-PIPE MODE SUBCARRIER RECOVERY

### 5.1 Introduction

In the bent-pipe mode of Shuttle payload data transmission, the data are not detected at the Shuttle payload interrogator. They go through the Shuttle repeater, where they are low-pass filtered, hard-limited, and modulated onto the high-power channel of the subcarrier UQPSK modulator. In this section the performance of the Costas loop recovering the subcarrier in the ground station receiver is studied for this case and compared with an implementation which does not include a hard limiter in the bent-pipe link. The results show a slight degradation of the loop performance when a hard-limiter is used. This advantage is offset, however, by the tight power control afforded by the limiter which reduces the effects of interference on the other two data channels.

### 5.2 Problem Statement

In the detached-payload bent-pipe mode the binary data stream is received by the Shuttle payload interrogator immersed in additive white Gaussian noise. This signal goes through the Shuttle repeater, where it is low-pass filtered and hard-limited. Then it is modulated onto the high-power phase of the 8.5 MHz subcarrier. This is shown in Figure 5.1.

For the analysis of the 8.5 MHz subcarrier recovery, we may assume that the carrier has been recovered perfectly. This leads to the link model of Figure 5.2.

We wish to characterize the phase-recovery performance of the Costas loop. The theory is developed for an arbitrary signal format at the Shuttle repeater output. The results are then applied to

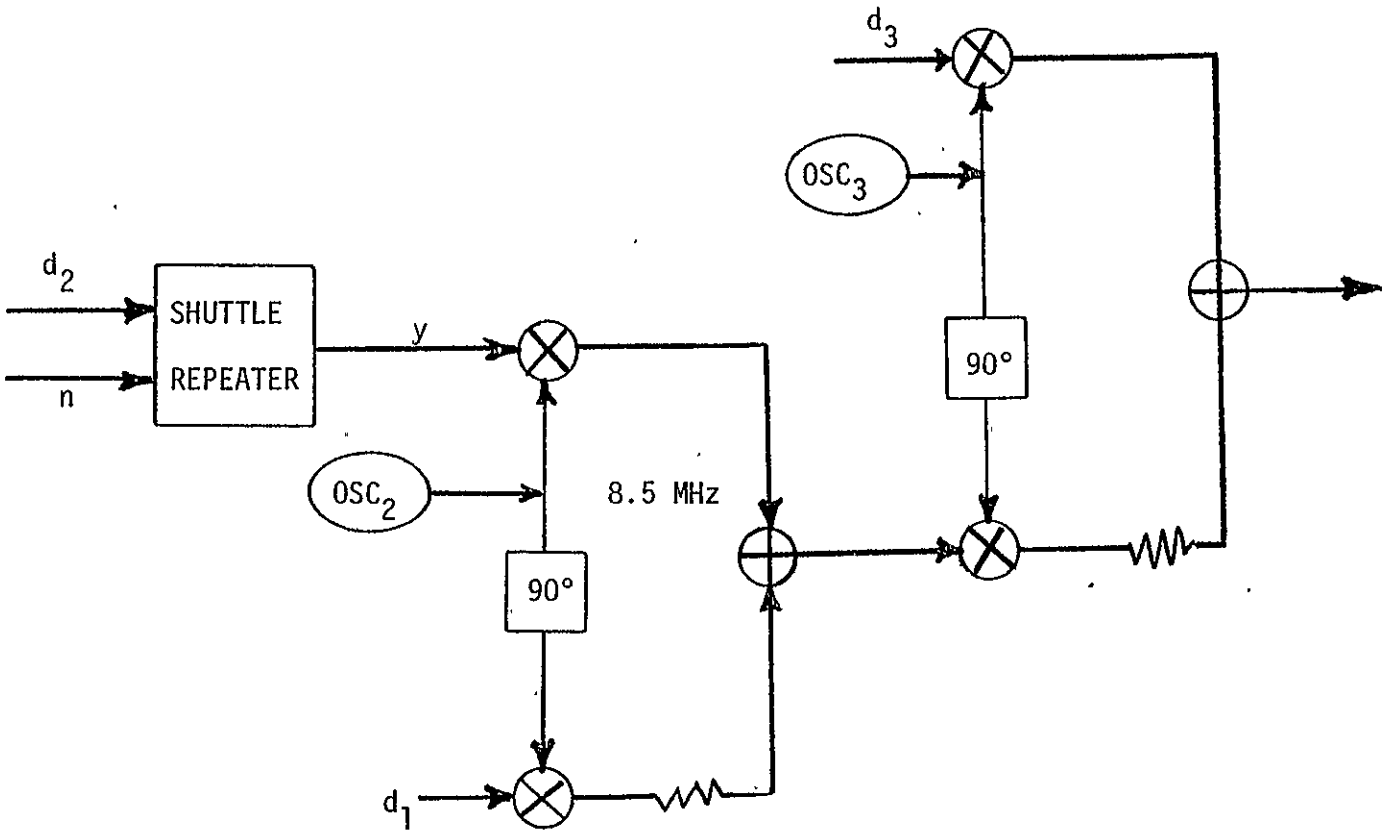


Figure 5.1. Three-Channel Transmitter in Bent-Pipe Mode

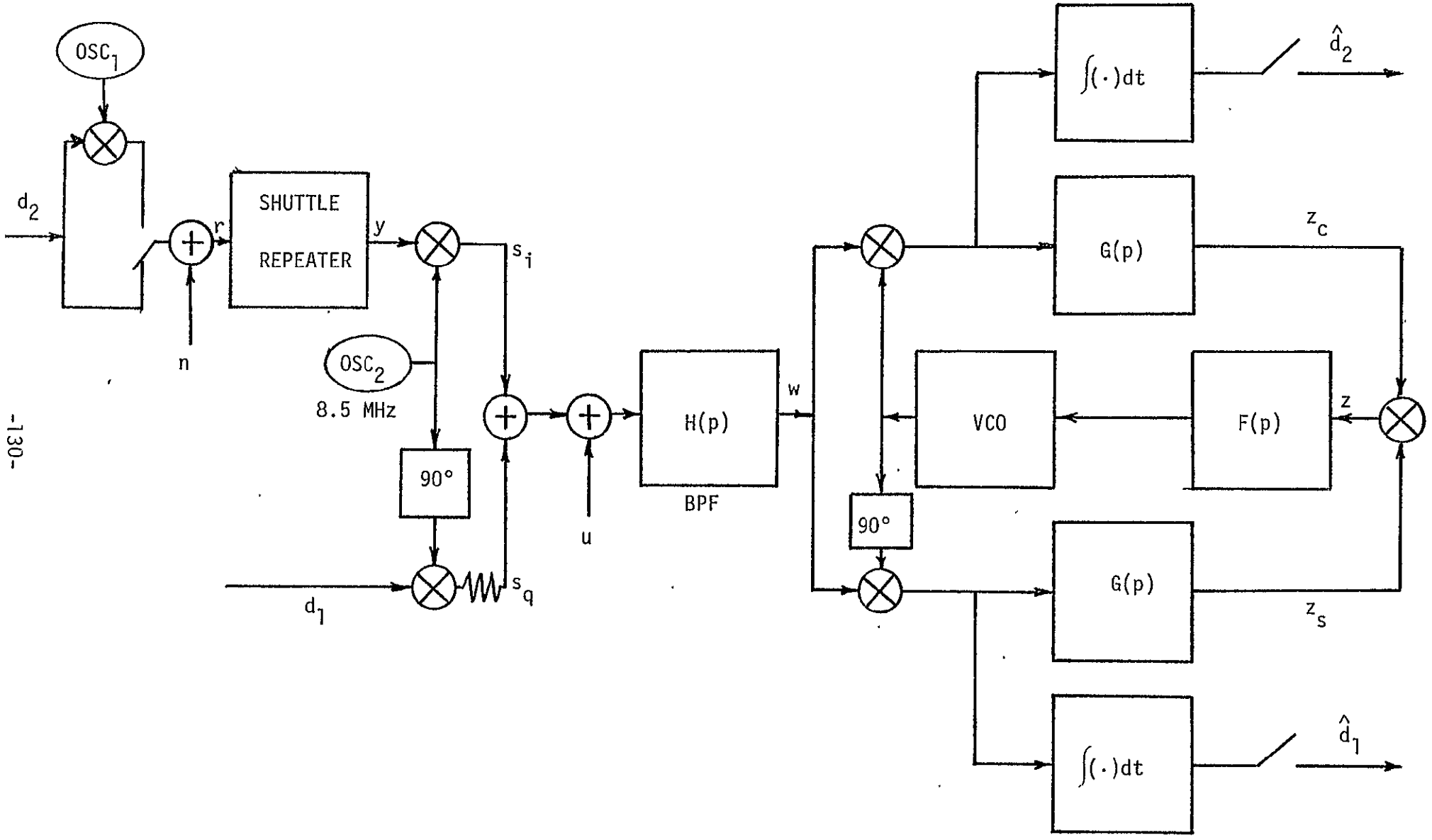


Figure 5.2. Simplified Link Diagram.

the case of baseband data with two different implementations for the Shuttle repeater: a hard-limiter preceded by a wide low-pass filter which does not affect the data signal and an arbitrary low-pass filter without hard-limiter.

5.3 Costas Loop Model (Following Reference 1)

The input signal to the Costas loop is the random process (see Fig. 5.2),

$$w(t) = H(p)(s_i(t) + s_q(t) + u(t)) \qquad (1)$$

where $H(p)$ is the ground station receiver filter, $s_i(t)$ is the high-power bent-pipe signal, $s_q(t)$ is the low-power digital voice signal and $u(t)$ is the downlink thermal noise. This signal can be written

$$w(t) = \sqrt{2}a(t) \sin \Phi(t) + \sqrt{2}b(t) \cos \Phi(t) \qquad (2)$$

for some random processes $a(t)$ and $b(t)$, where $\Phi(t) \equiv \omega_2 t+\theta(t)$ and $\theta(t) = \Omega_0 t+\theta_0$ is the input phase to be estimated. Let $\hat{\Phi}(t)$ be the loop estimate of $\Phi(t)$. In the upper arm of the loop, $w(t)$ is multiplied by $\sqrt{2K_1} \cos \hat{\Phi}(t)$, in the lower arm by $\sqrt{2K_1} \sin \hat{\Phi}(t)$. The multiplier units have gain $\sqrt{K_m}$ and are insensitive to the double-frequency terms. Each output passes through a filter corresponding to $G(p)$, yielding the upper-arm signal $z_c(t)$ and the lower-arm signal $z_s(t)$.

$$z_c(t) = \sqrt{K_1 K_m}\, G(p)[a(t) \sin \varphi(t) + b(t)\cos \varphi(t)] \qquad (3)$$

$$z_s(t) = \sqrt{K_1 K_m}\, G(p)[a(t)\cos \varphi(t) - b(t)\sin \varphi(t)] \qquad (4)$$

where $\varphi(t) \equiv \Phi(t)-\hat{\Phi}(t)$ is the loop phase error. The two signals are multiplied together, with unit gain, to produce the dynamic error signal

$$z(t) = z_c(t)z_s(t) \tag{5}$$

We assume that $\varphi(t)$ varies much more slowly than a(t) and b(t) and that the G(p) filter is sufficiently wide so that

$$z(t) = \{[(G(p)a(t))^2-(G(p)b(t))^2]\frac{1}{2}\sin(2\varphi(t)) - [G(p)a(t)G(p)b(t)]\cos(2\varphi(t))\}K_1K_m \tag{6}$$

The instantaneous frequency of the VCO output is related to z(t) by

$$\frac{d\hat{\Phi}(t)}{dt} = K_V F(p)z(t) + \omega_2 \tag{7}$$

where $K_V$ is a gain constant. Hence, the stochastic integro-differential equation of operation of the loop is

$$2\frac{d\varphi(t)}{dt} = 2\Omega_0 - 2K_V F(p)z(t) \tag{8}$$

Conditioned on $\varphi$, z(t) can be partitioned into a nonrandom part and a zero-mean random process:

$$z(t) = S(\varphi) + n_z(t,\varphi) \tag{9}$$

where

$$S(\varphi) = E\{z(t)|\varphi\} \tag{10}$$

$$n_z(t,\varphi) = z(t) - S(\varphi) \tag{11}$$

This allows us to rewrite (8) as

$$2\frac{d\varphi(t)}{dt} = 2\Omega_0 - 2K_V F(p)S[\varphi(t)] - 2K_V F(p)n_z(t,\varphi) \tag{12}$$

This equation describes a non-Markovian diffusion process. However, under suitable conditions (in particular, if the process $n_z(t,\varphi)$ is considerably faster than the process $\varphi(t)$) it can be approximated by a Markov process and Fokker-Planck techniques can be applied to characterize the stationary distribution of the modulo-$2\pi$-reduced phase noise process as well as the cycle-slipping rate. For this analysis the S-curve $S(\varphi)$ and the statistics of the equivalent noise process $n_z(t,\varphi)$ are needed.

5.4 Costas Loop S-Curve

We will assume that $\Omega_0=0$ and that the baseband equivalent of the H(p) filter is symmetric. We first obtain the input signal to the Costas loop.

We will denote a narrowband signal a(t) with center frequency $\omega_2$ by

$$a(t) = \sqrt{2}\ \mathrm{Re}[a'(t)e^{j\omega_2 t}] \tag{13}$$

where a'(t) is the baseband equivalent to a(t).

Defining the payload signal as

$$s_i(t) = \sqrt{2P_2}\ y(t)\ \sin(\omega_2 t) \tag{14}$$

where y(t) is normalized such that $E\{y^2(t)\} = 1$, we find

$$s_i'(t) = -j\sqrt{P_2}\ y(t) \tag{15}$$

$$x_i'(t) \equiv H'(p)s_i'(t) \tag{16}$$

where H'(p) is the baseband equivalent of H(p).

For the low-power signal we have

$$s_q(t) = -\sqrt{2P_1}\, d_1(t)\cos(\omega_2 t) \tag{17}$$

$$s_q'(t) = -\sqrt{P_1}\, d_1(t) \tag{18}$$

$$x_q'(t) \equiv H'(p)s_q'(t) \tag{19}$$

Now we consider the noise u(t), a narrowband Gaussian process with center frequency $\omega_2$.

$$u(t) = \sqrt{2}u_1(t)\cos(\omega_2 t) - \sqrt{2}u_2(t)\sin(\omega_2 t) \tag{20}$$

The spectral density of u(t) is

$$S_u(f) = S_{u'}(f-f_2) + S_{u'}(-f-f_2) \tag{21}$$

for some real function $S_{u'}(f)$, where $f_2 = \omega_2/(2\pi)$. We define

$$R_{u_i}(\tau) = E[u_i(t)u_i(t+\tau)] \ , \quad i = 1,2 \tag{22}$$

$$R_{u_{ik}}(\tau) = E[u_i(t)u_k(t+\tau)] \ , \quad i \neq k \tag{23}$$

Letting $R_{u'}$ be the inverse Fourier transform of $S_{u'}$ we have

$$R_{u_1} = R_{u_2} = \text{Re } R_{u'} \tag{24}$$

$$R_{u_{12}} = -R_{u_{21}} = \text{Im } R_{u'} \tag{25}$$

We assume that $S_{u'}(f)$ is symmetric about 0, so that

$$R_{u_1} = R_{u_2} = R_{u'} \tag{26}$$

$$R_{u_{12}} = -R_{u_{21}} = 0 \tag{27}$$

Since we assumed that the $H'(p)$ filter is symmetric then $H'(p)u_1(t)$ and $H'(p)u_2(t)$ are real-valued processes.

Now we go into the Costas loop.

In the upper arm the input signal is multiplied by $\sqrt{2K_1K_m}\cos(\omega_2 t-\phi)$ and the double-frequency terms are dropped. The same result is obtained if the baseband equivalent of the signal is multiplied by $\sqrt{K_1K_m}\ e^{j\phi}$ and the real part is taken. In the lower arm of the loop, the input signal is multiplied by $\sqrt{2K_1K_m}\sin(\omega_2 t-\phi)$ and the double-frequency terms are dropped. This is the same as multiplying the baseband equivalent by $j\sqrt{K_1K_m}\ e^{j\phi}$ and taking the real part, or multiplying it by $-\sqrt{K_1K_m}\ e^{j\phi}$ and taking the imaginary part.

Since $z_c$ and $z_s$ are each linearly related to $s_i$, $s_q$, and $u$, we may write

$$z_c(t) = z_c(t;s_i) + z_c(t;s_q) + z_c(t;u) \qquad (28)$$

$$z_s(t) = z_s(t;s_i) + z_s(t;s_q) + z_s(t;u) \qquad (29)$$

where, for example, $z_c(t;s_i)$ is $z_c(t)$ when the loop input is just $H(p)s_i(t)$.

For $s_i(t)$ we have

$$z_c(t;s_i) = G(p)\left[\sqrt{K_1K_m}\ \mathrm{Re}(x_i'(t)e^{j\phi})\right]$$

$$= \sqrt{K_1K_m}\ G(p)[\hat{x}_i'(t)\cos\phi - \tilde{x}_i'(t)\sin\phi] \qquad (30)$$

since $s_i, s_q$, and u are assumed independent and have zero mean.

$$E[z_c(t;s_i)z_s(t;s_i)|\varphi] = \frac{K_1K_m}{2} P_2[G(p)G^*(p)H'(p)H'^*(p)R_y(0)]\sin(2\varphi) \quad (40)$$

$$E[z_c(t;s_q)z_s(t;s_q)|\varphi] = -\frac{K_1K_m}{2} P_1[G(p)G^*(p)H'(p)H'^*(p)R_{d_1}(0)]\sin(2\varphi) \quad (41)$$

$$E[z_c(t;u)z_s(t;u)|\varphi] = 0 \quad (42)$$

since $u_1(t)$, $u_2(t)$ were assumed independent. Therefore,

$$S(\varphi) = \frac{K_1K_m}{2} G(p)G^*(p)H'(p)H'^*(p)(P_2R_y(0) - P_1R_{d_1}(0))\sin(2\varphi) \quad (43)$$

5.5 Spectral Density of the Equivalent Noise

Now we will obtain the spectral density of z for fixed $\varphi$.

We introduce the notation

$$\bar{a}(t) = G(p)H'(p)a(t) \quad (44)$$

for any signal a(t). Then

$$R_{\bar{a}}(\tau) = G(p)G^*(p)H'(p)H'^*(p)R_a(\tau) \quad (45)$$

Let $C = K_1K_m$. Then we have

$$z_c(t;s_i) = \sqrt{C}\sqrt{P_2}\sin(\varphi)\bar{y}(t) \quad (46)$$

$$z_c(t;s_q) = -\sqrt{C}\sqrt{P_1}\cos(\varphi)\bar{d}_1(t) \quad (47)$$

$$z_c(t;u) = \sqrt{C}(\cos(\varphi)\bar{u}_1(t) - \sin(\varphi)\bar{u}_2(t)) \quad (48)$$

$$z_s(t;s_i) = \sqrt{C}\sqrt{P_2}\cos(\varphi)\bar{y}(t) \quad (49)$$

where $\hat{x}_i'(t)$ and $\tilde{x}_i'(t)$ are real. Since

$$x_i'(t) = -j\sqrt{P_2}H'(p)y(t) \tag{31}$$

then

$$z_c(t;s_i) = \sqrt{K_1K_m}\sqrt{P_2}[G(p)H'(p)y(t)]\sin\varphi \tag{32}$$

Similarly,

$$z_s(t;s_i) = -G(p)\left[\sqrt{K_1K_m}\ \ \mathrm{Im}(x_i'(t)e^{j\varphi})\right]$$

$$= -\sqrt{K_1K_m}\ G(p)[\hat{x}_i'(t)\sin\varphi + \tilde{x}_i'(t)\cos\varphi]$$

$$= \sqrt{K_1K_m}\sqrt{P_2}[G(p)H'(p)y(t)]\cos\varphi \tag{33}$$

For the $s_q(t)$ effect, we use the fact that

$$x_q(t) = -\sqrt{P_1}\ H'(p)d_1'(t) \tag{34}$$

We find that

$$z_c(t;s_q) = -\sqrt{K_1K_m}\sqrt{P_1}[G(p)H'(p)d_1'(t)]\cos\varphi \tag{35}$$

$$z_s(t;s_q) = \sqrt{K_1K_m}\sqrt{P_1}[G(p)H'(p)d_1'(t)]\sin\varphi \tag{36}$$

For the $u(t)$ effect we have

$$z_c(t;u) = \sqrt{K_1K_m}G(p)\{\mathrm{Re}[H'(p)u_1(t)+jH'(p)u_2(t))e^{j\varphi}]\}$$

$$= \sqrt{K_1K_m}G(p)[H'(p)u_1(t)\cos\varphi - H'(p)u_2(t)\sin\varphi] \tag{37}$$

$$z_s(t;u) = -\sqrt{K_1K_m}G(p)[H'(p)u_1(t)\sin\varphi + H'(p)u_2(t)\cos\varphi] \tag{38}$$

Now we can calculate $S(\varphi)$.

$$S(\varphi) \equiv E[z(t)|\varphi] = E[z_c(t)z_s(t)|\varphi]$$

$$= E[z_c(t;s_i)z_s(t;s_i)|\varphi] + E[z_c(t;s_q)z_s(t;s_q)|\varphi] \tag{39}$$

$$+E[z_c(t;u)z_s(t;u)|\varphi]$$

$$z_s(t;s_q) = \sqrt{C}\sqrt{P_1}\sin(\phi)\bar{d}_1(t) \tag{50}$$

$$z_s(t;u) = \sqrt{C}(-\sin(\phi)\bar{u}_1(t)-\cos(\phi)\bar{u}_2(t)) \tag{51}$$

$$S(\phi) \equiv E[z(t)|\phi] = \frac{C}{2}(P_2 \cdot R_{\bar{y}}(0)-P_1 R_{\bar{d}_1}(0))\sin(2\phi) \tag{52}$$

Hence,

$$\frac{1}{C}(z(t) - E[z(t)|\phi])$$

$$= \frac{1}{2}P_2(\bar{y}^2(t)-R_{\bar{y}}(0))\sin(2\phi)- \frac{1}{2}P_1(\bar{d}_1^2(t)-R_{\bar{d}_1}(0))\sin(2\phi)$$

$$- \sqrt{P_1P_2}\cos(2\phi)\bar{y}(t)\bar{d}_1(t)$$

$$+ \sqrt{P_2}\cos(2\phi)\bar{y}(t)\bar{u}_1(t) - \sqrt{P_2}\sin(2\phi)\bar{y}(t)\bar{u}_2(t)$$

$$+ \sqrt{P_1}\sin(2\phi)\bar{d}_1(t)\bar{u}_1(t) + \sqrt{P_1}\cos(2\phi)\bar{d}_1(t)\bar{u}_2(t)$$

$$- \frac{1}{2}\sin(2\phi)\bar{u}_1^2(t) - \cos(2\phi)\bar{u}_1(t)\bar{u}_2(t)$$

so $$+ \frac{1}{2}\sin(2\phi)\bar{u}_2^2(t) \tag{53}$$

$$\frac{1}{C^2}R_z(\tau|\phi) \equiv E\{(z(t)-E[z(t)|\phi])(z(t+\tau)-E[z(t+\tau)|\phi])\}$$

$$= \frac{1}{4}P_2^2(E[\bar{y}^2(t)\bar{y}^2(t+\tau)]-R_{\bar{y}}^2(0))\sin^2(2\phi)+\frac{1}{4}P_1^2(E[\bar{d}_1^2(t)\bar{d}_1^2(t+\tau)]$$
$$-R_{\bar{d}_1}^2(0))\sin^2(2\phi))$$

$$+ P_1P_2\cos^2(2\phi)R_{\bar{y}}(\tau)R_{\bar{d}_1}(\tau) + P_2\cos^2(2\phi)R_{\bar{y}}(\tau)R_{\bar{u}_1}(\tau)$$

$$+ P_2\sin^2(2\phi)R_{\bar{y}}(\tau)R_{\bar{u}_1}(\tau) + P_1\sin^2(2\phi)R_{\bar{d}_1}(\tau)R_{\bar{u}_1}(\tau)$$

$$+ P_1\cos^2(2\phi)R_{\bar{d}_1}(\tau)R_{\bar{u}_1}(\tau) + \frac{1}{4}\sin^2(2\phi)E[\bar{u}_1^2(t)\bar{u}_1^2(t+\tau)]$$

$$- \frac{1}{4}\sin^2(2\phi)R_{\bar{u}_1}^2(0) + \cos^2(2\phi)R_{\bar{u}_1}^2(\tau)$$

$$- \frac{1}{4}\sin^2(2\phi)R_{\bar{u}_1}^2(0) + \frac{1}{4}\sin^2(2\phi)E[\bar{u}_1^2(t)\bar{u}_1^2(t+\tau)] \tag{54}$$

This equation for $R_z(\tau|\phi)$ holds because we have assumed $\bar{u}_1(t)$ and $\bar{u}_2(\tau)$ are independent and identically distributed for any choice of t and $\tau$. We must obtain $E[\bar{u}_1^2(t)\bar{u}_1^2(t+\tau)]$. To do this, we define the two random

variables $X = \bar{u}_1(t)$, $Y = \bar{u}_1(t+\tau)$. Then $E[\bar{u}_1^2(t)\bar{u}_1^2(t+\tau)] = E[X^2Y^2]$. Let $\sigma = \sigma_X = \sigma_Y$, $\rho = \frac{E(XY)}{\sigma^2}$. To calculate $E[X^2Y^2]$, we introduce the zero-mean Gaussian random variable

$$W \equiv Y - \rho X . \tag{55}$$

Since $E[XW] = E[X(Y-\rho X)] = 0 = E(X)E(W)$, then X and W are independent. We have

$$\sigma_W^2 \equiv E(W^2) = E[Y^2-2\rho XY+\rho^2X^2] = \sigma^2(1-\rho^2) \tag{56}$$

Then

$$\begin{aligned} E[X^2Y^2] &= E[X^2(W^2+2\rho XW+\rho^2X^2)] \\ &= \sigma^2\sigma_W^2 + \rho^2E(X^4) \\ &= \sigma^4(1-\rho^2) + \rho^2 3\sigma^4 \\ &= \sigma^4(1+2\rho^2) \end{aligned} \tag{57}$$

Thus,

$$\begin{aligned} E[\bar{u}_1^2(t)\bar{u}_1^2(t+\tau)] &= \sigma^4(1+2\rho^2(\tau)) \\ &= R_{\bar{u}_1}^2(0) + 2R_{\bar{u}_1}^2(\tau) \end{aligned} \tag{58}$$

so

$$\begin{aligned} \frac{1}{C^2} R_z(\tau|\varphi) = \frac{1}{4} &\sin^2(2\varphi)\,[P_2^2R_{\bar{y}2}(\tau)+P_1^2R_{\bar{d}_1^2}(\tau)] \\ &+ P_1P_2\cos^2(2\varphi)R_{\bar{y}}(\tau)R_{\bar{d}_1}(\tau) + P_2R_{\bar{y}}(\tau)R_{\bar{u}_1}(\tau) \\ &+ P_1R_{\bar{d}_1}(\tau)R_{\bar{u}_1}(\tau) + R_{\bar{u}_1}^2(\tau) \end{aligned} \tag{59}$$

## 5.6 Nonlinear Costas Loop Theory

We are now in a position to investigate the Costas loop performance.

To keep the notation manageable we will develop the theory for a first-order loop only.

The equation of loop operation (12) can be rewritten for a first-order loop as

$$\frac{d\varphi(t)}{dt} = \Omega_0 - K_V S(\varphi) - K_V \sigma_n(\varphi) n_z(t) \tag{60}$$

where $n_z(t)$ is a unit-variance zero-mean random process. Approximating $n_z(t)$ by a delta-correlated Gaussian process the above equation can be rewritten as an Ito stochastic differential equation

$$d\varphi(t) = \left[ \Omega_0 - K_V S(\varphi) + \frac{1}{2} K_V^2 \sigma_n(\varphi) \frac{d\sigma_n(\varphi)}{d\varphi} \right] dt - K_V \sigma_n(\varphi) dW(t) \tag{61}$$

where $W(t)$ is a Brownian motion process. Introducing the notation

$$K_1(\varphi) = \Omega_0 - K_V S(\varphi) + \frac{1}{2} K_V^2 \sigma_n(\varphi) \frac{d\sigma_n(\varphi)}{d\varphi} \quad \text{(drift coefficient)} \tag{62}$$

$$K_2(\varphi) = - K_V \sigma_n(\varphi) \quad \text{(diffusion coefficient)} \tag{63}$$

the equation takes the form

$$d\varphi(t) = K_1(\varphi) dt + K_2(\varphi) dW(t) \tag{64}$$

and we may use the standard techniques to characterize the stationary behavior of $\varphi$. In particular, the p.d.f. of $\phi$, the modulo $2\pi$ reduced phase error, is given by

$$p(\phi) = \frac{1}{K_2^2(\phi)} \exp[-U_0(\phi)] \cdot [C - 2J \int_{-\pi}^{\phi} \exp U_0(s) ds] \tag{65}$$

where

$$U_0(s) = -\int_{-\pi}^{s} \frac{2K_1(x)}{K_2^2(x)}\, dx \qquad (66)$$

C is a normalization constant and J is the average rate of cycle slips $N_+ - N_-$. In the absence of loop stress the density function is therefore

$$p(\phi) = \frac{C}{K_2^2(\phi)} \exp[-U_0(\phi)] \quad . \qquad (67)$$

5.7 Hard-Limiting Shuttle Repeater

The hard-limiting repeater implementation is illustrated in Figure 5.3a. The low-pass filter before the hard-limiter is assumed to be wide enough to pass the signal undistorted.

Assume that signal + noise before the hard-limiter is

$$r(t) = \sqrt{P}\, d_2(t) + n(t) \qquad (68)$$

and $y(t)$ is signal + noise after the hard-limiter, i.e.,

$$y(t) = \operatorname{sgn} r(t) \qquad (69)$$

From Reference 2 we obtain the correlation function of $y(t)$,

$$\begin{aligned} R_y(\tau) &\equiv E[y(t)y(t+\tau)] \\ &= E[\operatorname{sgn}(r(t)r(t+\tau))] \\ &= \operatorname{erf}^2\left(\frac{\sqrt{P}}{\sqrt{2}\sigma_n}\right) R_{d_2}(\tau) \\ &\quad + \frac{1}{\pi} \exp\left(\frac{-P}{\sigma_n^2}\right) \sum_{k=1}^{\infty} \left(\frac{R_n(\tau)}{\sigma_n^2}\right)^k \frac{1}{k!} He_{k-1}^2\left(\frac{\sqrt{P}}{\sigma_n}\right) [(1+R_{d_2}(\tau)) \\ &\quad - (-1)^k (1-R_{d_2}(\tau))] \end{aligned} \qquad (70)$$

where $\sigma_n^2 = R_n(0)$, $He_k$ is the kth Hermite polynomial,

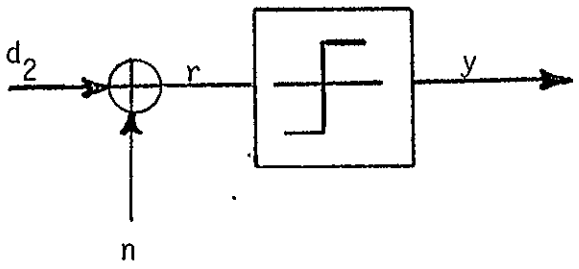


(a) With Hard-Limiter

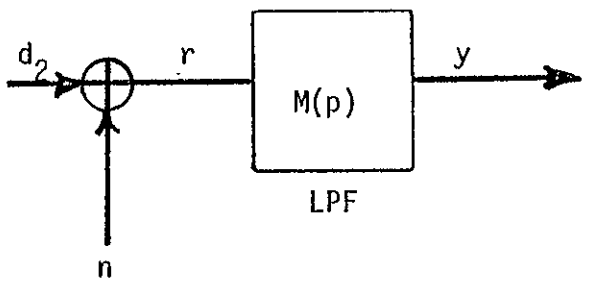


(b) Without Hard-Limiter

Figure 5.3. Two Shuttle Repeater Implementations Studied

$$\text{erf}(x) = \frac{2}{\sqrt{2\pi}}\int_0^{\sqrt{2}x} e^{-u^2/2}du = \frac{2}{\sqrt{\pi}}\int_0^{x} e^{-u^2}du \qquad (71)$$

$$R_{d_2}(\tau) = \begin{cases} 1-|\tau|/T_2, & |\tau| \le T_2 \\ 0\ ; & |\tau| > T_2 \end{cases} \quad \textbf{(NRZ)}$$

$$= \begin{cases} 1 - 3|\tau|/T_2, & |\tau| \le T_2/2 \\ |\tau|/T_2 - 1, & T_2/2 \le |\tau| \le T_2 \\ 0\ , & |\tau| \ge T_2 \end{cases} \quad \textbf{(BIPHASE)} \qquad (72)$$

where $T_2$ is the pulse duration of $d_2$. If $G(p)H'(p)$ is identity, then the equivalent noise correlation function is particularly simple. We have

$$R_z(\tau|\varphi) = C^2[P_1P_2\cos^2(2\varphi)R_y(\tau)R_{d_1}(\tau) + P_2R_y(\tau)R_{u_1}(\tau) + P_1R_{d_1}(\tau)R_{u_1}(\tau) + R^2_{u_1}(\tau)] \qquad (73)$$

The equivalent noise spectral density evaluated at zero frequency is then

$$S_z(0|\varphi) = C^2[P_1P_2\cos^2(2\varphi)\int_{-\infty}^{\infty} R_y(t)R_{d_1}(t)dt + P_2\int_{-\infty}^{\infty} R_y(t)R_{u_1}(t)dt + P_1\int_{-\infty}^{\infty} R_{d_1}(t)R_{u_1}(t)dt + \int_{-\infty}^{\infty} R^2_{u_1}(t)dt] \qquad (74)$$

where $C=K_1K_m$, $R_y(t)$ is given in (70), and

$$R_{d_1}(\tau) = \begin{cases} 1 - \frac{3|\tau|}{T_1}\ , & |\tau| \le T_1/2 \\ \frac{|\tau|}{T_1} - 1\ , & T_1/2 \le |\tau| \le T_1 \\ 0\ , & |\tau| \ge T_1 \end{cases} \qquad (75)$$

since channel 1 always uses the biphase data format. We use the estimate that $S_z(f|\varphi) = s_z(0|\varphi)$ for small f.

5.8 Linear Shuttle Repeater

Now consider the case where the hard-limiter is not used and M(p) is general, illustrated in Figure 5.3b. Then before the LPF we have

$$r(t) = \sqrt{P}d_2(t) + n(t) \tag{76}$$

After it we have

$$y(t) = \frac{1}{\sqrt{R_b(0)+R_v(0)}}\, b(t) + \frac{1}{\sqrt{R_b(0)+R_v(0)}}\, v(t) \tag{77}$$

where

$$b(t) = \sqrt{P}M(p)d_2(t) \tag{78}$$

$$v(t) = M(p)n(t) \tag{79}$$

and we have scaled y(t) so that $E[y^2(t)] = 1$. We see that

$$R_b(\tau) = PM(p)M^*(p)R_{d_2}(\tau) \tag{80}$$

$$R_v(\tau) = M(p)M^*(p)R_n(\tau) \tag{81}$$

Then

$$R_y(\tau) = \frac{1}{R_b(0)+R_v(0)}\,(R_b(\tau)+R_v(\tau)). \tag{82}$$

$$R_{\bar{y}}(\tau) = \frac{1}{R_b(0)+R_b(0)}(R_{\bar{b}}(\tau) + R_{\bar{v}}(\tau)) . \tag{83}$$

For the statistics of $\bar{y}^2$ we find

$$\bar{y}^2(t) = \frac{1}{R_b(0)+R_v(0)}\,[\bar{b}^2(t) + 2\bar{b}(t)\bar{v}(t) + \bar{v}^2(t)] \tag{84}$$

$$R_{\bar{y}2}(\tau) = E[\bar{y}^2(t)\bar{y}^2(t+\tau)] - R_{\bar{y}}^2(0)$$

$$= \frac{1}{(R_b(0)+R_v(0))^2}\{E[\bar{b}^2(t)\bar{b}^2(t+\tau)] + 2R_{\bar{b}}(0)R_{\bar{v}}(0)$$

$$+ 4R_{\bar{b}}(\tau)R_{\bar{v}}(\tau) + E[\bar{v}^2(t)\bar{v}^2(t+\tau)] - (R_{\bar{b}}(0)+R_{\bar{v}}(0))^2\}$$

$$= \frac{1}{(R_b(0)+R_v(0))^2}\{E[\bar{b}^2(t)\bar{b}^2(t+\tau)] + 2R_{\bar{b}}(0)R_{\bar{v}}(0)$$

$$+ 4R_{\bar{b}}(\tau)R_{\bar{v}}(\tau) + R_{\bar{v}}^2(0) + 2R_{\bar{v}}^2(\tau) - (R_{\bar{b}}(0)+R_{\bar{v}}(0))^2\}$$

$$= \frac{1}{(R_b(0)+R_v(0))^2}\{E[\bar{b}^2(t)\bar{b}^2(t+\tau)] - R_{\bar{b}}^2(0) + 4R_{\bar{b}}(\tau)R_{\bar{v}}(\tau)$$

$$+ 2R_{\bar{v}}^2(\tau)\} \qquad (85)$$

To obtain $E[\bar{b}^2(t)\bar{b}^2(t+\tau)] - R_{\bar{b}}^2(0)$, we note that

$$\bar{b}(t) = \sum_i c_i q(t-iT) \qquad (86)$$

where $c_i = \sqrt{P}$ or $-\sqrt{P}$ each with probability $\frac{1}{2}$ and $q(t)$ is the response of the $G(p)H'(p)M(p)$ filter to a data pulse (NRZ or bi-phase) of duration $T \equiv T_2$ and absolute height 1.

$$\bar{b}^2(t) = \sum_i \sum_k c_i c_k q(t-iT)q(t-kT)$$

$$= P\sum_i q^2(t-iT) + \sum_i \sum_{k\neq i} c_i c_k q(t-iT)q(t-kT) \qquad (87)$$

so

$$R_{\bar{b}2}(\tau) = E[\bar{b}^2(t)\bar{b}^2(t+\tau)] - R_{\bar{b}}^2(0)$$

$$= P^2\left\langle \sum_i q^2(t-iT)\sum_\ell q^2(t+\tau-\ell T)\right\rangle$$

$$+ \left\langle E\left[\sum_i \sum_{k\neq i} c_i c_k \sum_\ell \sum_{n\neq \ell} c_\ell c_n q(t-iT)q(t-kT)q(t+\tau-\ell T)\right.\right.$$

$$\left.\left. \cdot q(t+\tau-nT)\right]\right\rangle - P^2\left(\left\langle \sum_i q^2(t-iT)\right\rangle\right)^2$$

$$= P^2\left\langle \sum_i q^2(t-iT) \sum_\ell q^2(t+\tau-\ell T)\right\rangle - P^2\left(\left\langle \sum_i q^2(t-iT)\right\rangle\right)^2$$

$$+ 2P^2\left\langle \sum_i \sum_{k\neq i} q(t-iT)q(t-kT)q(t+\tau-iT)q(t+\tau-kT)\right\rangle$$

$$= P^2\left\langle \sum_i q^2(t-iT) \sum_\ell q^2(t+\tau-\ell T)\right\rangle - P^2\left(\left\langle \sum_i q^2(t-iT)\right\rangle\right)^2$$

$$+ 2P^2\left\langle \left(\sum_i q(t-iT)q(t+\tau-iT)\right)^2\right\rangle - 2P^2\left\langle \sum_i q^2(t-iT)q^2(t+\tau-iT)\right\rangle \tag{88}$$

where $\langle\cdot\rangle$ denotes the average over any time interval of length T. A similar expression holds for $R_{\bar{d}_1^2}(\tau)$, with q(t) replaced by the response of the G(p)H'(p) filter to a biphase pulse of duration $T_1$.

$$S_z(0|\varphi) = C^2\left\{\frac{1}{4}\sin^2(2\varphi)\left[\left(\frac{P_2}{R_b(0)+R_v(0)}\right)^2\int_{-\infty}^{\infty}[R_{\bar{b}^2}(t)+4R_{\bar{b}}(t)R_{\bar{v}}(t)+2R_{\bar{v}}^2(t)]dt + P_1^2\int_{-\infty}^{\infty}R_{\bar{d}_1^2}(t)dt\right]\right.$$

$$+ \frac{P_1P_2}{R_b(0)+R_v(0)}\cos^2(2\varphi)\int_{-\infty}^{\infty}(R_{\bar{b}}(t)+R_{\bar{v}}(t))R_{\bar{d}_1}(t)dt$$

$$+ \frac{P_2}{R_b(0)+R_v(0)}\int_{-\infty}^{\infty}(R_{\bar{b}}(t)+R_{\bar{v}}(t))R_{\bar{u}_1}(t)dt$$

$$\left. + P_1\int_{-\infty}^{\infty}R_{\bar{d}_1}(t)R_{\bar{u}_1}(t)dt + \int_{-\infty}^{\infty}R_{\bar{u}_1}^2(t)dt\right\} \tag{89}$$

where $R_b(t)$ and $R_v(t)$ are given in (80) and (81) and $C = K_1K_m$. We use the estimate that $S_z(f|\varphi) = S_z(0|\varphi)$ for small f. To evaluate (89) we may use the fact that

$$\int_{-\infty}^{\infty} R_{\bar{w}}(t)R_{\bar{x}}(t)dt = \int_{-\infty}^{\infty} |G(f)H'(f)|^4 S_w(f)S_x(f)df \qquad (90)$$

where w and x are signals and $S_w$ and $S_x$ are the Fourier transforms of $R_w$ and $R_x$, respectively.

5.9 S-Curve Amplitude Plots

Figures 5.4 through 5.9 are plots of the amplitude $S_a$ of the S-curve.

$$S_{\bar{a}} \equiv \frac{2}{K_1 K_m P_2} [S(\varphi)/\sin(2\varphi)]$$

$$= G(p)G^*(p)H'(p)H'^*(p)\left(R_y(0) - \frac{P_1}{P_2} R_{d_1}(0)\right) \qquad (91)$$

It is plotted as a function of Shuttle repeater input $E_b/N_0$, for channel 2 having NRZ or biphase pulses and rates of $R_2$ of 2000,192,16Kbps. The channel-1 data rate is 192 Kbps. Recall that the S-curve is independent of the ground station receiver noise. At the top of each figure are curves for the case where the repeater is a hard limiter and at the bottom are curves for the case of a lowpass-filter repeater. Each curve corresponds to a different bandwidth of the combined LPF $G(f)H'(f)$ in units of $R_2$.

Following are the assumptions made in obtaining the curves. The combined filter $G(f)H'(f)$ is a one-pole Butterworth filter. In the case of HL repeater, the spectrum of this repeater input noise is rectangular with a bandwidth of 1.5 $R_2$. In the case of LPF repeater, the input white noise and signal are both filtered by a four-pole Butterworth filter of bandwidth 1.5 $R_2$. In both cases, $P_1/P_2 = .25$.

Figure 5.4. $S_a$ for $R_2$ = 2000 Kbps, Channel 2 NRZ.

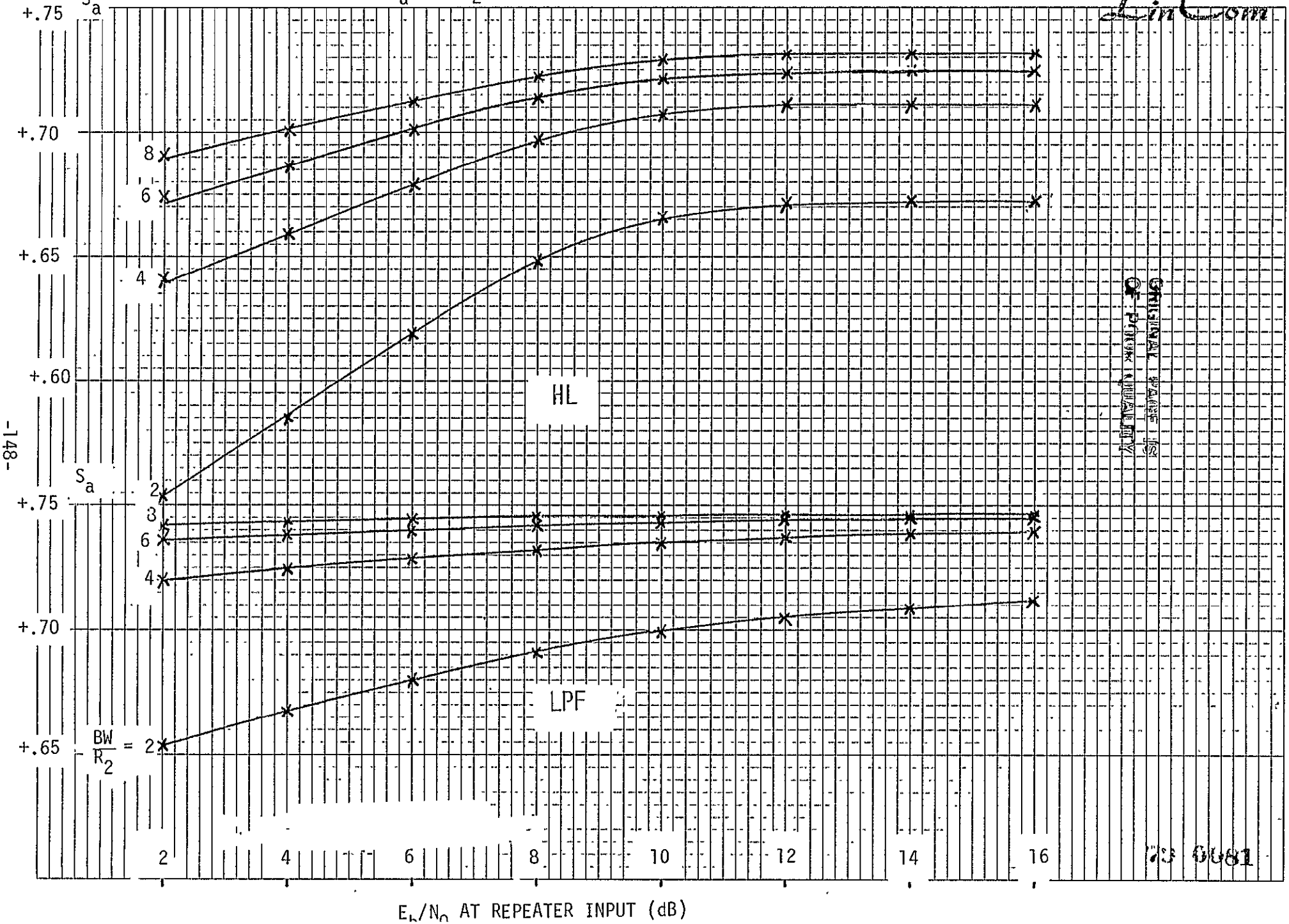

Figure 5.5. $S_a$ for $R_2$ = 192 Kbps, Channel 2 NRZ.

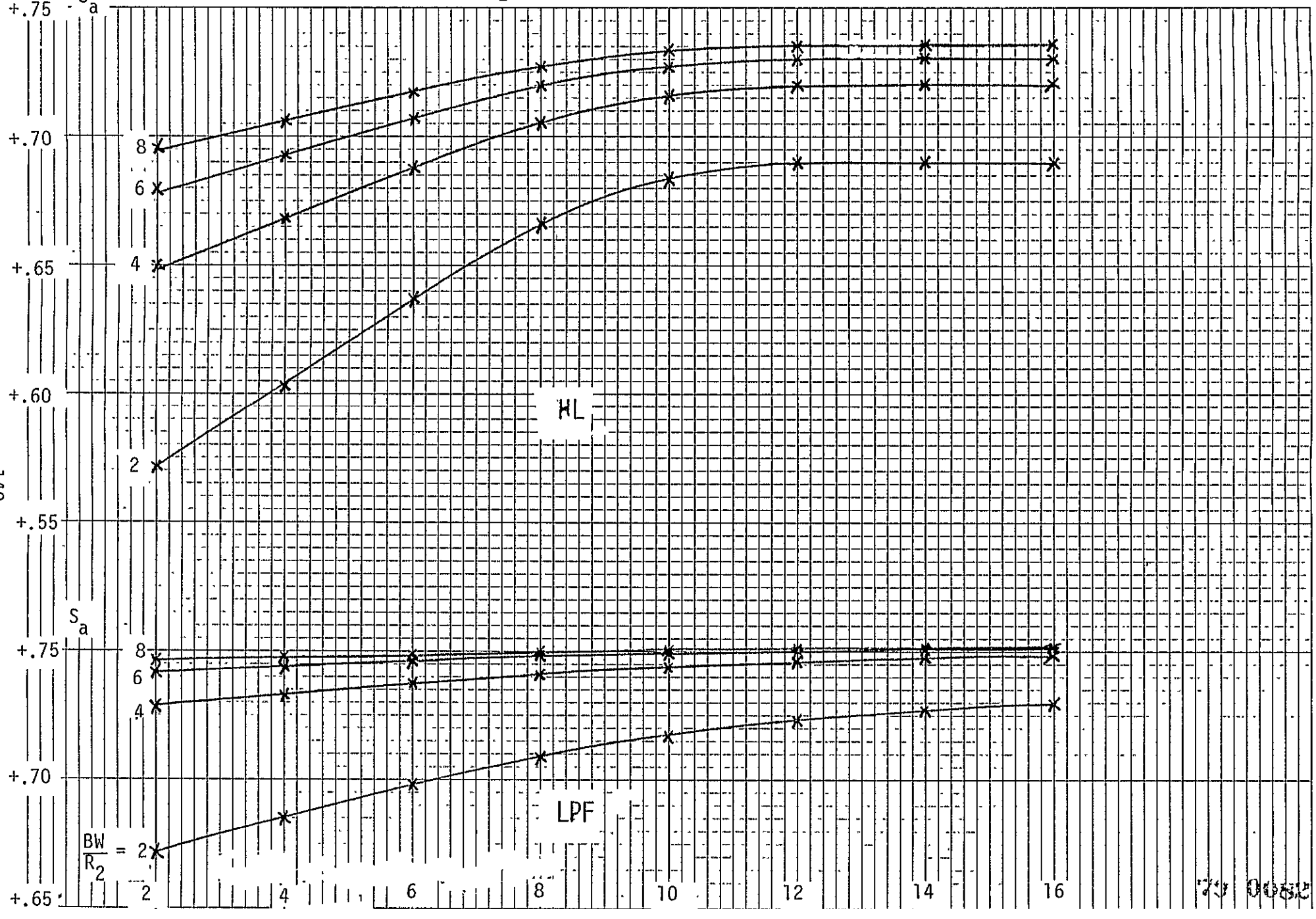

Figure 5.6. $S_a$ for $R_2$=16 Kbps, Channel 2 NRZ.

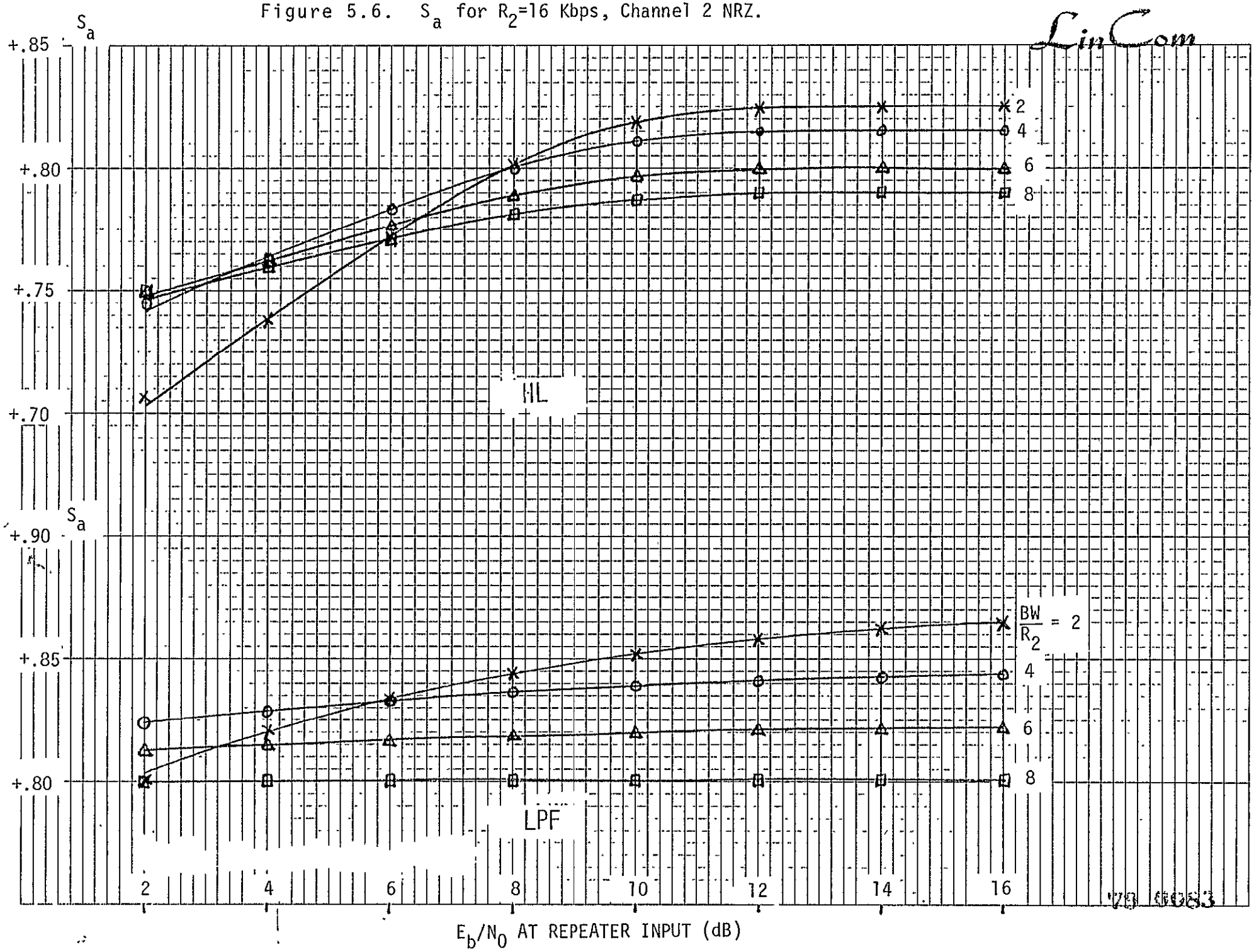

Figure 5.7. $S_a$ for $R_2$ = 2000 Kbps, Channel 2 Biphase.

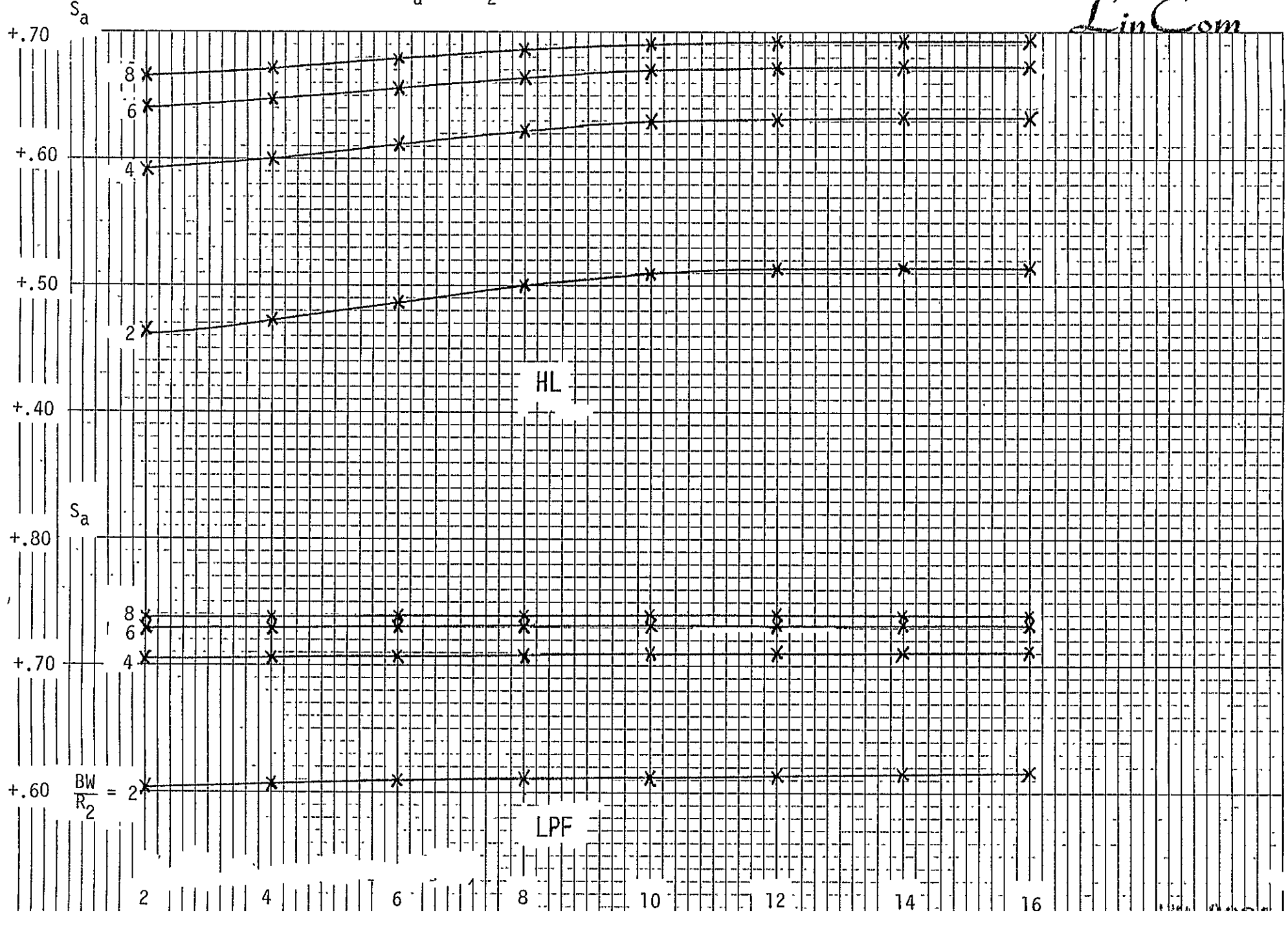

Figure 5.8. $S_a$ for $R_2$ = 192 Kbps, Channel 2 Biphase.

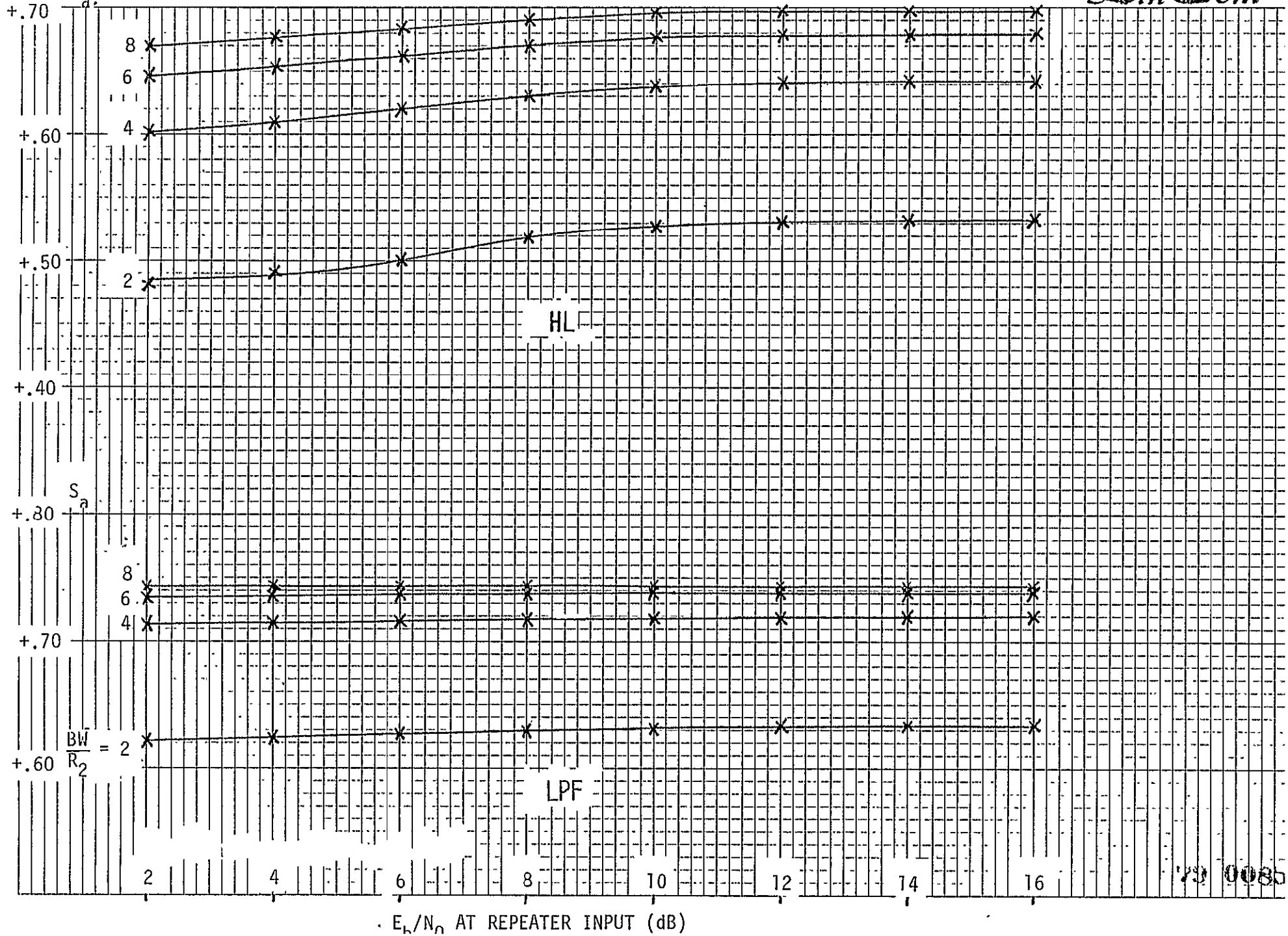

Figure 5.9. $S_a$ for $R_2$ = 16 Kbps, Channel 2 Biphase.

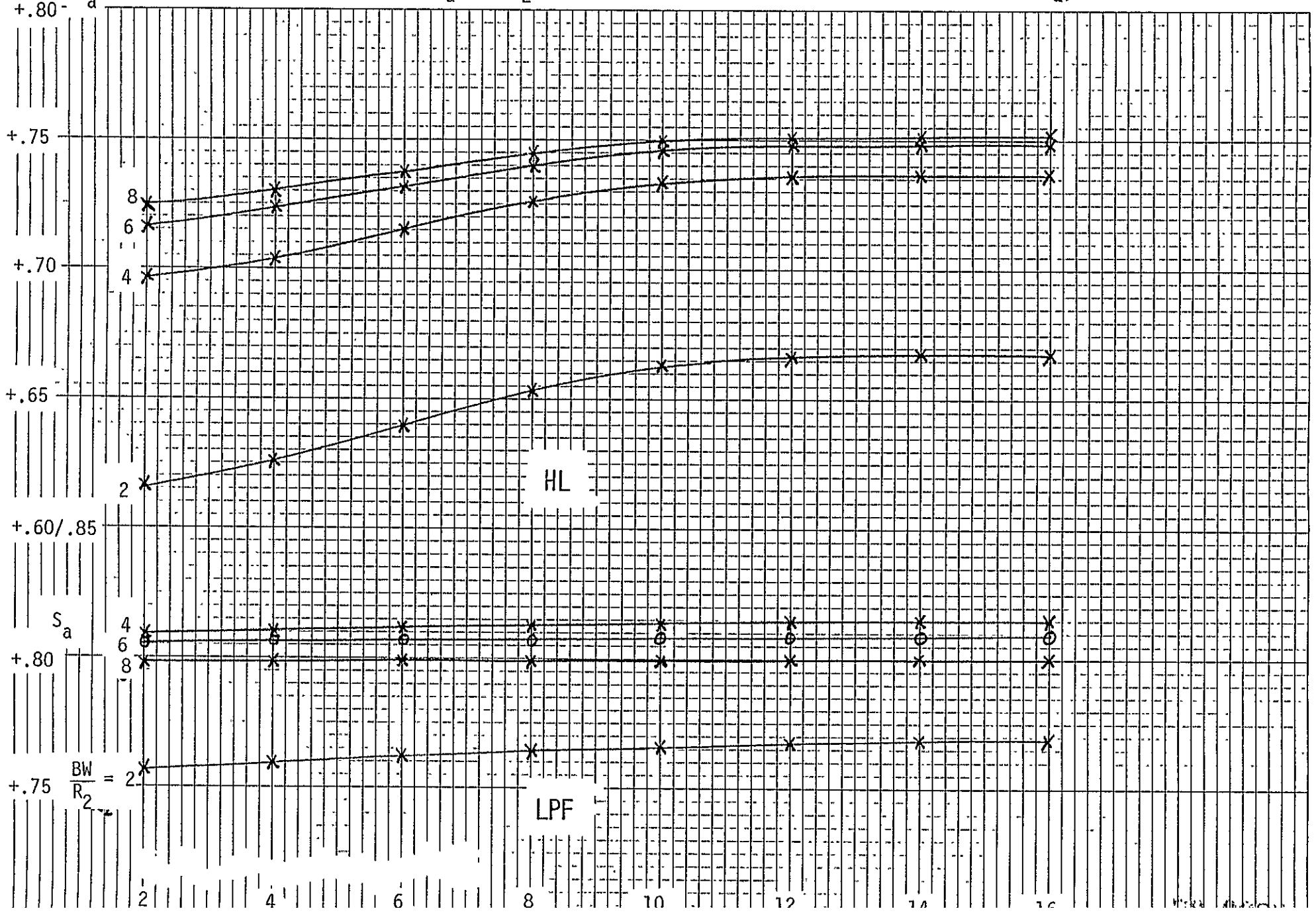

## 5.10 Variance of Loop Phase Error

From Reference 3 we have for loop phase error $\phi$,

$$\sigma_\phi^2 \triangleq \frac{N_0' B_L}{(S'(0))^2} \tag{91}$$

where $N_0'/2 = S_z(f=0|\varphi=0)$ and $B_L$ is the loop bandwidth, when the bandwidth of the equivalent noise is much wider than $B_L$. It can be shown that $R_2 S_z(0|0)$ does not depend on $R_2$ but only on $R_1/R_2$, if the bandwidth of the $G(f)H'(f)$ filter is taken as a multiple of $R_2$. We plot

$$\frac{N_0' R_2}{(S'(0))^2} \triangleq \frac{\sigma_\phi^2}{B_L/R_2} \tag{92}$$

in Figures 5.10 through 5.15, using NRZ or biphase pulses and three different data rates for channel 2. Each figure shows results for both repeaters considered. Assumptions made include those noted in the previous section. Additionally, $E_b/N_0 = 10$ dB for $s_i$ and u processes and the spectrum of u is assumed flat over its bandwidth.

## 5.11 Filter Bandwidth Selection

As shown by equation (43), the Costas loop S-curve contains two terms whose relative magnitudes depend on the UQPSK power split, the payload interrogator bandwidth, the data rates and the IF and arm filter bandwidths in the ground station. In the desired mode of operation the first term, which depends on the channel 2 statistic, is larger than the second term which is determined by the low-rate channel 1. However, if the combined IF and arm filter are too narrow they will reduce the channel 2 power to the point where the second term is larger than the first. In this instance the Costas loop will track the low-

Figure 5.10 $\frac{\sigma_{\varphi}^2}{B_L/R_2}$ $R_2$ = 2000 Kbps, Channel 2 NRZ, $E_b/N_0$ = 10 dB for s, and u.

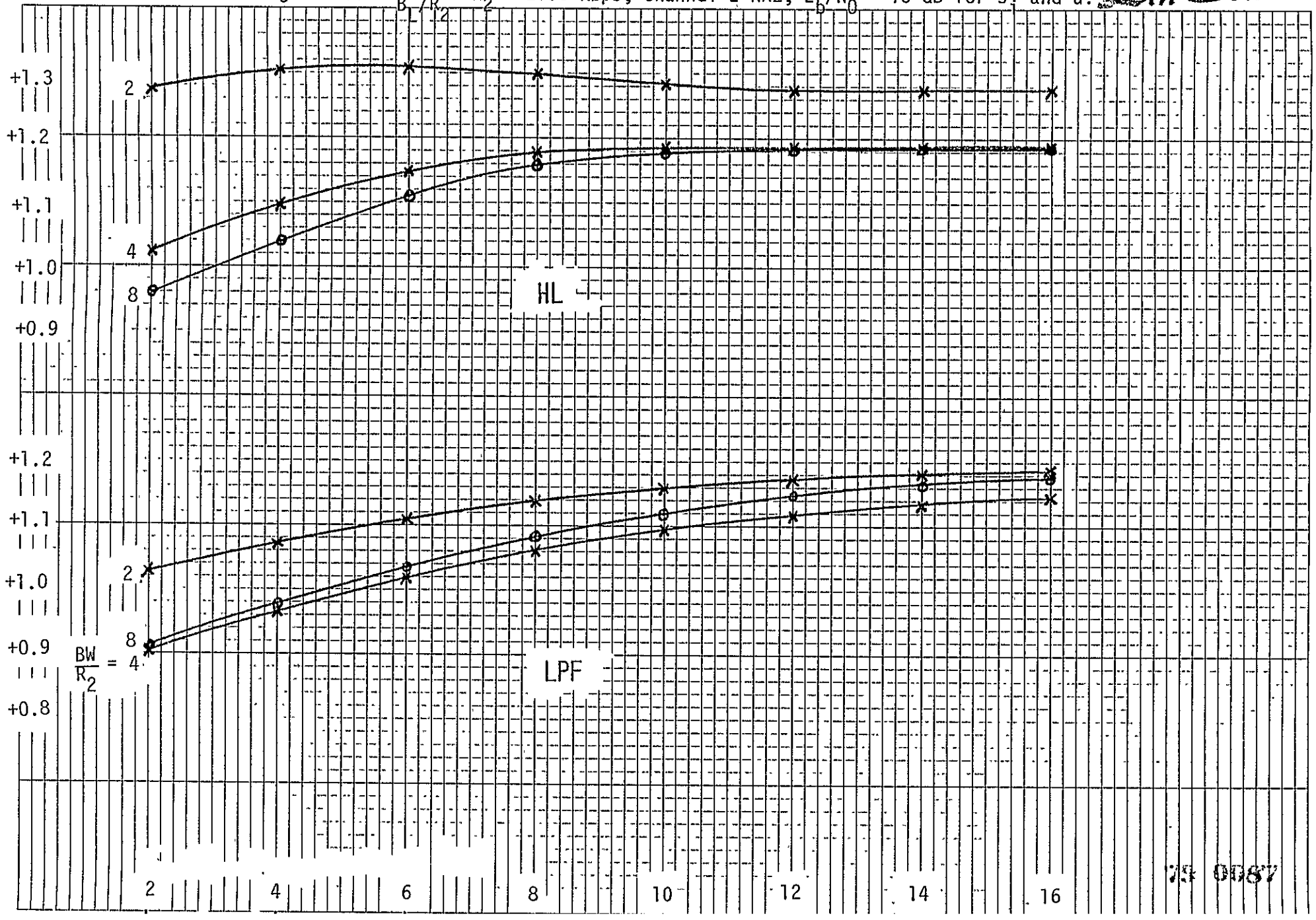

Figure 5.11. $\frac{\Phi}{B_L/R_2}$ for $R_2$ = 192 Kbps, Channel 2 NRZ, $E_b/N_0$ = 10 dB for $s_i$ and $u_i$

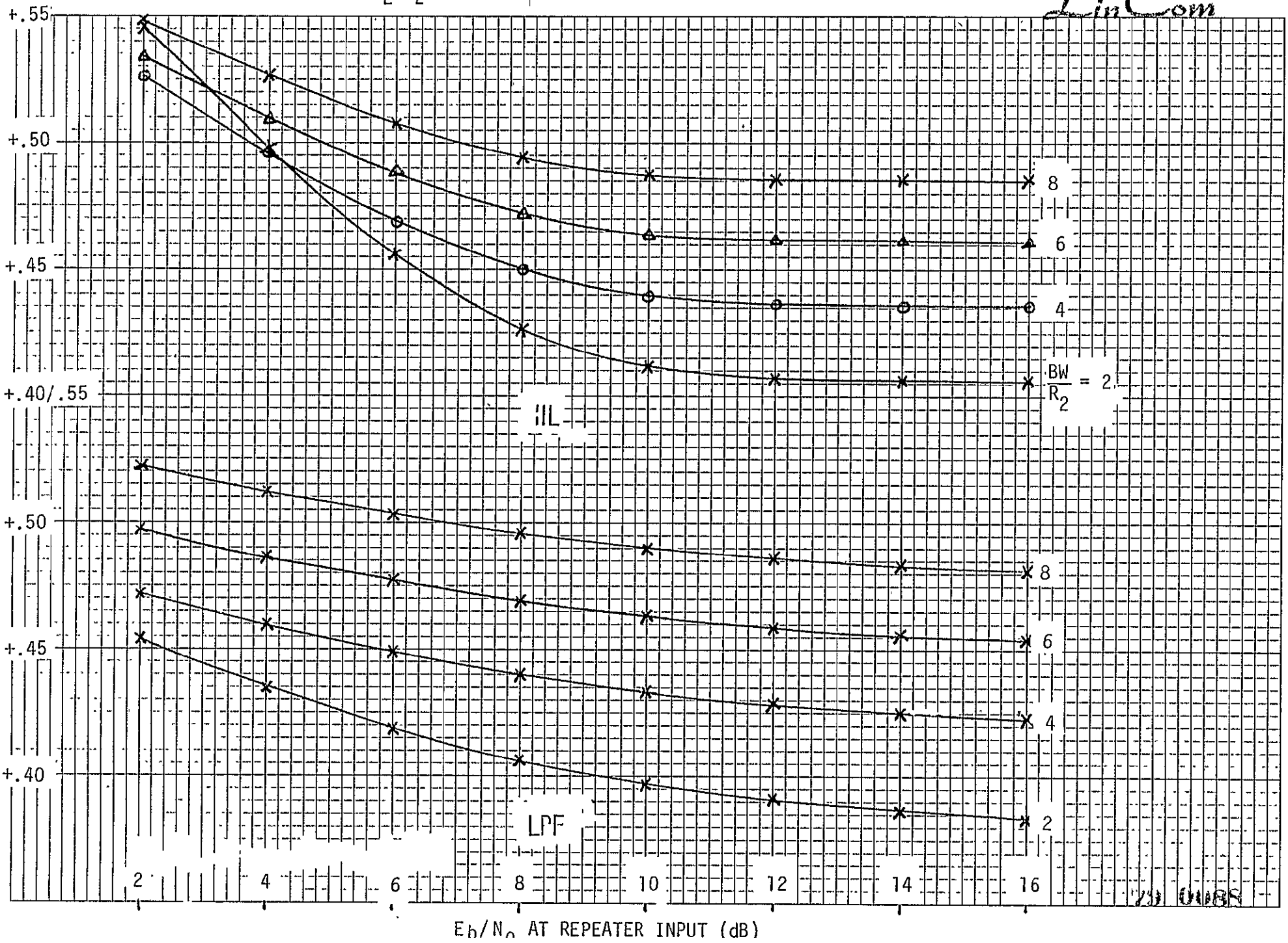

Figure 5.12. $\frac{\sigma_{\varphi}^2}{B_L/R_2}$ for $R_2$ = 16 Kbps, Channel 2 NRZ, $E_b/N_0$ = 10 dB for $s_i$ and $u$.

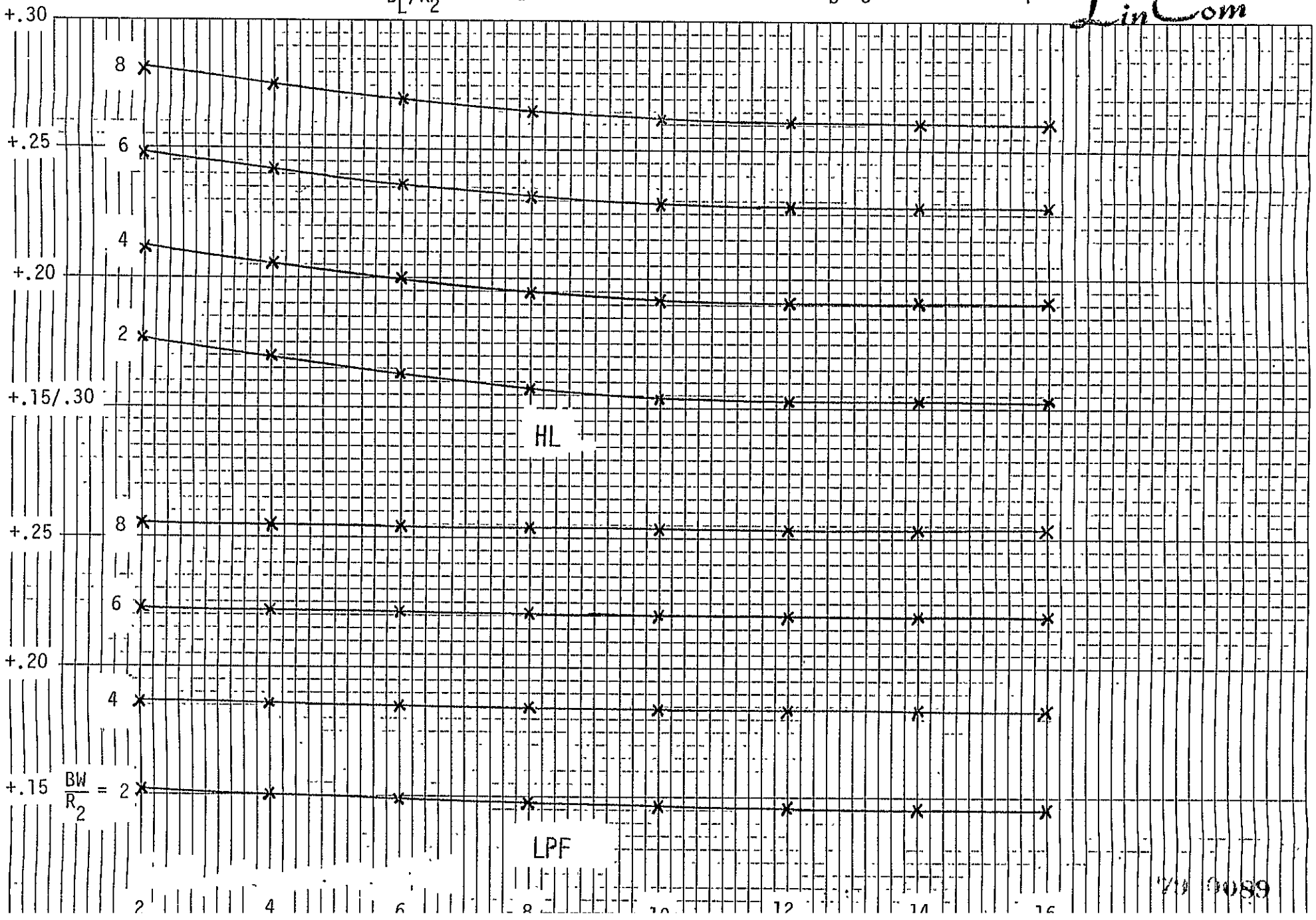

Figure 5.13. $\frac{\sigma}{B_L/R_2}$ for $R_2 = R_2 = 2000$ Kbps, Channel 2 Biphase, $E_b/N_0$=10 dB for s and u

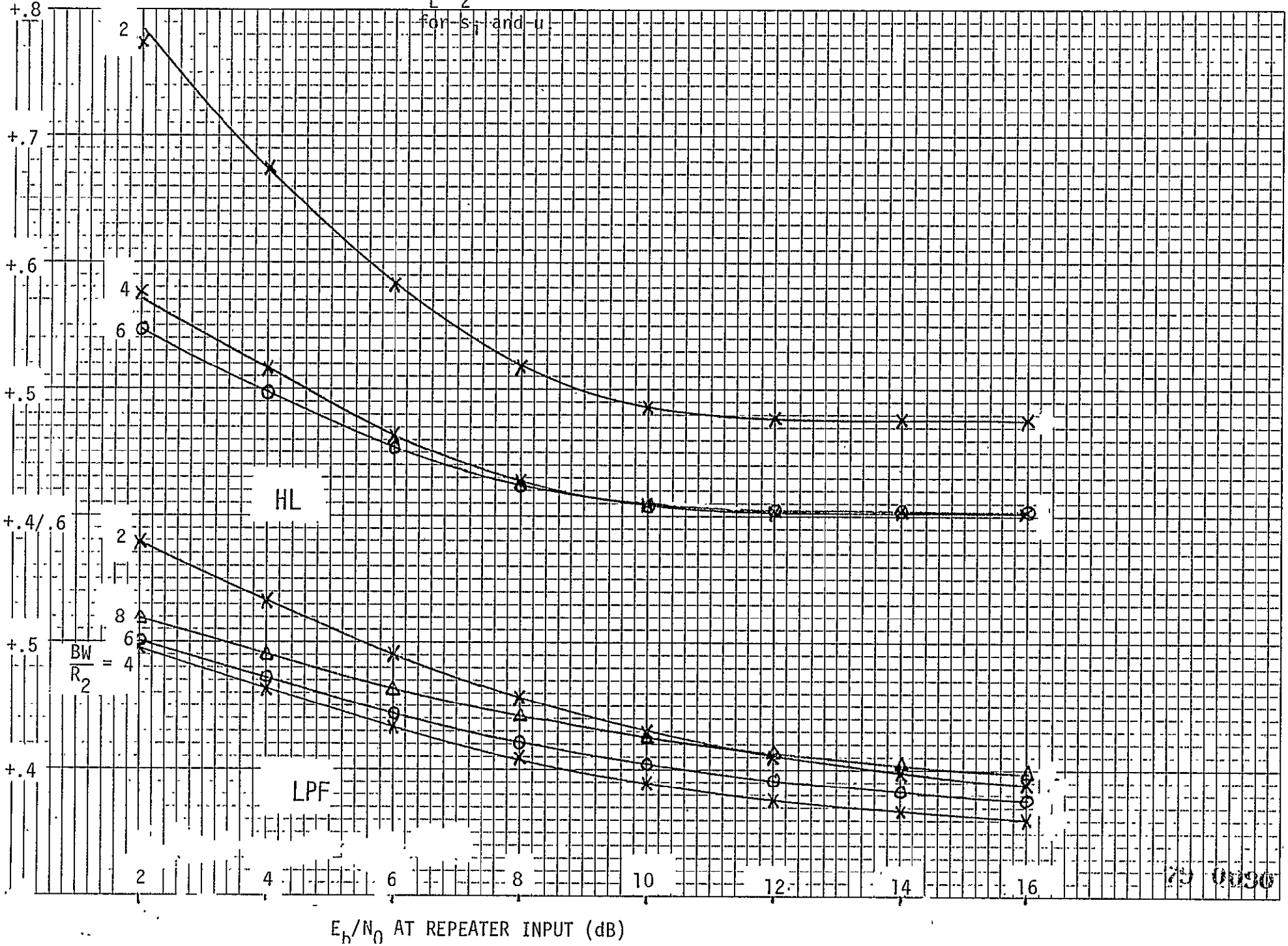

Figure 5.14. $\frac{\sigma^2_{c\phi}}{B_L/R_2}$ for $R_2$ = 192 Kbps, Channel 2 Biphase, $E_b/N_0$ = 10 dB for $s_i$ and u.

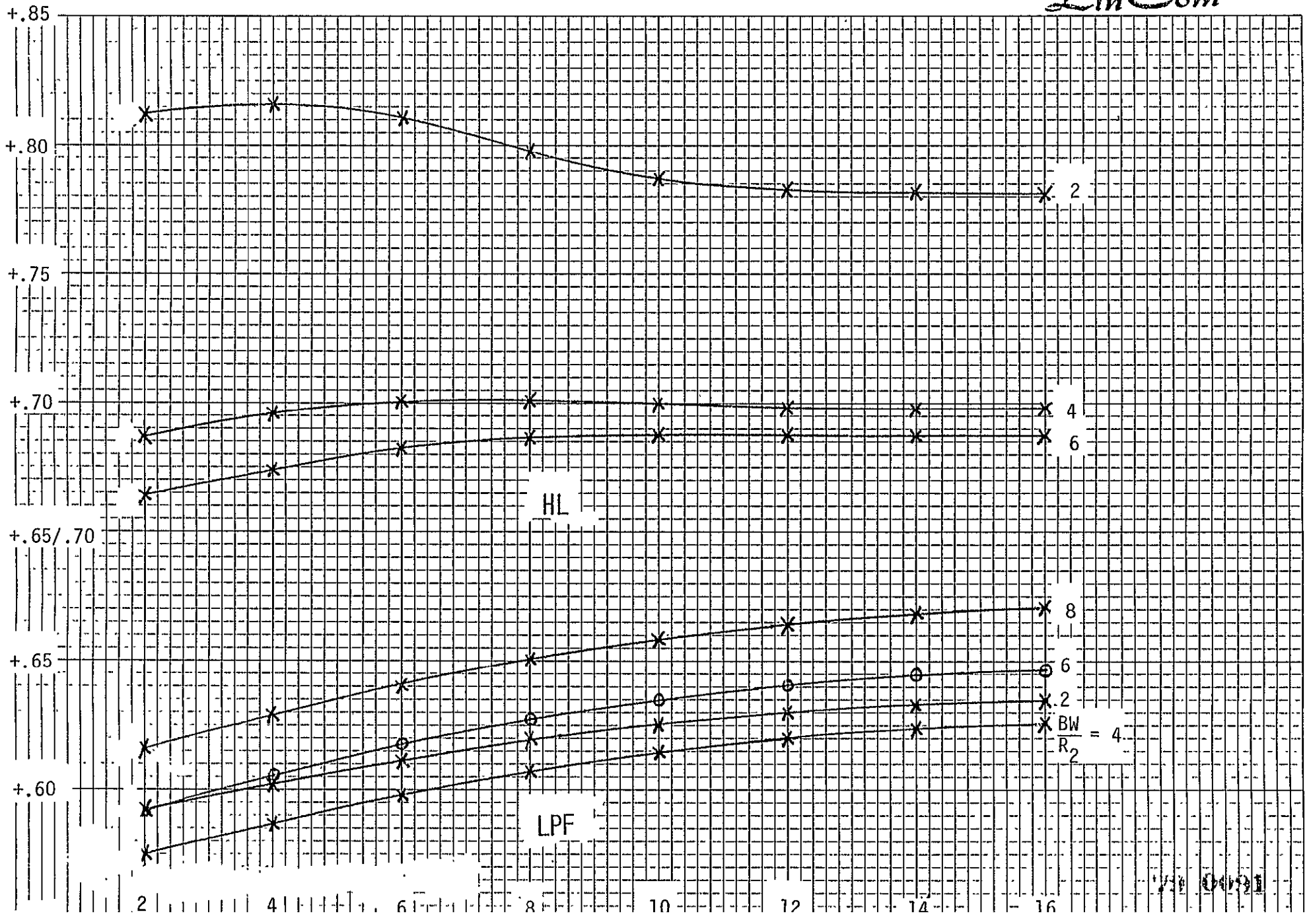

Figure 5.15. $\frac{\dot{}}{B_L/R_2}$ for $R_2$ = 16 Kbps, Channel 2 Biphase, $E_b/N_0$ = 10 dB for $s_i$ and u.

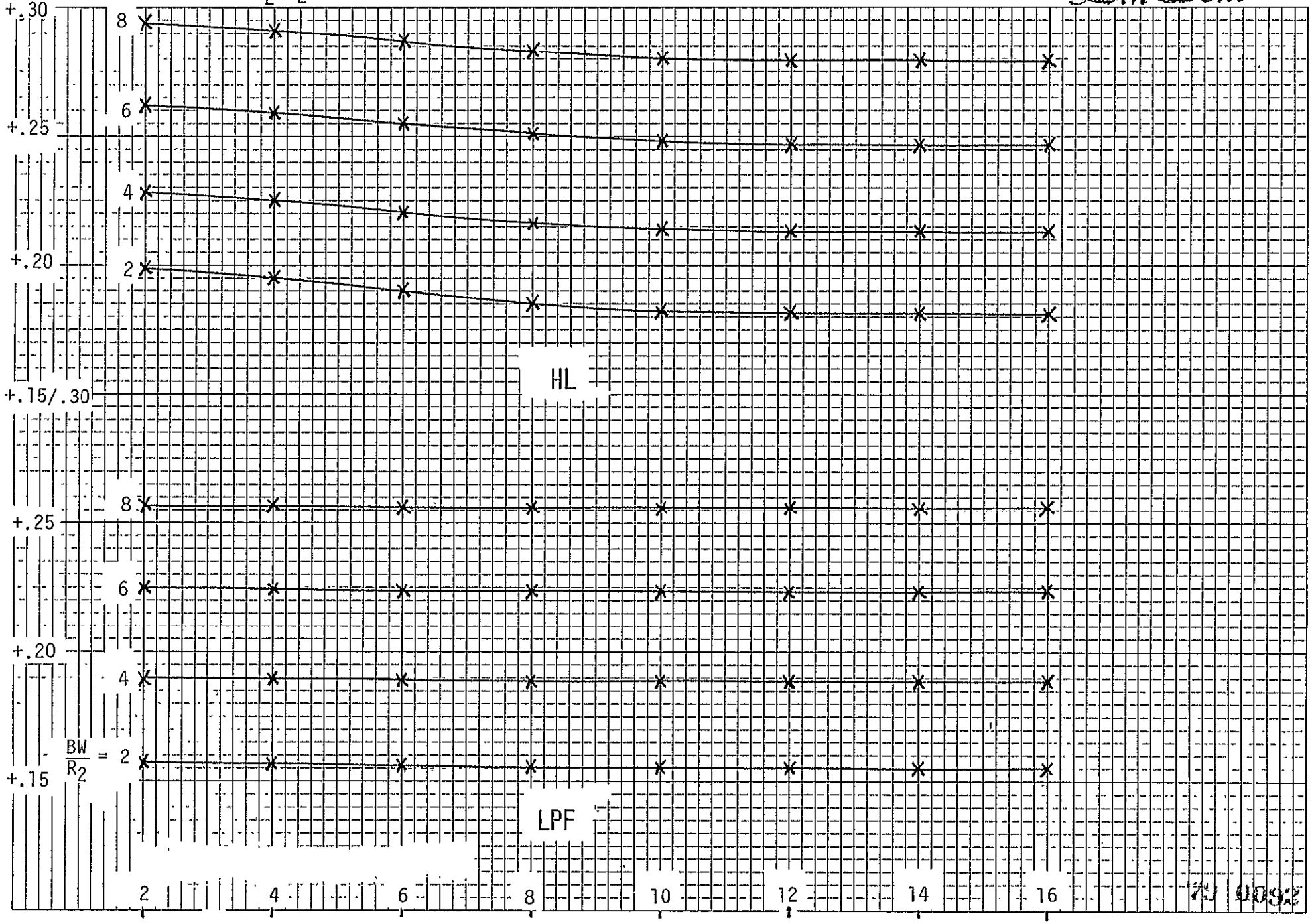

power channel. This problem is particularly serious if the payload signal drops out and the payload interrogator receives noise only. Assuming a rectangular spectrum for the noise process n (Fig. 5.2) the output spectrum is still almost rectangular (Fig. 5.16) with the same bandwidth. Since the combined IF and arm-filters do not affect the low-rate channel 1 power we can expect the Costas loop lock-point to shift by 90 degrees when the arm-filter bandwidth is less than approximately 1/4 at the payload interrogator bandwidth for a UQPSK power split of 4:1. In the transition region, i.e. when the arm filter bandwidth is approximately one quarter of the interrogator bandwidth, the loop will either track unsatisfactorily or not at all. These conclusions agree with the findings in [4].

5.12 Conclusions

From the plots, Fig. 5.4 to 5.15 it is clear that the payload interrogator implementation could be slightly improved, as far as subcarrier recovery is concerned, by remvoing the hard-limiter. This is borne out by the fact that the resulting S-curve amplitudes are higher and less sensitive to the carrier-to-noise ratio at the payload interrogator. This small improvement comes at the expense of reduced power control for channel 2 which will result in higher crosstalk into channel 1.

For the worst-case conditions (lowest data rate on channel 2, $E_b/N_0$ = 10 dB, i.e. no margin) and for a loop bandwidth of 500 Hz the expected rms phase error in the detector will be 5 degrees. If the possibility of losing the payload signal exists the relationship between the payload interrogator bandwidth and the Costas loop arm filter bandwidth has to be selected carefully to avoid tracking

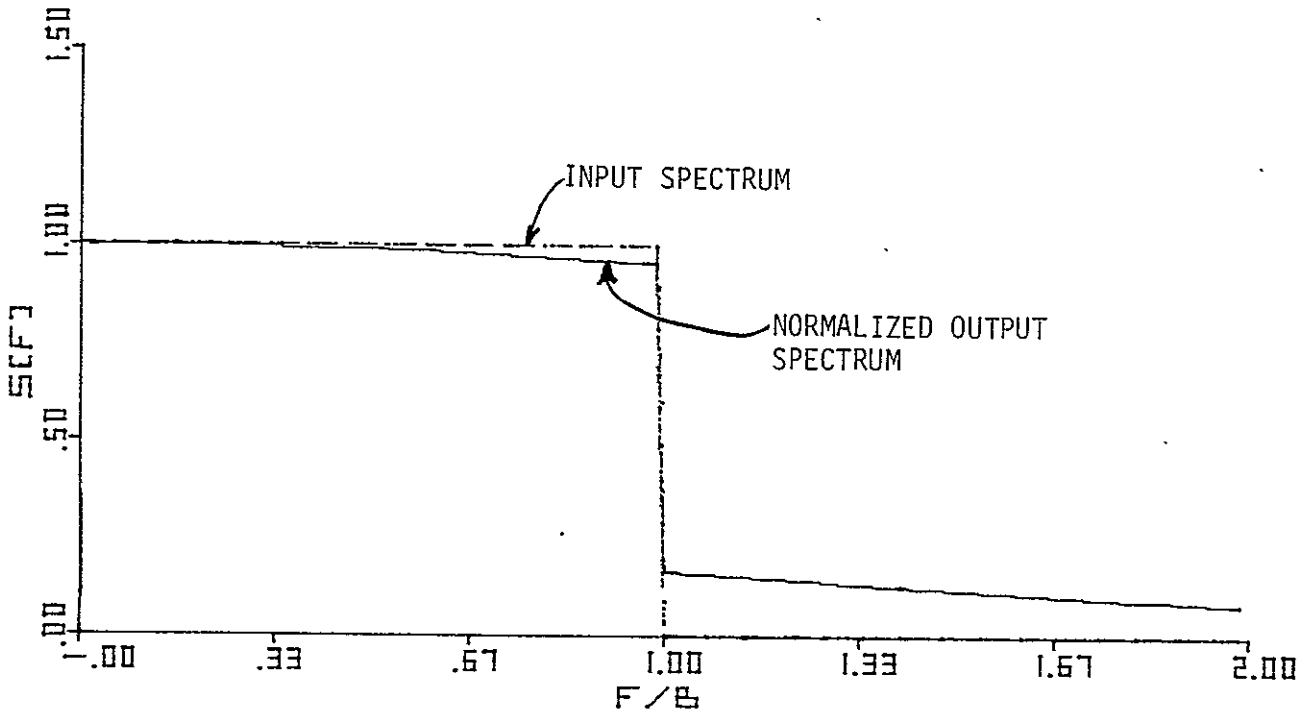


Figure 5.16. Noise Output Spectrum of Hard-Limiter.

the signal with a 90 degree offset.

NOTE:

In mode 1 of Ku-band return link, the subcarrier is a square wave and not a sine wave as assumed in this analysis. The spectrum of the modulated subcarrier then is like that of the sine-wave subcarrier near 8.5 MHz but has additional harmonics. For the case of the LPF repeater, even when $R_2$ is as large as 2 Mbps, there is almost no overlapping of various parts of the spectrum because the bandwidth of the LPF is 1.5 $R_2$, which is less than 4.25 MHz. When the repeater is a HL, there may be more overlapping when $R_2$ is 2 Mbps. Assuming no overlapping, which is true for practically all values of $R_2$, then as long as the loop arm multipliers are insensitive to signals above 4.25 MHz, the arm signals $z_c$ and $z_s$ will be the same for square-wave subcarrier as for sine-wave subcarrier if the average power of both channels is multiplied by $\pi^2/8$.

## REFERENCES

1. W. C. Lindsey, "Optimum Performance of Costas Type Receivers," Axiomatix Report R7502-1, Feb. 18, 1975.

2. W. C. Lindsey and W. R. Braun, "Tracking and Data Relay Satellite System (TDRSS) Communication Analysis and Modeling Study, Phase I Report," LinCom Corp., prepared under NASA Contract No. NAS 5-23591, October 15, 1976, pp. 93-94.

3. W. R. Braun and W. C. Lindsey, "Carrier Synchronization Techniques for Unbalanced QPSK Signals," prepared under NASA Contract NAS 5-23591, to be published in IEEE Transactions on Communications, September 1978.

4. Shuttle Ku-Band and S-Band Communications Implementation Study, Final Report, Axiomatix Report No. R7902-3, February 28, 1979.